"THE DEVELOPMENT OF A STANDARD CALORIMETRIC DOSIMETER SYSTEM FOR MEGAVOLTAGE RADIATION"

by

JOHN EDWARD PATTISON

Fellowship Diploma (Applied Physics) -
Royal Melbourne Institute of Technology.

Bachelor of Science -
Australian National University.

A thesis
presented for the degree
of
Master of Science
in the
University of Adelaide.

Based on work performed in the
Department of Radiotherapy, Royal Adelaide Hospital
in association with the
Department of Physics, University of Adelaide.

August, 1971.

TABLE OF CONTENTS

SUMMARY vi

ACKNOWLEDGEMENTS ix

STATEMENT OF AUTHENTICITY x

MAIN TEXT

Chapter I HISTORICAL INTRODUCTION

I.1 The Early Period 1

I.2 Development of Ionization Methods 6

I.3 Limitations of the Roentgen and the emergence of the Rad 10

I.4 Standard Chemical Systems 14

I.5 The Calorimetric Systems 15

Chapter II CALORIMETER DESIGN AND PROPERTIES

II.1 Calorimeter Materials

1.1 Calorimeter Absorber Material 20

1.2 Calorimeter Design 23

1.3 Masses and Heat Capacities of Calorimeter Components 24

II.2 Thermodynamic Considerations

2.1 Possible Approaches 26

2.2 Thermal Insulation 28

2.3 Estimation of Thermal Constants for the Calorimeter 29

2.4 Effect of an External Temperature Change upon the Calorimeter Element 31

II.3	Temperature Measurement System	
3.1	Temperature Sensors	34
3.2	Temperature Measuring Circuit	36
3.3	Bridge Potential and Thermistor Self-Heating	38
3.4	Bridge Sensitivity and Linearity	42
II.4	Calibration Method	
4.1	Approach	44
4.2	Calibration Circuit	46
4.3	Practical Details	47
4.4	Estimation of Weighting Resistance	49
4.5	Calibration Equations	49
4.6	Simulation of Electric Calibration to Radiation Measurement	50
4.7	Temperature Distribution due to Radiation Field	53
4.8	Temperature Distribution due to Electric Heating	58
II.5	Thermal Linearity of System	
5.1	General Considerations	63
5.2	Thermal Linearity of Element	64
5.3	Effect of Unbalanced Calibration Heating	66

Chapter III		AUXILIARY DOSIMETERS	
	III.1	Air-Cavity Ionization Chamber	
	1.1	Materials and Design	68
	1.2	Electrical Properties	71
	1.3	Determination of Collection Volume	74
	1.4	Calibration of the Ionization Chamber	78
	1.5	Experimental Procedure	81
	III.2	The Fricke, or Ferrous Sulphate, Dosimeter	
	2.1	Materials and Design	82
	2.2	Calibration of Fricke Dosimeter	85
	2.3	Experimental Procedure	88
Chapter IV		OPERATION OF CALORIMETER AND RESULTS	
	IV.1	Operation of Calorimeter	
	1.1	Analysis of Graphical Results	91
	1.2	Experimental Procedure	95
	IV.2	Preliminary Results	
	2.1	Initial Tests	97
	2.2	Linearity of Response	99
	IV.3	Results	
	3.1	Picker Teletherapy Unit	101
	3.2	Orbitron Teletherapy Unit	103
	3.3	Observations from Results	105
	3.4	Tests on Methods of Chart Analysis	107
Chapter V		CONCLUSIONS	109

APPENDICES

I	Masses and Heat Capacities of Calorimeter Components	xi
II	Calculation of Thermal Transfer Coefficients	xvi
III	Calibration Heater Resistance Values	xxii
IV	Calculation of Typical Ionization Chamber Result	xxiii
V	Calculation of Typical Fricke Dosimeter Result	xxiv
VI	Calculation of Typical Calorimeter Result	xxvii

BIBLIOGRAPHY xxxi

SUMMARY

This thesis describes the development of a standard calorimetric system of radiation dosimetry which is to be used in the Department of Radiotherapy of the Royal Adelaide Hospital.

The thesis commences by surveying briefly the historical background of the evolution of units and methods of radiation dosimetry in medicine. The necessity for developing a dosimeter system based on calorimetry, for use at photon energies greater than about 3 MeV, is indicated and an outline of the progress in the field of calorimetric dosimetry is presented. The fact that no particular design of a calorimetric system has yet been universally adopted for standard dosimetry is stressed.

The second chapter then describes, in some detail, the numerous theoretical factors involved in the design of a calorimetric dosimeter. The system developed is designed to simulate the absorption of radiation in a small segment of a large "tissue-equivalent" material. Thermodynamically it is a twin quasiadiabatic system employing thermistors as the temperature sensors in a D.C. Wheatstone bridge circuit. The calorimeter is calibrated in terms of fundamental quantities by means of Joule heating in discrete heaters embedded in the bulk of the absorbing material. Justification is given for all choices made during the design of the system. Considerable emphasis has been placed on the thermal properties of the system, such as, effect of external temperature variations, effect of thermistor

self-heating, the simulation of electric calibration to radiation absorption, thermal linearity, etc., since these detailed theoretical considerations had not been seen in previous published work on calorimetric dosimetry. It is concluded, on the basis of the theoretical work in this chapter, that the system so designed should have the properties desired of a standard dosimetric system, namely, linearity of response, adequate sensitivity and accuracy, and fundamental calibration.

To permit verification of the performance of the calorimetric system, two further dosimeters were constructed, one an air-cavity ionization chamber and the other a Fricke dosimeter. The third chapter describes the design and construction of these two auxiliary dosimeters. They were designed so as to be of similar materials and shape as the calorimeter while retaining their own calibrations.

Chapter four describes a number of tests, including an intercomparison of the three dosimeters using Co 60 γ-radiation, made over a period of twelve months. The two methods of analysing the calorimeter results are also investigated. From the various tests it is found that (i) the calorimeter behaves essentially as predicted from theory, and (ii) the results obtained with the calorimeter compare favourably with those obtained by the currently-used methods of dosimetry based on oxidation of ferrous sulphate, and on

ionization in air, the latter of which is only strictly applicable for photon energies less than about 3 MeV.

It is concluded, in chapter five, that the calorimeter developed during the course of this project may be used with confidence as an independent standard dosimeter. The calorimetric system was proven to be readily adaptable to each of the radiation machines within the Radiotherapy Department, namely, two Co60 telecurie units (a "Newton-Victor" Orbitron and a "Picker X-ray" C1000) and a 4MeV linear accelerator. The system compares favourably with regards to cost of construction, procedure of operation, etc., with those systems developed elsewhere and described in the various publications.

ACKNOWLEDGEMENTS

Thanks are due to Dr. S.I. Evans, Director of the South Australian Institute of Technology, where the author is a member of staff, for the granting of permission to undertake this work. Thanks are also due to Dr. G.L. Goodwin, Head of the School of Physics at the South Australian Institute of Technology, for arranging for facilities towards the production and publication of this thesis.

To his supervisors, Mr. B. Worthley of the Physics group of the Anti-Cancer Foundation of the University of Adelaide, at the Royal Adelaide Hospital, and Dr. S. Tomlin of the Department of Physics, University of Adelaide, the author is particulary indebted for inspiration, for advice and for criticism in discussion at all times.

To his colleagues in the Physics group of the Anti-Cancer Foundation of the University of Adelaide, and to the workshop staff who have assisted him in constructional matters, the author acknowledges his sincere gratitude.

STATEMENT OF AUTHENTICITY

This is to certify that this thesis contains no material which has been accepted for the award of any other degree or diploma in any other University, and that, to the best of my knowledge and belief, the thesis contains no material previously published or written by another person, except where due reference has been made in the text of this thesis.

Signed

(J.E. Pattison)

MAIN TEXT

CHAPTER I HISTORICAL INTRODUCTION

I.1 The Early Period

In an endeavour to place the present work into correct perspective the following short historical review is presented. It will be shown how the various concepts and techniques for the measurement of radiation dosage have evolved. In doing so both the aims and limitations that are involved in this work will be more clearly defined.

The application of x-radiation to diagnostic and therapeutic medicine came immediately after the announcement of its discovery by Roentgen in January 1896. A number of carcinomas were treated in 1896, possibly the first by GRUBBE (1933). In April 1896, Webster found that rheumatic pains were relieved by the repeated exposure of the joint to x-ray diagnosis. At the same time however the harmful effects of this new radiation were beginning to become apparent. Radiation dermatitis, epilation and radiation sickness were noted in 1896. The more severe effects were discovered some years later, such as sterilization in 1903. Although Villard had discovered the similarity of γ-rays to x-rays in 1898, γ-rays were not generally used for therapy until after 1904. In the case of γ-radiation the harmful effects were observed first. Both Becquerel (accidentally) and Pierre Curie (deliberately) exposed themselves to radium for a number of hours in 1901, and obtained skin erythemas

followed by skin ulceration (BECQUEREL and CURIE, 1901). As was the case with x-radiation, radium was grossly misused as a possible remedy for almost any ailment.

Although man was learning of the hazards associated with working with these new radiations, no serious organized efforts were made at radiation protection for the first twenty years of their use. A problem in the therapeutic uses of radiation was the necessity to apply them in a quantitative manner, not at that time either needed, or practised, in other branches of medicine. A further serious problem which hindered the development of the fields of radiation protection and therapy was the lack of suitable units of dose, and of instruments for quantitative dosimetry.

Roentgen had described how adding filters to an x-ray beam had made the beam become more penetrating, or "harder", thus showing that an x-ray beam is characterized by two factors; quantity (dosage or intensity) and quality (penetrating power or wavelength). An understanding of quality was built up slowly. At first it was estimated by the length of a spark gap, representing tube voltage. Then various filters came into use, and in 1913 Christen proposed the concept of "Half-Value Layer", which is still in use today. The problem of the measurement of quantity was not so easily overcome.

The mechanism of radiation induced effects on cells was not known in the early years and the difference in concepts between exposure, as related to the beam, and absorbed dose, as related to

the absorbing material, was only realized by a few persons around 1910. It took many more years before these concepts were clearly differentiated. Thus, the measurement of dosage was very confused in this early period and during it most of the physical, chemical and some of the biological effects, which were known to be related to the x-ray quantity, were tried as dosimetric systems, but most of them found only limited popularity for short periods of time. In each case the effect being measured and its units were intimately connected to the measuring technique employed.

Many of the early attempts at dosimetry are described by GLASSER (1941). They include, the first dosimeter, the "Osteoscope", which was based on density observations of substitute hands upon either fluoroscopic screens or photographs. For a short time, somewhat inaccurate empirical equations, based on physical factors, were used to compute x-ray dosages. Chemical systems such as the "Chromoradiometer" of Holzknecht, and the "pastilles" of Sabouraud and Noire were introduced just after 1900 and gained some popularity; the latter system was still being used in dermatological therapy until about 1940. Both methods were based upon the degree of discolouration of tablets of certain chemical mixtures when exposed to x-radiation. Other chemical effects, such as precipitation from solutions as in the "Kalomel radiometer", were used with limited success. These chemical systems were found to be unreliable due to their great dependence upon radiation quality and were not

advanced enough to provide a quantitative dosimetry until after 1950. Various fluoroscopic methods of dosimetry were tried, such as the "Fluorometer" of Contremoulins in 1902, and an improved version the "Roentgen Photometer" of Wintz and Rump in 1926. These early fluoroscopic methods never gained much favour, but modern versions are extremely important in practical dosimetry today. A popular photographic method of dosimetry was developed by Kienock in 1905, whereby depth doses were also able to be determined. Another popular dosimeter was introduced in 1915, the "Fuerstenau Intensimeter". The action of this device was based on the change of resistance of a Selenium cell when irradiated, but hysteresis, and other such effects, caused the intensimeter not to be used after about 1930. Each of these early dosimeters was a practical instrument and was not capable of being fundamentally calibrated, but had to be calibrated against some standard system. Since there was no such standard system in the early period, the instruments were calibrated in arbitary units, such as H, K, e, F, etc. Some people used, as a reference, the epilation or erythema dose as a biological unit, where the epilation dose is the quantity of radiation required to cause hair to fall out from the skin and the erythema dose is the quantity of radiation required to produce a reddening of the skin. Thus a certain number of H, K, etc., were specified to express the quantity of radiation that would produce the desired skin reaction. In 1920, the "Unit skin dose", based on observations of skin erythemas, was defined by Seitz and

Wintz; and so for a while, the erythema dose came to be the first standard of dosage. Other biological systems were also suggested as practical dosimeters, such as the "Biological ionization chamber" of WOOD (1929), which consisted of Drosophila (fruit fly) eggs. As has since been verified, the same dose would invariably cause the same percentage of eggs not to hatch. The first attempt at the specification of a tolerance dose was in terms of the erythema dose in 1925 by Mutscheller.

This biological standard of dosage was, however, difficult to realize in practice with any accuracy or consistency. The erythema dose depends upon numerous other factors besides the radiation intensity, for example, size of the irradiated area, dose rate, region of the body exposed, age and race of the individual exposed, training of the observer, etc. Furthermore the biological standard did not avoid the difficulty that doses of different radiations, which are equal in the defining system, may produce unequal reactions in other systems, and consequently a better standard of dosage was required. A grim picture was painted by EWING (1934), when reminiscing over the decades before 1920, "At one period the prescription of (therapy) dose was so uncertain and the results apparently so capricious that all one could really do was to place the patient under the machine and hope for the best". The same problem of units and dosimetry applied to radium therapy where, for many years, the dosage was simply

expressed in terms of milligrams of radium and the exposure time. Some years elapsed before it was realized that γ-ray doses could be specified in the same units as x-rays.

I.2 The Development of Ionization Methods

During the early years a few people were interested in the ionizing effects of radiation; Roentgen, Robb and Perrin had each discussed these effects in 1896, however they were nearly lost sight of as means of dosimetry in the following years. Villard in 1908 was the first to propose a quantitative unit of radiation intensity based on the ionization of air. This proposal was given little consideration at the time, although the unit suggested was essentially that which was finally adopted twenty years later. Szilard, Duane, Friedrich, Christen and others kept the idea alive in the following years. By 1920 the difference in concepts between radiation intensity, or exposure, and the energy absorbed, or dose, was generally realized.

The International Congress of Radiology (ICR) met for the first time in 1925 and in that year established the International Commission on Radiological Units and Measurements (ICRU), which has become the principal organization responsible for selecting and defining radiation quantities and units.

Improvements in ionization chamber techniques, especially the development of sensitive electrometers, led to the unit "roentgen", based on ionization in air, being tentatively accepted by the second ICR in 1928. The definition of the roentgen was built around the practical means of measuring it and measures a property of the radiation at a given point in air. Since the x-ray absorption per unit mass of air and of tissue are very similar over a very wide range of radiation qualities, the use of the roentgen focussed the attention of many workers on the energy absorption in tissues. Gradually the advantages of this unit were appreciated but it took another nine years before it was officially adopted.

Following a better understanding of the significance of secondary electron ranges, "free-air" ionization chambers were being developed with success in the late 1920's. In 1932, Taylor of the US-NBS developed the American standard free-air ionization chamber to determine the roentgen and to intercompare international dosage units. The work was supplemented by such persons as Behnken, Failla, Fricke, Glasser, Holthusen and others, who eliminated discrepencies between their units by consultation and discussion. International agreement was reached in 1932 on the experimental establishment of the roentgen, by means of the free-air ionization chamber. A number of special techniques have since been developed for use with the free-air ionization chamber for specialized applications.

Besides the standard ionization chambers, small practical chambers came into use in the 1920's. These "thimble" chambers were brought into use for the measurement of x-ray doses at points in, or on, "phantoms" which simulate the soft tissue under irradiation. They were, in principle, calibrated against a standard chamber although the need for "air-wall" equivalence was not at first realized and some early chambers were made from aluminium. Such chambers came into general use after Fricke and Glasser developed their thimble chamber with an air-wall in 1925. The thimble chamber was further improved in 1928, by Glasser, Portmann and Seitz, by its attachment to a condenser and a string electrometer. The resulting "condenser" chamber became one of the most versatile methods of radiation measurement and is still in common use today. Other specialized forms of ionization chambers have since been developed, such as the "extrapolation" chamber by Failla in 1937. The proper basis for the design of the cavity type ionization chamber is embodied in the "Bragg-Gray principle" which gives a method for obtaining the dose to the walls of a small gas filled cavity from a knowledge of the ionization measured in the cavity. The principle was developed by GRAY (1929, 1936) and can be stated somewhat simply as follows. The energy dissipated per unit mass of the wall material, E_m, is related to the cavity ionization per unit mass of the gas, J_m, by means of the relation: $E_m = s\ W\ J_m$; where s is the ratio of the mass stopping powers for the material

relative to air, and W is the energy required to produce an ion pair in air. The Bragg-Gray principle has been investigated by many persons since its original formulation and has been greatly generalized to cover many other effects in the cavity gas other than ionization.

Finally, a definition of a standard unit, the roentgen (r), was accepted at the fifth ICR in 1937; thereby recognizing the weight of the preceding twenty years experimental work. The roentgen was defined as "that quantity of x or γ-radiation such that the associated corpuscular emission per 0.001293 gm of air produces, in air, ions carrying 1 esu of quantity of electricity of either sign". The problem of realizing the roentgen is thus resolved into two parts (i) segregating a known mass of air ionized by the beam in question, and (ii) measuring the number of ions produced in that mass of air. In this method of intensity measurement the dependence upon radiation quality is readily controlled and reproduced.

Although the 1937 definition of the roentgen has undergone some slight modifications since its original formulation, ionization methods upon which it is based have served the needs of radiation dosimetry well over the following years, and generally still do today. Ionization methods will most likely remain the basis of practical dosimetry for some years to come, but as

standards they have slowly been shown to have limitations and an alternative system is becoming sufficiently developed to possibly take their place.

I.3 Limitations of the Roentgen and the Emergence of the Rad.

As multimillion volt machines came into use, it was found that increasing difficulties stood in the way of realizing the 1937 definition of the roentgen. In addition to the practical problem that a free-air ionization chamber useful for such high voltages would be required to be of enormous dimensions, there is a further inherent problem due to the fact that the ionization process considered in the 1937 definition is no longer representative of the basic situation which we wish to measure. The former problem can be overcome, to some extent, by using pressurized chambers but the latter problem, due to a basic failure of the principle on which the concept of the roentgen is based, proves insurmountable. Since at high energies, the secondary electrons travel a substantial distance from their point of origin it follows that the flow of high energy x or γ-rays at any point is no longer related clearly and directly to the ionization produced at that point. The roentgen remains useful as long as the penetration of the radiation is much greater than that of the associated electrons, and this is generally true for photon energies up to about 3 MeV.

A source of some confusion with the early definitions of the roentgen was that they did not clearly indicate the particular property of the radiation of which the roentgen was said to be the unit. Another problem that emerged was the need to introduce a new quantity which could be more directly correlated with the local biological and chemical effects of the radiation. It would be expected that, within limits, the effect produced should be proportional to the energy absorbed. Thus, the amount of energy dissipated by the radiation in each portion of the material represents the most obvious and physically sound term of reference for discussing the effects produced by the radiation in that material. An advantage of using such a system is that it matters little whether the energy dissipation stems originally from x-rays or from any other type of ionizing radiation, and hence, it becomes possible to adopt a common basis of dosimetry for all such radiations.

At the sixth ICR in 1950 it was decided that, in general, doses of radiation should be expressed in terms of the energy absorption by the material of interest, at the point in question, namely in erg/gm (Recomm. of I.C.R.U., LONDON, 1950). It was, however, recognized at that time, that the direct measurement of absorbed dose was not usually practical and that, in general, the value would be based on ionization measurements.

By this time it was becoming evident that the absorbed dose, although quite important, was not the only factor concerned in dosimetry; for example, the manner of energy release along the track of the ionizing particle (or linear energy transfer, LET), and other such factors were found to be important. However, these other factors are roughly constant for a given type and energy of radiation and may be summarized by the term "relative biological effectiveness" (RBE).

The outcome of these early considerations and attempts to define essentially an energy unit was the agreement in 1953 to the use of the "rad" as the unit of radiation absorbed dose; where one rad was defined as 100 erg/gm of the absorbing material. Coupled with this was the definition of the "roentgen equivalent man" (rem) as the unit of dose equivalence, combining the rad with an RBE factor, in an endeavour to put the dosimetry of all ionizing radiations on a common basis. The quantity, absorbed dose, had a generality and simplicity which greatly facilitated its acceptance and in not too many years it had become widely used in every branch of radiation dosimetry. The introduction of absorbed dose into medical and biological fields was further assisted by the defining of the rad, since one rad is approximately equal to the absorbed dose delivered when soft tissue is exposed to one roentgen of medium voltage x-radiation.

The ICRU in 1958, set up an Ad Hoc committee whose task was to review the fundamental concepts, quantities and units which are required in radiation dosimetry and, in general, to "tighten standards of rigor". The recommendations of this committee (ICRU Rept. 10a) give the quantities and units currently in use, and for details of these, and the conditions under which they are to be realized, reference should be made to this report.

As a result of the 1958 ICRU report it now appears that we have a fairly well defined and consistent system of quantities and units. The rad is used soley for absorbed dose and the roentgen only for exposure. The ideal unit of dose would be one which would produce the same biological effect independent of the kind and energy of the radiation. Such an ideal is probably unattainable because of the extreme complexity of radiation induced damage in living systems. In practice we employ a physical dose unit which gives nearly the same biological effect independent of the energy of a given kind of radiation. Thus the rad occupies a useful position in modern dosimetry, even though more sophisticated measures of radiation fields, such as LET, have assumed important positions in recent years in the fields of biophysics and radiobiology.

I.4 Standard Chemical Systems

In the past decade or two, numerous other dosimeter systems have been developed, many of which have their foundation in the early period. However, all but certain of the chemical systems are practical dosimeters requiring calibration against a standard. In the majority of the chemical systems the details of the irradiation produced effects in the solutions are poorly understood. The production of radicals to which the sensing element will respond usually has to be determined experimentally and the system calibrated against a standard. The yield of such a system is generally specified in terms of "G" values, i.e. the number of radicals formed per 100 eV of energy absorbed in the medium. The most common and best understood system is the Ferrous Sulphate, or Fricke, dosimeter, which is based on the oxidation of ferrous ions to ferric ions. This system, and also possibly the ceric - cerous system, are capable of being used as fundamental standards of dosage, although their G-values are essentially found by calibration. The original work for the Fricke dosimeter was published by FRICKE and MORSE (1929), but it was only after about 1950 that it was available as a standard. These chemical systems are sensitive to chemical and container purity and other factors, and require care and experience for stable reproducible readings. The use of these systems is generally restricted to special applications where their small size is an advantage and large doses are available.

I.5 The Calorimetric Systems.

Calorimetric systems rely on the principle that the absorbed energy is eventually degraded to heat and hence can be measured in terms of the rise in temperature of the absorbing material. In absorbing materials where no endothermic processes occur, calorimetry is the most basic and direct method of measuring absorbed dose. The most important limiting factor in the early calorimetric dosimeters was for many years the inadequacy of the thermometer systems.

From the beginning, there were people who realized that dose could be specified in terms of absorbed energy and as early as 1910 Duddel proposed a measurement of absorbed dose which anticipated the rad. There were even isolated attempts to measure the amount of energy absorption. Dorn in 1897 used an air thermometer to measure the heat produced by the complete absorption of x-rays in metals. Other investigators have tried different methods and absorbing materials to measure the energy content of an x-ray beam; Rutherford and McCluny (1900), Wien (1905), Bumstead (1906), Adams (1907), Boos (1922), Grebbe (1924), Kulenkampff (1926), Rump (1927) and others. Following the discovery of the rapid and continuous emission of heat from radium, a number of various calorimetric methods were tried for its measurement by such persons as Curie and Dewar (1904), Angstrom (1905), and Schweiller and Hess (1908). RUTHERFORD and ROBINSON (1913) measured the heat

output by means of a twin calorimeter incorporating two platinum resistance thermometers in opposite arms of a Wheatstone bridge. Due to the smallness of the temperature rise, all of these early attempts, and most of those that followed, measured the total energy absorption from the beam, which gave a measure of the intensity of the x-ray beam or radioactive source.

The temperature changes to be measured are generally small relative to those that can be measured accurately by resistance changes, thermoelectric effect, physical expansion of the absorber, etc.. However, since about 1945, a more sensitive temperature detecting element has been available. This was the thermistor, which is a metallic oxide semiconductor having a high negative temperature coefficient of resistance. The introduction of the thermistor came at a very opportune time, when the limitations of the roentgen were being realized, and thus a new era in calorimetry was opened.

This revived activity was, however, mainly restricted to establishments possessing multimillion volt machines. One of the first attempts was by Ham and Trout in 1950. Also in that year, KERST and PRICE (1950) made a calorimetric determination of the output flux of a 320 MeV Betatron, but they preferred to use thermocouples. Further work followed; LAUGHLIN and BEATTIE (1951), LAUGHLIN *et al.* (1953), EDWARDS and KERST (1953), GENNA and

LAUGHLIN (1955), GREENING *et al.* (1968). In the instruments of these workers, the radiation was totally absorbed, usually in heavy metals such as lead or gold, and the energy fluence estimated. Further, many of the early calorimeters required machines with large outputs for their measurements to be of reasonable accuracy. FAILLA (1955), renowned in the field of radiation dosimetry, considered that calorimetry was definitely worthwhile, especially as an aid to improving ionization chamber methods, which he believes calorimeters will probably never replace. In his opinion calorimeters will remain within the domain of standards laboratories.

The measurement of absorbed dose was somewhat more difficult and consequently developed a little more slowly. The successful operation of an absorbed dose calorimeter was originally described by GENNA and LAUGHLIN (1956) who used both copper and polystyrene as absorbing materials. The field was further developed by BERNIER *et al.* (1956), PETREE (1958), REID and JOHNS (1961), PETREE and WARD (1962), BEWLEY (1963), SCHLEIGER and GOLDSTEIN (1964), and others. Many of these systems were measurements of absorbed dose in an isolated mass, not in a segment of an irradiated medium which would closer simulate the situation of biological and clinical interest.

In addition to the measurement of energy fluence and the absolute determination of absorbed dose under specified conditions, comparisons with ionization chambers and certain chemical dosimeters were carried out under identical conditions to those experienced by the calorimeters, and these measurements provided independent determinations of the values of W, and of G for the chemical systems investigated. LAZO, DEWHURST and BURTON (1954) made an estimation of the value of G for the Fricke dosimeter. BERNIER *et al.* (1956) used their calorimeter to estimate W. GOODWIN (1959) determined the value of W by means of a total absorption calorimeter using lead as the absorbing material and Cs^{137} γ-radiation. DAVIES *et al.* (1963) made a comparison of ionization, calorimetric and Fricke dosimetry. ALMOND (1967) used an aluminium calorimeter to determine G for the Fricke dosimeter for 6 to 18 MeV electrons. Occasionally some investigators still prefer to use thermocouples as the temperature sensors, such as FLEMING (1970).

It is important to note that each of the calorimeters developed so far is different, not only in details, but in some cases quite different thermodynamic principles are used. No single design of a calorimeter to realize the rad has yet been universally adopted and the field is still open to new developments. The instrument that has been developed, and which will now be described, has been designed with a specific purpose, namely to

suit the needs for standard dosimetry in the Radiotherapy Department of the Royal Adelaide Hospital.

CHAPTER II CALORIMETER DESIGN AND PROPERTIES

In this chapter the design of the calorimeter is described in some detail, giving reasons for the choices made. A number of theoretical factors are discussed which give an insight into the behaviour of the calorimeter under irradiation.

II.1 Calorimeter Materials

II.1.1 Calorimeter Absorber Material.

In radiotherapy the dose received in such materials as muscle tissue, bone and other various types of organ tissues is required. Ideally the calorimeter should be constructed from such materials, but in practice this is not possible, since they have poor mechanical, electrical and thermal properties as well as being generally nonhomogeneous. It should be remembered that in applying calorimetric methods to dose measurements, that it is assumed that all of the absorbed energy from the radiation is eventually degraded to heat. There are however some possible physical and chemical endothermic processes which may occur, such as increases in the rest masses of nuclei, crystal lattice displacements, changes in interatomic bond energies, excitation or ionization of electrons used in covalent bonds with a possible resultant change in molecular structure (especially in the more complex organic molecules), etc.. The latter effect is obviously

the basis of radiotherapy. All of these endothermic processes are, in practice, only a small fraction of the energy that is eventually degraded to heat within the material. In the most extreme cases it is of the order of a percent. MILVY *et al.* (1958) estimated that tissue-equivalent plastic under irradiation from Co^{60} γ-radiation had a thermal defect (the percentage of the absorbed energy not degraded to heat) of 2.3%. FLEMING and GLASS (1969) irradiated a Shonka-type tissue-equivalent plastic (which is mainly polyethylene) with 1.7 MeV protons and found that the initial thermal defect was 4.2% which decreased with absorbed dose to a saturation value of 3.7%. It is expected that these values would be somewhat less for radiation of lower LET value.

Graphite was chosen as the absorbing material since, as it is composed of a single element, it does not undergo any chemical endothermic effects when irradiated and the possible physical effects are negligible. Further, graphite has reasonable electrical and thermal properties and, with care, can be machined. The atomic number of carbon is 6, which is close to that for tissue materials. The effective atomic number of tissues depends upon the effect considered. In the present case, where photon energies greater than 1 MeV are considered, then the photoelectric effect is negligible. Compton scattering, which predominates at the lower energies in this range, is nearly independent of atomic

number, while pair production, which becomes important at higher photon energies, varies linearly with atomic number. The effective atomic numbers ($\overline{Z}$) for pair production of tissue materials are given by SPIERS (1956) and are shown in Table II.1.

Table II.1

Effective atomic numbers ($\overline{Z}$) for pair production of tissue material.

material	$\overline{Z}$
air	7.4
water	6.6
muscle	6.6
subcutaneous fat	5.2
bone	10.0

Thus, as far as radiation absorption is concerned, graphite is closely tissue-equivalent for energies > 1 MeV.

The graphite used in the construction of the present calorimeter was grade AGSR, which has a maximum grain size of 0.015 inch, uses a graphite type binder and gives a 0.11% ash. The ash consists mainly of sulphur and small amounts of iron and aluminium, with traces of other elements. As will soon be shown, these percentage impurities are trivial compared with those added during the construction of the calorimeter. The density of the graphite (ρ) was experimentally determined to be:

$$\rho = (1.60 \pm 0.005)\ gm/cm^3.$$

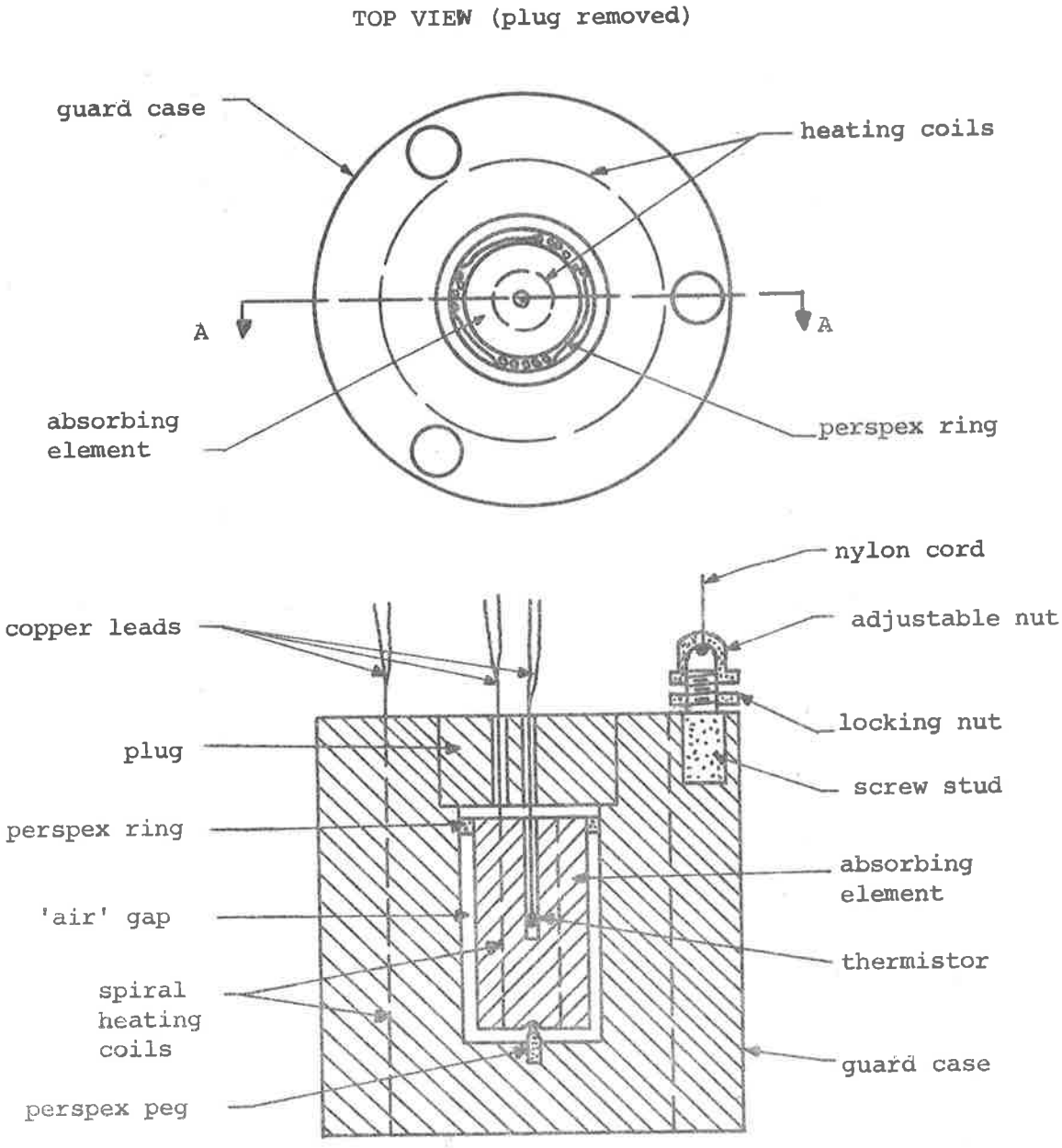

Fig.II.1 Internal Structure of Calorimeter.

II.1.2 Calorimeter Design.

The internal structure of the calorimeter is shown in Figure II.1. There were a number of factors considered during the design of the calorimeter element - the mass in which the absorbed dose is to be measured. The element had to be an elementary mass such that further reduction in size did not significantly change the value of the dose measured, while at the same time it had to be large enough to avoid statistical considerations. The calorimeter parts generally had to be fairly homogeneous so as to not significantly perturb the radiation field within the material in so far as the energy absorption within the absorbing material was concerned. Foreign materials such as 'Perspex' (methyl methacrylate plastic), 'Araldite' (epoxy resin), wire, etc., must not significantly effect the energy absorbed. This limitation is small in practice, except for low energy photons where the photoelectric effect predominates.

The absorbing element contains a thermistor for temperature measurement (refer II.3) and a spiral heating coil for calibration purposes (refer II.4). The element is totally surrounded by, but thermally insulated from, a massive guard case. The mass of this case is approximately 96% of the total mass of the calorimeter. The case, which also contains a spiral heating coil, simulates the effect of bulk tissue around the mass in which the dose is being

measured, while at the same time providing a thermal baffle for the element. The case also ensures that radiation equilibrium exists for photon energies up to about 12 MeV, but at the same time may produce excess attenuation at energies below 1 MeV.

The element was thermally insulated from the case by means of an 'air' gap of 2 mm and perspex supports. The gap was sufficiently small so that the radiation field was not significantly perturbed. BEWLEY (1963) estimated that the perturbation effect upon a beam due to a 2 mm gap in graphite is less than 0.1%.

The complete calorimeter was suspended within a vacuum chamber by means of three nylon cords attached to adjustable height screws on the case. A similar calorimeter, without the heating coils, was also constructed and was used as a reference calorimeter in the differential temperature measurement approach employed (refer II.3).

II.1.3 Masses and Heat Capacities of Calorimeter Components.

A knowledge of the mass of the element of the test calorimeter was required to give measurements in terms of absorbed dose. Further, the masses of all the other parts of both the test and reference calorimeters were measured so that it could be shown that the two calorimeters were reasonably identical and that the percentage of non-graphite materials in both was small.

The heat capacities of the case and element of both were also able to be calculated. The mass of each component was accurately measured on a Sauter balance during assembly, the results being tabulated in Appendix I. It should be noted that the masses of the elements of both the test and reference calorimeters were altered during the course of the work. The perspex ring of each was originally solid and both their mass and thermal conductance was considered excessive. The mass of the ring was originally 3.0% of the mass of the element and was subsequently reduced to 2.0% by drilling many small holes within the ring. A further modification was made to the calorimeters at the same time (refer II.4.3). From Appendix I we have: Test calorimeter I, mass of element (m_e) = (9.289 ± 0.005) gm, which is 3.55% of the total mass of the calorimeter. The composition of the element is 96.02% graphite, 3.89% 'organic' (low Z) and 0.09% 'metallic' (high Z). The heat capacity of the element (H_e) = 1.620 cal/^{o}C. For Test calorimeter II, mass of element (m_e) = (9.228 ± 0.005) gm. The composition is closely the same as in I, and its heat capacity (H_e) = 1.589 cal/^{o}C.

The specific heat values (c) for the various materials used in the calorimeter were obtained from various handbooks and in some cases estimates were made from the available information. It should be noted that, except for graphite and perspex, the other values need be only approximate since they contribute

little to the overall heat capacities. From Appendix I it can be seen that the case and element of both the test and reference calorimeters are nearly identical in mass, heat capacity and composition. It can now be seen that the original impurities in the graphite are insignificant compared with those added during assembly. The impurities have been broadly classified as 'organic' and 'metallic'. The 'organic' impurity is mainly perspex and may suffer from some endothermic reactions. If the thermal defect of the 'organic' impurity is of the order of 1% then the energy lost by this effect is less than 0.1%, since it constitutes less than 4% of the mass of the element. The effective atomic number for perspex for pair production is about 6.2 and hence does not disturb the tissue-equivalence of the system. The effect of the 'metallic' impurity is to increase the effective atomic number of the calorimeter and thus increase the amount of energy absorbed. However, the amount of this impurity is so small that the increase in the dose rate is insignificant.

Consequently, the measurement of absorbed dose with the calorimeter will simulate the absorption of radiation energy in a small segment of a large "tissue-equivalent" material.

II.2 Thermodynamic Considerations.

II.2.1 Possible Approaches.

As in any calorimetry, there are three basic thermodynamic approaches that may be considered: (i) Isothermal, where the outside

wall of the calorimeter is kept at a constant temperature. As would be expected the heat losses for such a system are great, possibly as high as 5 to 10%, unless special precuations are taken, such as using an ultra high vacuum ($<10^{-5}$torr), reducing heat transfer by radiation, using thermal baffles, etc.. (ii) Adiabatic, where the outside wall temperature is continuously, and usually automatically, adjusted to remain at the same temperature as the calorimeter element. This lowers heat losses but does not allow for their evaluation and possible correction. (iii) Quasiadiabatic, where a guard case is placed around the element and is of the same material as the element. Both element and case are exposed to the radiation to the same extent and hence their temperature rises are closely equal. Heat losses from the element are low, although possibly not as low as in the adiabatic system, however the losses can now be evaluated and the final result corrected for the effect of cooling. A disadvantage of this method compared with the others, is that the results must now be taken in a graphical form, from which the cooling corrections are obtained.

In the present work the quasiadiabatic approach was employed, since it is basically simple and the case also serves the other functions previously mentioned (refer II.1.2).

II.2.2 Thermal Insulation.

Heat losses from the element are further reduced by enclosing the calorimeters within a vacuum system and operating at reduced pressure. The design of the vacuum system is very simple. Two vacuum chambers are used, one to contain the test calorimeter and the other to contain the reference calorimeter. A suitable vacuum is attained with only a two stage rotary pump, giving an ultimate pressure of 5×10^{-3} torr after a 3 hour pumping time. Most previous authors have used pressures of the order of 10^{-5} torr in an endeavour to completely remove heat losses by conduction through the air. However, below 10^{-3} torr, there is little discernible decrease in the thermal conductivity of the air and losses by thermal radiation become the most significant form of heat loss. Unless special care is taken to minimize thermal heat losses then using a pressure below 10^{-3} torr is of little benefit. The vacuum chamber walls are chrome plated on the interior, although not polished. The vacuum chambers are constructed from ½ inch brass and are thermally coupled to give a large heat capacity. This is, to some extent, an advantage but also produces a somewhat large attenuation (about 40%) of the radiation beam and consequently limits the minimum dose rate that can be measured with accuracy. The chambers used in this work were readily available at the time, but, in the future, chambers of overall smaller size may be employed, possibly with wall thicknesses about ¼ inch.

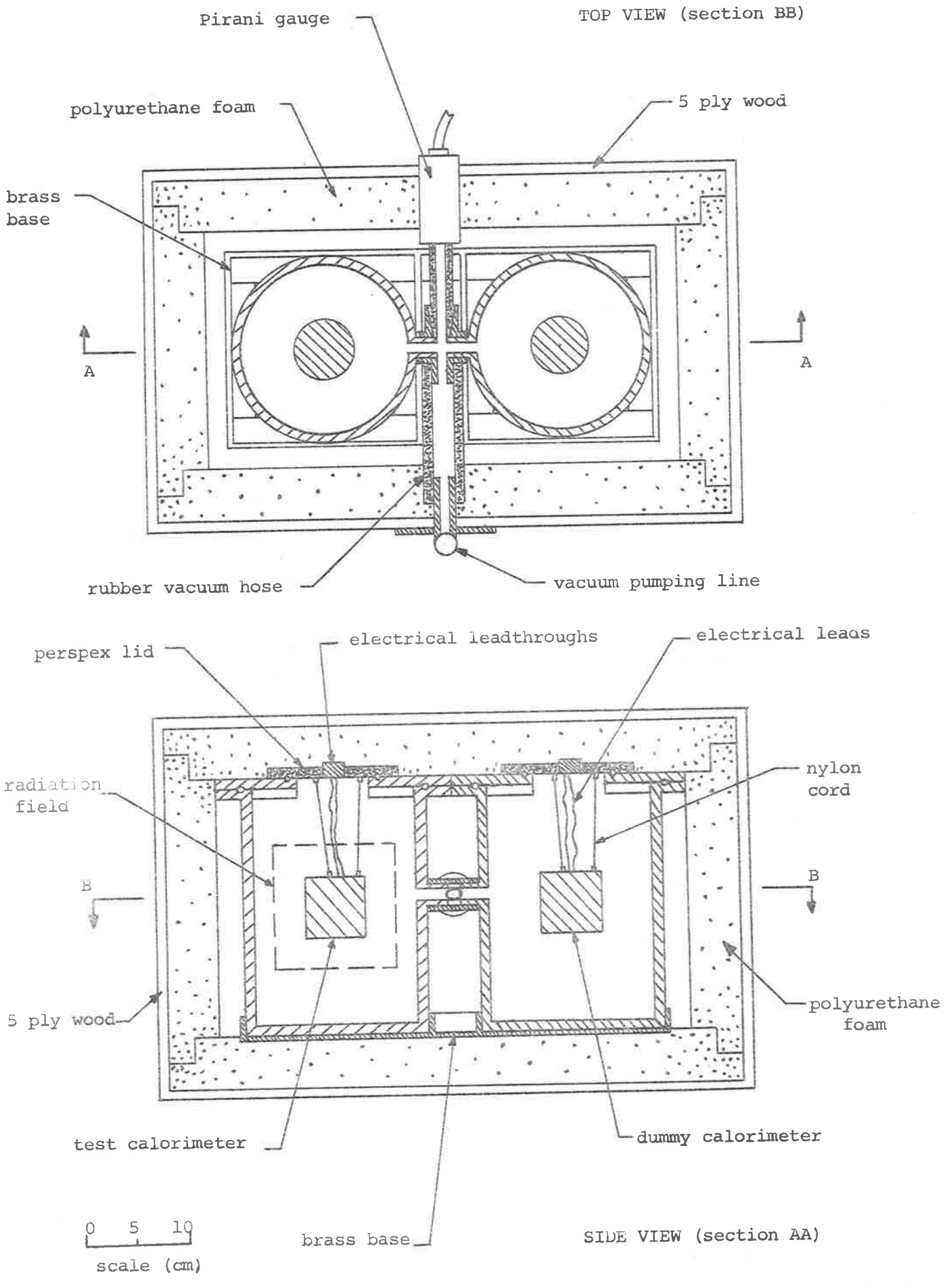
TOP VIEW (section BB)
Pirani gauge
polyurethane foam
5 ply wood
brass
base
A
A
rubber vacuum hose
vacuum pumping line
perspex lid
electrical leadthroughs
electrical leads
radiation
field
nylon
cord
B
B
5 ply wood
polyurethane
foam
test calorimeter
dummy calorimeter
0 5 10
scale (cm)
brass base
SIDE VIEW (section AA)

The present system, however, proved suitable for the dose rates encountered during the course of the work described. At least one previous author dispensed with the need for using a vacuum at all. GOODWIN (1959) used Santocell foam insulation which he considered gave as good a result with the advantage of producing a more compact and rigid system.

The vacuum chambers were further thermally insulated and housed in a box constructed of 5-ply wood and lined with a 2 inch layer of polyurethane foam, as shown in Figure II.2. This equipment was mounted on a metal carriage and was quite portable enabling it to be moved from room to room. Both the vacuum chambers and the carriage were earthed to ground potential. Correct alignment with the radiation machines was achieved by means of markers on the outside of the wooden box, which were determined geometrically and checked radiographically with the test calorimeter in position.

II.2.3 Estimation of Thermal Constants for the Calorimeter.

It is expected, from the previous section, that any changes occuring in the ambient room temperature will be much reduced by the time the effect reaches the calorimeter elements. To investigate this effect it was necessary to have at least an estimate of the thermal constants of the calorimeter. The heat capacities (H) have already been considered in section II.1.3.

The specific heat of graphite (c) varies from 0.160 cal/gm ^{o}C at 20^{o}C to 0.170 cal/gm ^{o}C at 25^{o}C, that is, a variation of about 1.1%/^{o}C. In all calculations a value of 0.165 cal/gm ^{o}C has been used since it corresponds to a typical temperature (~22.5^{o}C) encountered during the course of this work. It is possible to define a temperature sensitivity of the calorimeter element given by, $dT/dE = 1/m_e c = 0.654$ ^{o}C/cal.

For small temperature differences $(T - T_o)$ it is well known that the heat transfer rate (dE/dt) can be represented by equation (II.1).

$$\frac{1}{A}\frac{dE}{dt} = -h(T - T_o) \qquad \ldots\ldots \text{(II.1)}$$

where A is the cross-sectional area and h is the total thermal transfer coefficient for all of the modes of heat transfer involved. The product (Ah) = K is referred to as the total thermal 'conductance' for the given system, keeping in mind that other forms of heat transfer besides conduction may be involved. To determine the value of the thermal conductance for the present system it was convenient to divide the calorimeter into two separate regions as shown in Figure II.3. The first region is for heat transfer between the vacuum chamber and the calorimeter case, which gives the value K_1, and the second region is for heat transfer between the case and the element, which gives the value K_2. The detailed calculations are shown in Appendix 2 and the final results are:

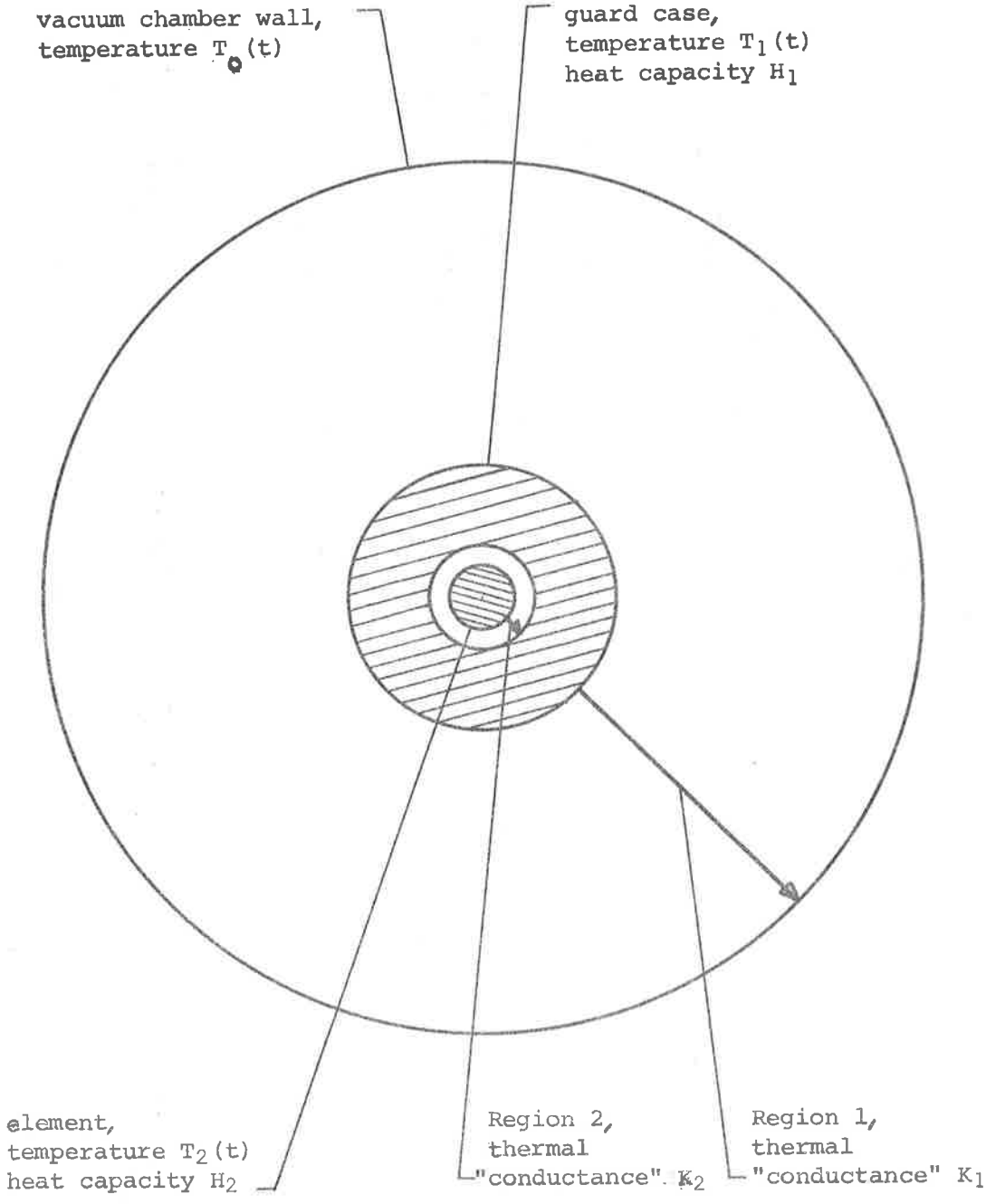

Fig.II.3 Regions of Heat Transfer.

$$K_1 = 2.04 \times 10^{-2} \quad \text{cal/sec}^{\circ}\text{C}$$

$$K_2 = 0.244 \times 10^{-2} \quad \text{cal/sec}^{\circ}\text{C}$$

Define the constant ξ, the reciprocal of thermal time constant, by:

$$\xi \equiv \frac{K}{H} \text{ sec}^{-1}$$

Thus, for the case we have $\xi_1 = 4.785 \times 10^{-4}$ sec^{-1}

and, for the element we have $\xi_2 = 15.36 \times 10^{-4}$ sec^{-1}

Also define $\xi_{21} \equiv \frac{K_2}{H_1} = 0.572 \times 10^{-4}$ sec^{-1}

Note that ξ_{21} is about 2.8% of the value of $(\xi_1 + \xi_2)$, thus

$\xi_{21} << (\xi_1 + \xi_2)$ is valid.

Owing to the similar design, masses and heat capacity values, etc., of the test and reference calorimeters it is assumed that these values of ξ are closely similar for both calorimeters.

The thermal conductivity (k) of the graphite was estimated by a thermal comparator method and was found to be $k \simeq 0.3$ cal cm/cm^{2}sec$^{\circ}$C, thus giving an estimate of the thermal diffusivity (α) of the graphite.

$$\alpha = \frac{k}{c\rho} \simeq 1.0 \text{ cm}^2/\text{sec}$$

This relatively high thermal diffusivity ensures that no large temperature differences are set up within the bulk of the calorimeter.

II.2.4 Effect of an External Temperature Change upon the Calorimeter Element.

In the following analysis it will be shown how a temperature change of the vacuum chamber wall affects the

temperature of the calorimeter element. Due to the high thermal diffusivity of the graphite it is assumed that the temperatures across both the case and element cross-sections are uniform. This assumption is verified in section II.4.8. Consider the system shown in Figure II.3 In the following derivation we are only interested in the variations of temperature with respect to the ambient temperature. Thus, $T_o(t)$, $T_1(t)$ and $T_2(t)$ are the variations in temperature with respect to the ambient temperature, and further, we have that $T_o(0) = T_1(0) = T_2(0) = 0$. Applying the law of conservation of energy to each region of heat transfer gives the following equations:

$$K_1\int_o^t\{T_o(t) - T_1(t)\}dt = H_1T_1(t) + K_2\int_o^t\{T_1(t) - T_2(t)\}dt \quad ...(II.2a)$$

and $$K_2\int_o^t\{T_1(t) - T_2(t)\}dt = H_2T_2(t) \quad ...(II.2b)$$

Applying Laplace Transforms gives, after some rearrangement,

$$\xi_1 L\{T_o(t) - T_1(t)\} = pL\{T_1(t)\} + \xi_{21}L\{T_1(t) - T_2(t)\} \quad ...(II.3a)$$

and $$\xi_2 L\{T_1(t) - T_2(t)\} = pL\{T_2(t)\} \quad ...(II.3b)$$

Now assume that the temperature variation on the vacuum chamber wall is of the form of a rectangular pulse, of height $T_o\,^oC$ and width a secs..

That is, assume $$T_o(t) = T_o\{H(t) - H(t - a)\} \quad ...(II.4a)$$

where H(t) is the Unit Step Function.

Applying Laplace Transforms to equation (II.4a) gives:

$$L\{T_o(t)\} = \frac{T_o}{p}\left(1 - e^{-ap}\right) \quad ...(II.4b)$$

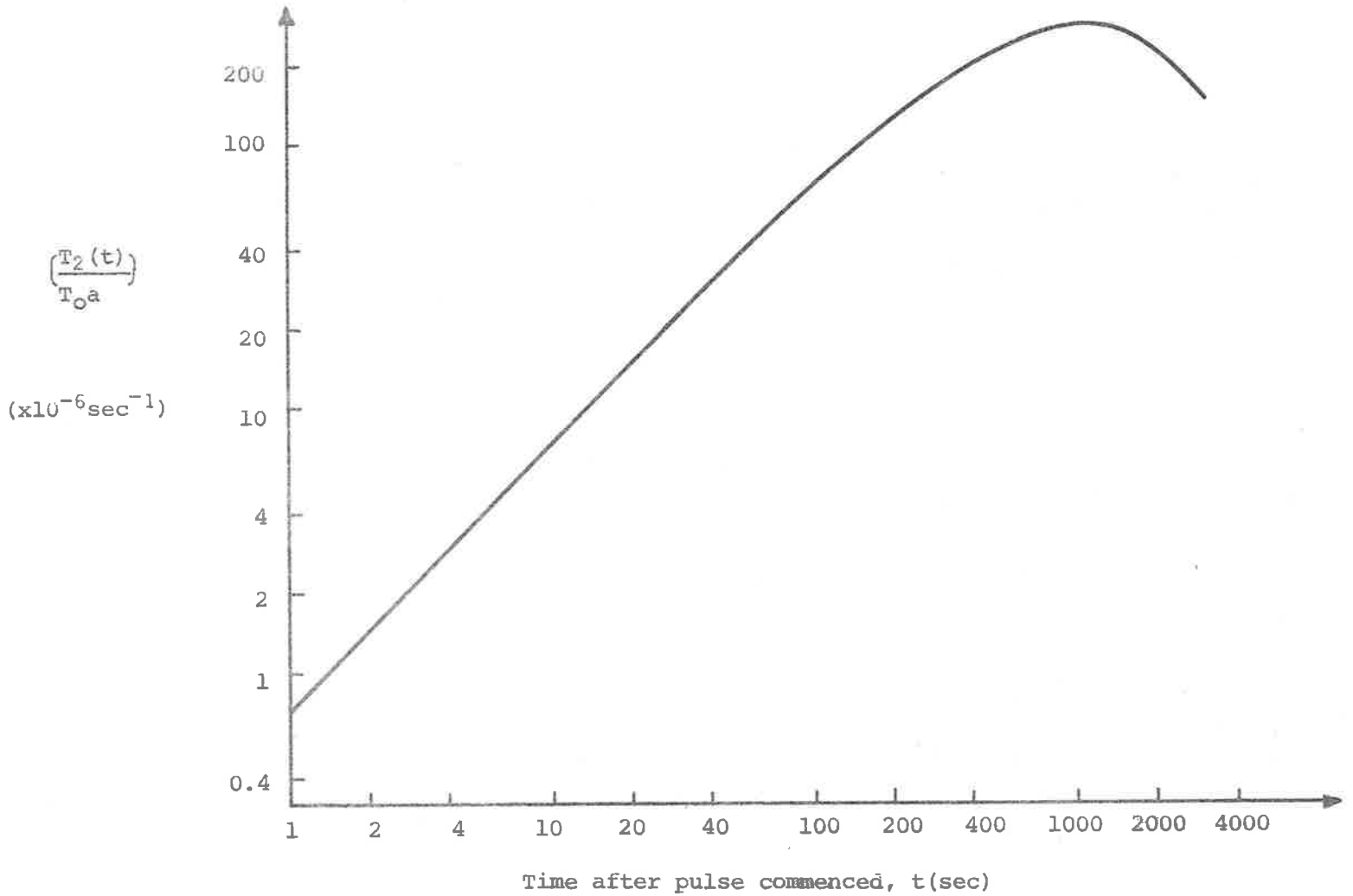

Fig.II.4 Effect on the Temperature of the Element, $T_2(t)$, due to a Temperature Variation of the Vacuum Chamber Wall in the Form of a Rectangular Pulse of Height $T_o{}^{\circ}C$ and Width a sec, as a Function of Time After the Pulse Commenced.

Solving equations (II.3a), (II.3b) and (II.4b) simultaneously, and making use of the approximation $\xi_{21} << (\xi_1 + \xi_2)$, gives the following solution for $T_2(t)$:

$$T_2(t) = T_o\left(1 - \left(\frac{\xi_2}{\xi_2-\xi_1}\right)e^{-\xi_1 t} + \left(\frac{\xi_1}{\xi_2-\xi_1}\right)e^{-\xi_2 t}\right)$$
$$-T_o H(t-a)\left(1-\left(\frac{\xi_2}{\xi_2-\xi_1}\right)e^{-\xi_1(t-a)}+\left(\frac{\xi_1}{\xi_2-\xi_1}\right)e^{-\xi_2(t-a)}\right) \quad \ldots(II.5)$$

Consider the special case when a is short, such that $\xi_2 a << 1$, and consider times $t > a$, then equation (II.5) is simplified to:

$$T_2(t) = T_o a\left(\frac{\xi_1\xi_2}{\xi_2-\xi_1}\right)\left(e^{-\xi_1 t}-e^{-\xi_2 t}\right) \quad \ldots(II.6)$$

Equation (II.6) is shown graphically in Figure II.4. It can be seen that the original pulse is smoothed in the process of reaching the element, with a maximum temperature occuring in the element at a time t_{max} after the pulse starts on the wall, where t_{max} is given by:

$$t_{max} = \left(\frac{\ell n \xi_2 - \ell n \xi_1}{\xi_2 - \xi_1}\right)$$

In the present calorimeter the maximum temperature rise of the element is $T_2(max) = 3 \times 10^{-4}(T_o a)\,^{o}C$ about 18.4 minutes after the pulse commenced. For example, consider a pulse with $T_o = 0.1^{o}C$ and $a = 0.1$ sec., then the effect of this pulse is to increase the temperature of the element by $7 \times 10^{-8}\,^{o}C$ after 10 secs., $7 \times 10^{-7}\,^{o}C$ after 100 secs and a maximum of $3 \times 10^{-6}\,^{o}C$ after about 18.4 minutes. It will be shown that this temperature rise of the element is not detectable by the temperature measuring system, even though the original pulse is much larger than would be expected ever to occur.

Thus, the thermal properties of the system, as far as external disturbances are concerned, are quite satisfactory. It has yet to be shown that the losses from the element, under normal use, are within tolerable limits (refer II.5).

II.3 Temperature Measurement System.

II.3.1 Temperature Sensors.

The expected temperature rise for a dose of one rad in the calorimeter element is of the order of only 10^{-5}°C, and the only two devices which have sufficient sensitivity to detect such temperature changes are the thermocouple and the thermistor. The thermocouple has the advantage of not introducing power into the system, by self-heating; but on the other hand it requires many junctions to attain an acceptable sensitivity, which in turn increases both the amount of impurity in the element and the heat losses from the element. Thermocouples are still occasionally used, but since thermistors have a greater sensitivity per unit mass, they are now preferred in this field.

The variation of resistance ($R_T\Omega$) of a thermistor with temperature ($T^{\circ}K$) is given by an equation of the form:

$$R_T = R_\infty e^{B/T} \qquad \ldots(II.7)$$

where $B(^{\circ}K)$ and $R_\infty(\Omega)$ are constants depending on the given type of thermistor. The thermistors employed in this work are STC type M15, having nominal resistance values of 100kΩ at 20°C and 79.5kΩ at 25°C,

or alternatively having B = 4050°K and R_∞ = 0.0995Ω. The thermistors were purchased as a matched pair (within 1%) which helps to overcome the problems of changes in ambient temperature, thermistor self-heating, etc.. LAUGHLIN and GENNA (1956) have shown that if the effect of mismatch of the thermistors is to be negligible (<0.1%) then they must be matched to within 1%. The temperature sensitivity of the thermistors (β) is readily obtained from equation (II.7).

$$\beta = \frac{\partial R_T}{\partial T} / R_T = -B/T^2 \qquad \ldots(II.8)$$

The value of B for the thermistors used in this work were experimentally determined and found to be B = 4079°K (0.7% from the nominal value). Thus, the sensitivity of these thermistors is 4.69%/°C at 22°C. The temperature variation of thermistor sensitivity is obtained from equation (II.8).

$$\frac{\partial \beta}{\partial T} = 2B/T^3 \qquad \ldots(II.9)$$

In the present case we have a value of 0.03%/°C^2 at 22°C, or alternatively a change of 0.6%/°C in the above value of β. Thus the variation of the thermistor sensitivity with temperature is quite small, and for the temperature ranges encountered during a normal measurement (<10^{-2}°C) the value of β can be considered constant to a very good approximation.

The M15 thermistor is a bead type encased in glass with a copper disc backing which can be simply prised off without harm to the thermistor. The resulting thermistor has a diameter of about 2 mm. The thermistor leads were insulated with varnish and the

thermistors firmly embedded, with a mixture of silicone grease and powdered graphite, into the holes provided in the respective calorimeter elements.

II.3.2 Temperature Measuring Circuit.

There are two possible techniques which may be used. A single calorimeter may be employed where it is endeavoured to determine accurately the energy absorbed by measuring the temperature rise of the element and correcting for energy losses, thermistor self-heating, etc.. Such an approach is usually coupled with the isothermal system, with the calorimeter surrounded by a temperature controlled bath. The other technique is to use two nearly identical calorimeters in similar environments, where only one of the calorimeters is irradiated and the other is a reference. In this differential system we do not have to correct for thermistor self-heating, changes in ambient temperature, etc..

The differential approach is used in this work, with the thermistors included in opposite arms of a D.C. Wheatstone bridge, as shown in Figure II.5. The fixed resistance arms, R_1' and R_2, are 0.1MΩ (nominal) steps on a "Yew" 1MΩ precision resistance box type WMT. The variable resistance, δR, is a "Pye" decade resistance box with a maximum resistance of 11,110Ω in steps of 1Ω, with a precision of ±0.1%. The bridge is excited by either, 1, 2 or 3 Hg cells as desired, each with a nominal voltage of

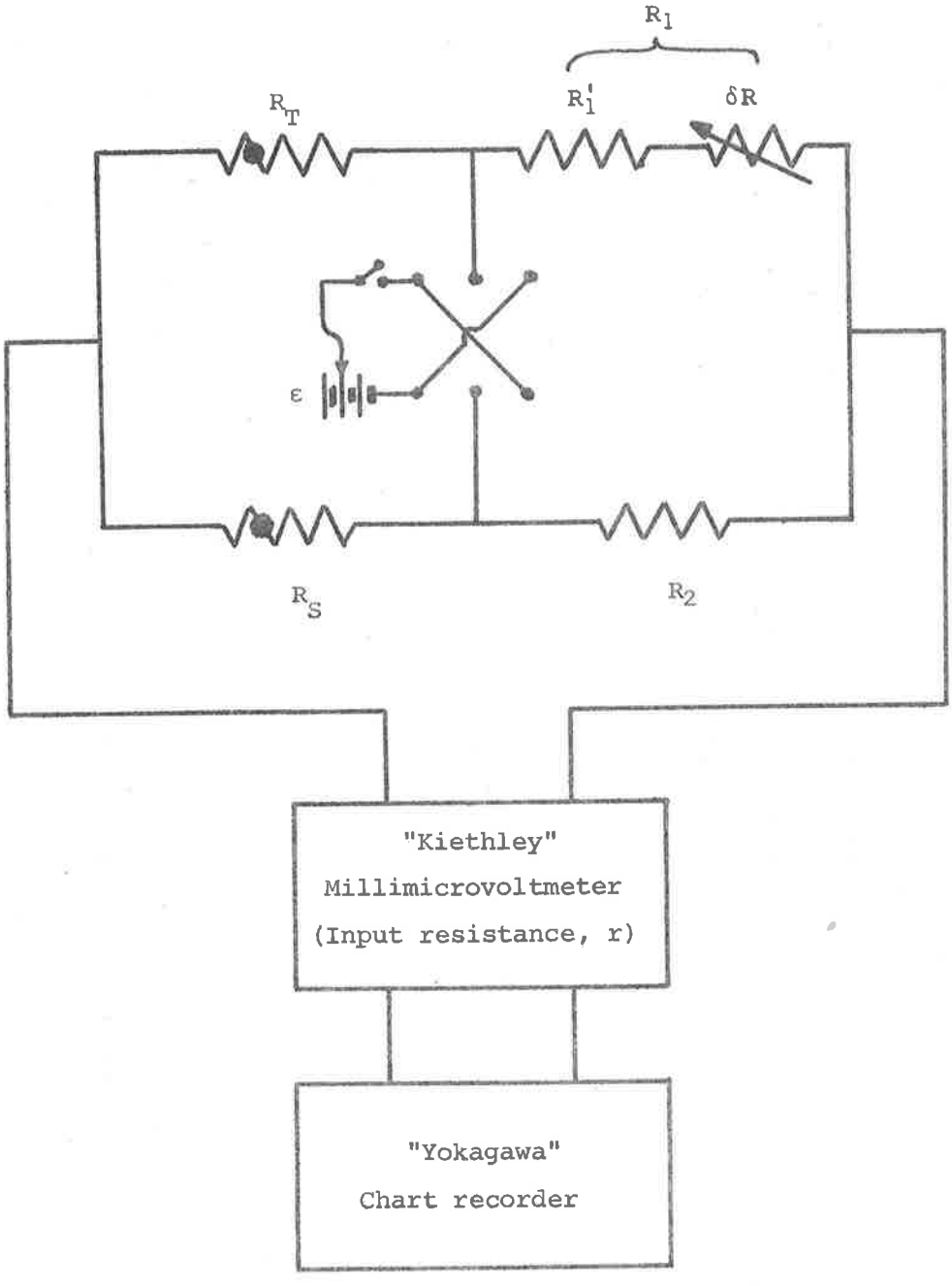

Fig.II.5 Temperature Measuring Circuit.

1.35 volts. The polarity of the potential can be reversed during measurements to allow for correction of any thermoelectric effects present in the bridge. The output of the bridge is detected by a "Keithley" millimicrovoltmeter type 149 which is supplied from the mains through a constant voltage transformer. One side of the bridge is earthed through the output of the millimicrovoltmeter. The meter has a nominal input resistance of 10MΩ for the range used. The output of the meter is passed through a potential drop network to a "Yokagawa" multichannel chart recorder, which gives a print out at 5 second intervals. The Hg cells, switches and resistive components of the bridge are housed in a thermally and electrically shielded box, which is at earth potential. The calorimeters are connected to the remainder of the bridge by means of a 12-core non-microphonic cable. Care has been taken to shield the circuit from external noise, but the limit of the bridge sensitivity is set by the thermal noise of the thermistors and connecting cable. Although the thermistors have a high temperature sensitivity, unfortunately, they also have a high noise factor due to their complex chemical composition. The measured noise, with the thermistors shorted out of the bridge by fixed 0.1MΩ resistors contained in the shielded box, was about ±0.5μV, which is close to the value expected from the Johnson noise equation using a frequency bandwidth of 100 c/s. The noise with the thermistors in the bridge was measured to be about ±3μV.

II.3.3 Bridge Potential and Thermistor Self-Heating.

There is not great freedom in the choice of the bridge potential. On the one hand an attempt should be made to use as large a potential as possible, since the bridge sensitivity is directly proportional to this potential (refer II.3.4). On the other hand the thermistor self-heating increases with the square of the bridge potential. The thermistor self-heating introduces a number of considerations. (i) The time taken for the system to reach thermal equilibrium after being turned on. It was found that with 1 Hg cell the system took ¼ hour to reach usable equilibrium, while with 2 and 3 cells it took 1 and 2 hours respectively. (ii) The temperature difference between the thermistor and the element must remain essentially constant so that an increase in the temperature of the element will produce an equal temperature rise in the thermistor. LAUGHLIN and GENNA (1956) have derived a relationship which gives the maximum bridge potential that can be used for the disturbance, due to a change in power dissipation in the thermistor, to be less than 0.1% of the change in temperature that is to be measured. The condition is:

$$\varepsilon^2_{max} < (16.8 \times 10^{-3})\frac{R_T K_T}{\beta} \qquad \ldots(II.10)$$

where ε_{max} is the maximum permissible bridge potential, K_T is the thermal conductance for heat transfer between the thermistor bead and the element, and R_T and β are the resistance and the temperature sensitivity of the thermistor, respectively.

The value of ϵ_{max} was estimated by two methods. (a) From the dimensions of the thermistor, and assuming the thermistor glass had a thermal conductivity of 2×10^{-3}cal cm/cm^{2}sec^{o}C. This gave a value of $K_T \simeq 0.03$ cal/sec^{o}C, which in turn gave the maximum permissible voltage as approximately 30 volts. (b) From the graph output, assuming that the observed time delay was due to the thermal barrier around the thermistor. A time delay of the order of 5 seconds was observed, which corresponded to a temperature difference of about 12×10^{-5}^{o}C for a power dissipation of about 13×10^{-6} cal/sec.. These gave a value of $K_T \simeq 0.1$ cal/sec^{o}C, which in turn gave the maximum permissible voltage as approximately 55 volts. Owing to the irregular geometry involved the first estimate was difficult and the value of the maximum permissible voltage obtained was considered a minimum. The second estimate was also difficult since the observed time delay may not have been due entirely to the thermal barrier, and the value of voltage obtained by this method was considered a maximum. However, in practice, the bridge potential used was lower than either of the above two maximum permissible values. (iii) The power dissipation in the thermistor, due to self-heating, should be a reasonably low value compared with the radiation power being measured. Since the differential system was employed this was not a critical consideration. The order of magnitude of the radiation dose rate was 40 rad/min $\equiv 6.2 \times 10^{-5}$ joule/sec.. One Hg cell produced a thermistor self-heating rate

of 7% of the radiation dose rate, while 2 and 3 Hg cells produced 30% and 66% of the radiation dose rate, respectively.

The question of thermal equilibrium was considered in some detail. The temperature of the thermistor, and the element, increases until it reaches such a value that the rate of energy loss from the element equals the rate of energy dissipation by the thermistor. If the thermistors and calorimeters were perfectly matched then the transient temperature variations would occur equally in both and hence the effect of the transients would not be observed in the output of the bridge. Such an ideal is virtually impossible to attain in practice, thus the output of the bridge will vary somewhat until both thermistors reach their own equilibrium temperatures in their own times. It is of interest to see how the calorimeter temperature varies with time, both for the element and for the case. Since the thermal transfer constants are not accurately known it is not possible to distinguish between the test or the reference calorimeters. The following analysis applies to a system containing a single calorimeter and, as such, shows the maximum times that are required for the system to come to equilibrium.

As was done in section II.2.4, assume that the temperature distributions over the graphite sections are uniform and that the temperatures $T_1(t)$ and $T_2(t)$ are with respect to the ambient

temperature. Let the rate of power dissipation due to thermistor self-heating be P_2 cal/sec, which can be considered a constant to a good approximation. Using the same notation as in Figure II.3 and applying the law of conservation of energy to each region of heat transfer, gives the following equations:

$$P_2 t = \xi_2 T_2(t) + K_2 \int_o^t \{T_2(t) - T_1(t)\} dt \qquad \ldots(II.11a)$$

$$K_2 \int_o^t \{T_2(t) - T_1(t)\} dt = \xi_1 T_1(t) + K_1 \int_o^t T_1(t) dt \qquad \ldots(II.11b)$$

Equations (II.11a) and (II.11b) are readily solved using Laplace Transforms, together with the approximation that $\xi_{21} << (\xi_1 + \xi_2)$, to give:

$$T_1(t) = \frac{P_2}{K_1}\left(1 - \left(\frac{\xi_2}{\xi_2 - \xi_1}\right)e^{-\xi_1 t} + \left(\frac{\xi_1}{\xi_2 - \xi_1}\right)e^{-\xi_2 t}\right) \qquad \ldots(II.12a)$$

and

$$T_2(t) = P_2\left(\frac{1}{K_1} + \frac{1}{K_2}\right)\left(1 - Ae^{-\xi_1 t} - Be^{-\xi_2 t}\right) \qquad \ldots(II.12b)$$

where $$A = \frac{\xi_{21}\xi_2}{(\xi_2 - \xi_1)(\xi_{21} + \xi_1)}$$

and $$B = \left(\frac{\xi_1}{\xi_{21} + \xi_1}\right)\left(1 - \frac{\xi_{21}}{\xi_2 - \xi_1}\right)$$

Define the functions $F_1(t)$ and $F_2(t)$ by the relationships:

$$T_1(t) = \left(\frac{P_2}{K_1}\right)F_1(t) = T_1(\infty)F_1(t)$$

$$T_2(t) = P_2\left(\frac{1}{K_1} + \frac{1}{K_2}\right)F_2(t) = T_2(\infty)F_2(t)$$

The functions $F_1(t)$ and $F_2(t)$, which show the relative increases in temperature with time of the case and element respectively, are shown graphically in Figure II.6 for the present calorimeter with $A = 0.155$ and $B = 0.845$. For the case when 2 Hg cells are used, $P_2 = 4.8 \times 10^{-6}$ cal/sec, then the final equilibrium temperatures are, for the element, $T_2(\infty) = 22 \times 10^{-4}$ °C and for

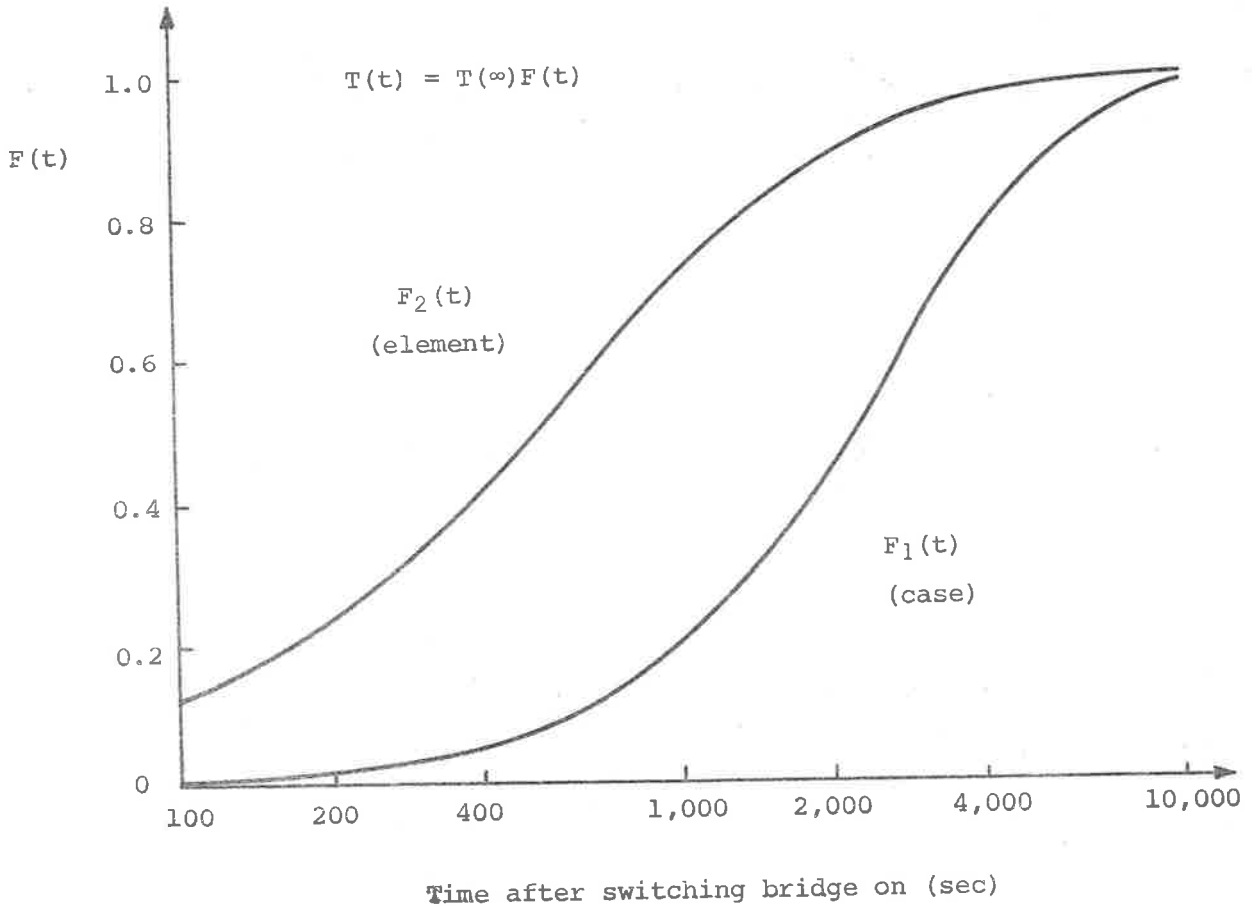

Fig.II.6 Variation of Thermistor Self-Heating Time Function, F(t), with Time after Switching Bridge On.

the case, $T_1(\infty) = 2 \times 10^{-4}$°C. The time it takes for the system to reach any desired state of equilibrium can be estimated from the slope of the function $F_2(t)$, or more precisely, from the differential of equation (II.12b) with respect to time, that is, from:

$$\frac{\partial T_2(t)}{\partial t} = P_2\left(\frac{1}{K_1} + \frac{1}{K_2}\right)\left(\frac{\xi_1\xi_2}{\xi_1+\xi_{21}}\right)\left(\left\{\frac{\xi_{21}}{\xi_2-\xi_1}\right\}e^{-\xi_1 t} + \left\{1 - \frac{\xi_{21}}{\xi_2-\xi_1}\right\}e^{-\xi_2 t}\right) \quad \ldots(II.13)$$

In the present calorimeter the output of the bridge must not vary by more than about 3μV/min, that is, the element temperature must not vary by more than about 10^{-6}°C/sec.. By considering equation (II.13) it can be determined that this rate of temperature variation is reached for the single calorimeter system about 2½ hours after switching the bridge on. In the present twin calorimeter system the time to reach this state of equilibrium is only one hour, hence the use of the twin system is justified.

Further, for the single calorimeter system, the element temperature variation is about 1.5×10^{-5}°C/sec. after one hour, while for the actual twin calorimeter the rate is about 1×10^{-6}°C/sec. or only about 8% of that for the single system. Thus, the test and reference calorimeters are at least reasonably matched.

II.3.4 Bridge Sensitivity and Linearity.

The equation for the 'out-of-balance' voltage of the Wheatstone bridge is:

$$v = \frac{\varepsilon r\,(R_1R_S - R_2R_T)}{(R_1 + R_2)(R_TR_S + R_Tr + R_Sr) + R_1R_2(R_T + R_S)} \quad \ldots(II.14)$$

where the symbols are defined in figure II.5. In practice the values of R_1 and R_2 are within 2% of each other, hence we can put, $R_1 = R_2 = R$, and equation (II.14) becomes:

$$v = \frac{r\varepsilon(R_S - R_T)}{(R_T + R_S)(R + 2r) + 2R_TR_S} \qquad \ldots(II.15)$$

The sensitivity of the bridge (σ volt/Ω/volt) to changes in the test thermistor resistance can be defined by:

$$\sigma \equiv \frac{1}{\varepsilon}\left|\frac{\partial v}{\partial R_T}\right| = \frac{1}{(AR_T^2 + BR_T + C)} \qquad \ldots(II.16)$$

where:
$$A = \frac{(R + 2R_S + 2r)^2}{2R_Sr(R + R_S + 2r)}$$

$$B = \frac{(R + 2R_S + 2r)(2r + R)}{r(R + R_S + 2r)}$$

$$C = \frac{R_S(2r + R)^2}{2r(R + R_S + 2r)}$$

The value of σ is dependent on the ambient temperature, through R_S, and is relatively independent of the value of r. Figure II.7 shows σ as a function of R_T, for three values of R_S. A typical value of σ being 2.75μV/Ω/volt at an ambient temperature of 22.5°C.

The linearity of response of the bridge can be determined by differentiating equation (II.16) with respect to temperature, giving:

$$\left|\frac{\partial\sigma}{\partial T}/\sigma\right| = \sigma\beta R_T(2AR_T + B) \qquad \ldots(II.17)$$

Substituting numerical values gives a value of 4.7%/°C. Consequently, over the temperature range encountered during a measurement, the variation in bridge sensitivity is <0.05%, and can be neglected.

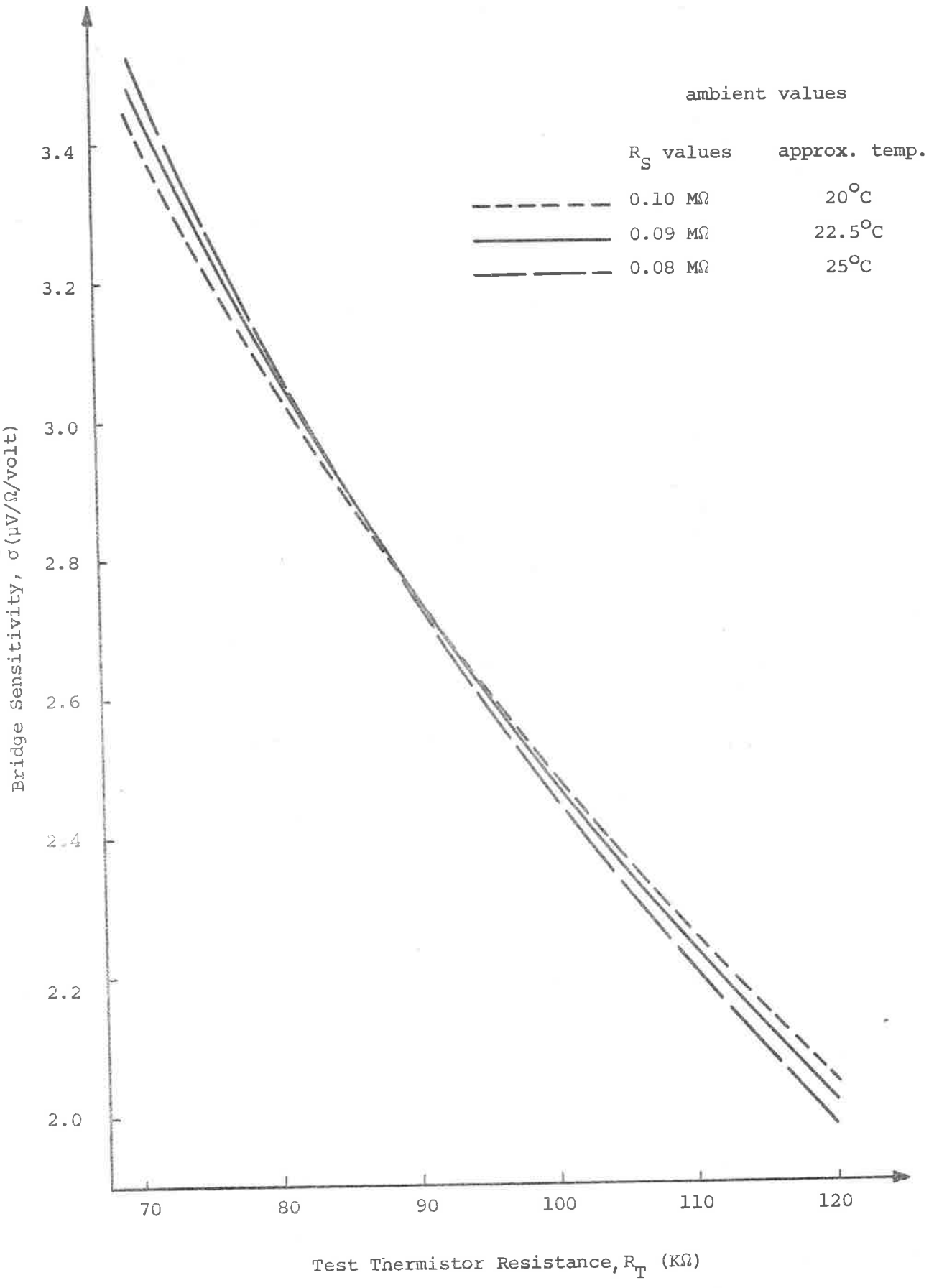

Fig.II.7 Variation of Sensitivity of Temperature Measuring Bridge as a Function of Test Thermistor Resistance, for Three Ambient Temperatures.

An alternative expression for the bridge sensitivity (σ' volt/Ω/volt) can be defined by putting $R_T = R_S$ in equation (II.14) and subsequently differentiating the resultant equation with respect to R_1, giving:

$$\sigma' \equiv \frac{1}{\varepsilon}\left|\frac{\partial v}{\partial R_1}\right| = \frac{1}{(A'R_1^2 + B'R_1 + C')} \qquad \ldots(II.18)$$

where:
$$A' = \frac{(R_T + 2r + 2R_2)^2}{2R_2 r(R_T + 2r + R_2)}$$

$$B' = \frac{(R_T + 2r)(R_T + 2r + 2R_2)}{r(R_T + 2r + R_2)}$$

$$C' = \frac{R_2(R_T + 2r)^2}{2r(R_T + 2r + R_2)}$$

The value of σ' is essentially independent of both the ambient temperature and the value of r. For this sensitivity we obtain the value of 2.39μV/Ω/volt. This sensitivity is important since it can be readily checked by varying the value of δR in the arm of R_1. Experimentally, σ' was found to be (2.36 ± 0.05) μV/Ω/volt. The agreement is satisfactory and confirms that the bridge is functioning correctly.

II.4 Calibration Method.

II.4.1 Approach.

There have been a number of approaches made to the problem of the calibration of calorimeters. Some previous authors have calibrated their instruments against standard ionization chambers, and at least one used the more indirect method of calibrating against a standard radiation field. These methods tend to defeat one of the

main advantages of calorimeters, namely the ability of determining absorbed dose directly in terms of fundamental quantities. However if these types of calibration procedures are carried out at photon energies where ionization methods are still applicable, then they at least guarantee that the calorimeter, when extended into the multi-million volt range, will give results which are continuous with the ionization methods. A further advantage with these methods is that the amount of impurities (i.e. non-tissue-equivalent materials) in the calorimeter, both case and element, is reduced.

The majority of previous authors have used an electrical method of calibration which depends upon the Joule heating effect in a known resistance. In this method there are two further approaches that can be used, both with the intention that the electric heating should closely simulate the heating produced during the absorption of radiation energy. The most common method is to use discrete heating wires of known resistance which are in good thermal contact with the absorbing material, but are not always within the bulk of the material. Some authors have thought that the discrete heaters would not simulate the radiation absorption closely enough and have tried to achieve closer simulation by using conducting (and usually tissue-equivalent) plastics as the absorbing material, and then passing the calibration current through the bulk of the calorimeter. The use of tissue-equivalent plastics was discussed in Section II.1.1. It is also possible that the resistance values of

such materials may not be sufficiently stable for standard purposes, perhaps depending upon such factors as surface condition, temperature, humidity, etc.. It is also not obvious that the use of conducting plastics will in fact give closer simulation of the absorption of radiation energy than the discrete heater method.

The present calorimeter employs the discrete heater approach and it will be shown that this method gives a reasonable approximation to the temperature field produced by radiation heating.

II.4.2 Calibration Circuit.

Since the calorimeter is in two sections, case and element, which are thermally insulated from each other, it is necessary to have a separate heating coil in both. The positions of the two heating coils within the calorimeters are shown in Figure II.1, while the calibration circuit is shown in Figure II.8. The ratio of the currents passing through each coil must be such as to produce equal rates of temperature rise in the case and the element, as is the situation during radiation exposures. This condition is achieved by the correct selection of the weighting resistance (R_W) in the element heater arm. The limiting resistance (R_L) allows various electric dose rates to be obtained and is usually selected so that the electric dose rate is close to the radiation dose rate being measured. Calibration 'exposure times' are made with a manual knife switch and are timed against a calibrated stopwatch. The 'exposure

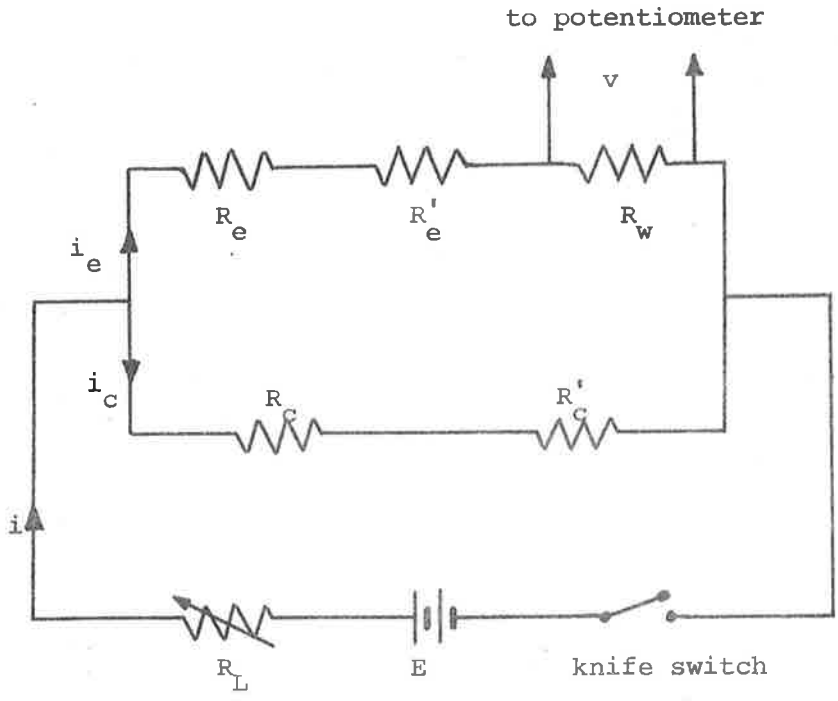

Fig.II.8 Electric Calibration Circuit.

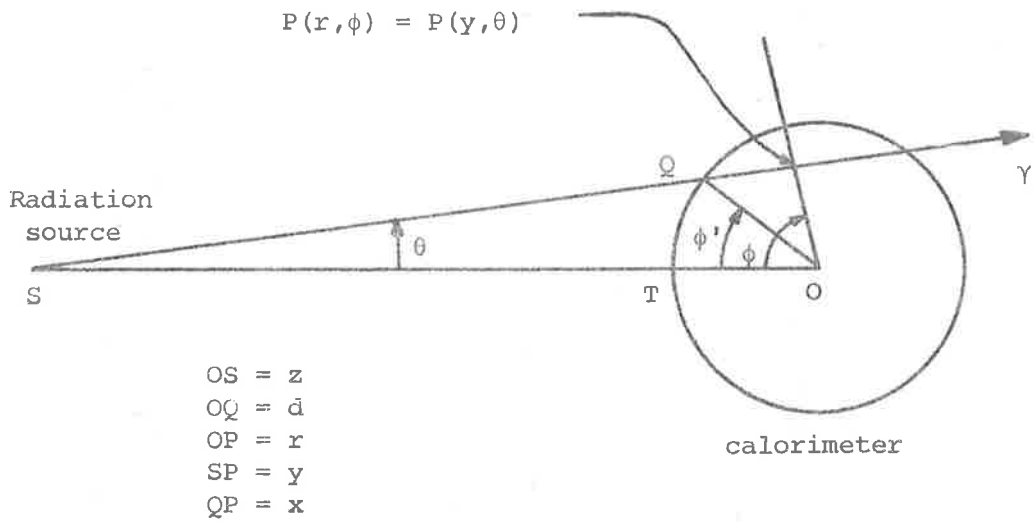

Fig.II.9 Geometry for the Determination of the Dose Distribution within the Calorimeter.

times' are usually about 5 minutes with an estimated uncertainty of ±0.1%. The element heater current is determined by measuring the potential drop across the weighting resistance with a "Cambridge" Precision potentiometer type 7565. Both the weighting resistance and the measured potential are known with an uncertainty of ±0.1%. Hence the power dissipated in the element heater can be determined with acceptable accuracy.

II.4.3 Practical Details.

The element heater consists of one spiral coil of 48 SWG eureka wire with a nominal resistance of 100Ω. The leads to this heater are 45 SWG copper wire. The case heater consists of four spiral coils of 36 SWG eureka wire, connected in parallel, with a nominal resistance of 3.8Ω. The leads to this heater are 44 SWG copper. The heaters are embedded in the bulk of the case and element material. This is done by winding the given coil in a spiral groove on the inner cylindrical section, then filling the groove with 'Aquadag' (colloidal graphite in water) and finally placing a tight fitting outer annular section over the inner section, to form either the case or the element. The placement of the heater coils was checked radiographically.

The resistances of the copper leads, from the eureka heaters to the vacuum chamber leadthroughs, are a small fraction (<1%) of the values for the heaters and the heat produced in them is assumed to

eventually pass into the calorimeter. The resistances of the copper leads can only be further reduced at the expense of increasing thermal losses along them. The wire gauges selected are considered to provide a compromise between low resistance and low thermal conductance. From the vacuum chamber leadthroughs, the calibration circuit passes along the 12-core cable, which also conveys the temperature measuring leads.

The resistance values of the heater coils, measured at the vacuum chamber leadthrougns, and of the heater coils plus cable, measured at the shielded box, were determined by two methods. The first was to compare the unknown resistance with a secondary standard resistance using the Cambridge Precision potentiometer. The accuracy of this method depends essentially upon the calibration of the reference resistances, which was ±0.1% in this case. The second method was to use a "Wayne Kerr Universal Bridge" type B221, which had a specified accuracy of ±0.1%. Both methods were intercompared and found to give results consistent within their tolerances. In the original calorimeter excessive lengths of eureka wire were left emerging from the graphite bulk (about 4 mm). This produced a relatively large heating effect outside of the graphite bulk which, together with the low thermal conductivity of the eureka, gave some concern as to whether all of the heating effect external of the graphite should be included in the total heating effect produced within the calorimeter. During the course of this work the eureka leads were

shortened (to about 1 mm) which caused the resistance values to change. The resistance values were measured on a number of occasions, for the two models, and are listed in Appendix 3.

II.4.4 Estimation of Weighting Resistance.

If the power dissipated in the element heater is P_e and, in the case heater, is P_c then their ratio (P_c/P_e) must be equal to the ratio of their heat capacities (H_1/H_2). Using the notation shown in Figure II.8 we have the condition that:

$$\left(\frac{P_c}{P_e}\right) = \left(\frac{R_w + R_e + R'_e}{R_c + R'_c}\right)^2 \left(\frac{R_c}{R_e}\right) = \left(\frac{H_1}{H_2}\right) \qquad \ldots(II.19)$$

The values of the heat capacities are in Appendix 1 and the values of the heater resistances in Appendix 3. The calculated value of R_w for Calorimeter I was found to be 21.7Ω but, for convenience, a value of 22.0Ω was used. For Calorimeter II the calculated value of R_w was 24.5Ω while the value used was 25.0Ω. The uncertainties in the calculated values of R_w are of the order of ±1Ω.

II.4.5 Calibration Equations.

The energy produced when a current i_e (amp) flows through the element heater of resistance R_e(Ω) for a time t (sec) is:

$$E = (i^2_e R_e t) \text{ joule}$$

The electric dose to the element of mass m_e(gm) is thus:

$$D = \left(\frac{i^2_e R_e t 10^5}{m_e}\right) \text{ rad} \qquad \ldots(II.20)$$

Substituting numerical values give the following equations:

Calorimeter I Dose (rad) = (0.1287) v^2(mV)t(min) ...(II.20a)

Calorimeter II Dose (rad) = (0.0947) v^2(mV)t(min) ...(II.20b)

The uncertainties in these calculated electric doses are ±0.6%.

The heater wire gauges set a limit to the maximum current that the heater coil can safely pass and this sets a limit to the maximum electric dose rate that can be obtained. The element heater can carry up to 3 mA, while the case heater (four wires in parallel) can carry 140 mA. The dose rate is thus limited, by the element heater, to a maximum of about 500 rad/min., which is more than sufficient for present needs. Usually an element current of <1 mA suffices, corresponding to dose rates of <60 rad/min..

II.4.6 Simulation of Electric Calibration to Radiation Measurement.

As mentioned earlier the calibration temperature distribution should be effectively the same as the temperature distribution due to the absorption of radiation energy. Since this problem has not been previously investigated by other workers in this field, it is examined in some detail in the following sections. It will be appreciated that an exact analysis of the situation would be prohibitively difficult and that certain simplifications will be necessary to make reasonable progress.

Before the temperature distribution, due to the radiation, can be determined it is at first necessary to derive an approximate dose distribution for the circular cross-section of the calorimeter. As mentioned in section II.1.2 the 2 mm gap between the element and the case causes negligible disturbance to the radiation field, and thus, for the purpose of determining the dose distribution, the gap is neglected.

Consider the geometry shown in Figure II.9. Point $P(r,\phi) = P(y,\theta)$ is a general point within the calorimeter where the dose is to be determined. Point S is the source of radiation and SQP is the path of the ray passing through point P from the source. The dose at point P is determined by three main factors, namely (i) the inverse square law attenuation of the primary beam, which is inversely proportional to y^2, (ii) the absorption of the primary beam after passing through a thickness x of the calorimeter material, which is proportional to $\exp(-\mu x)$, where μ is the linear absorption coefficient for the graphite (for $Co^{60}\gamma$-radiation, $\mu = 0.0427\ cm^{-1}$) and finally (iii) the scattered radiation. At photon energies >1 MeV the backscatter is of the order of 2% of the maximum forward scatter, and side scatter is similarly small. As a simplification, it is assumed that only forward scatter occurs and that it is given by a factor of the form: $\left(1 + b\{1 - \exp(-ax)\}\right)$. The form of this factor was determined

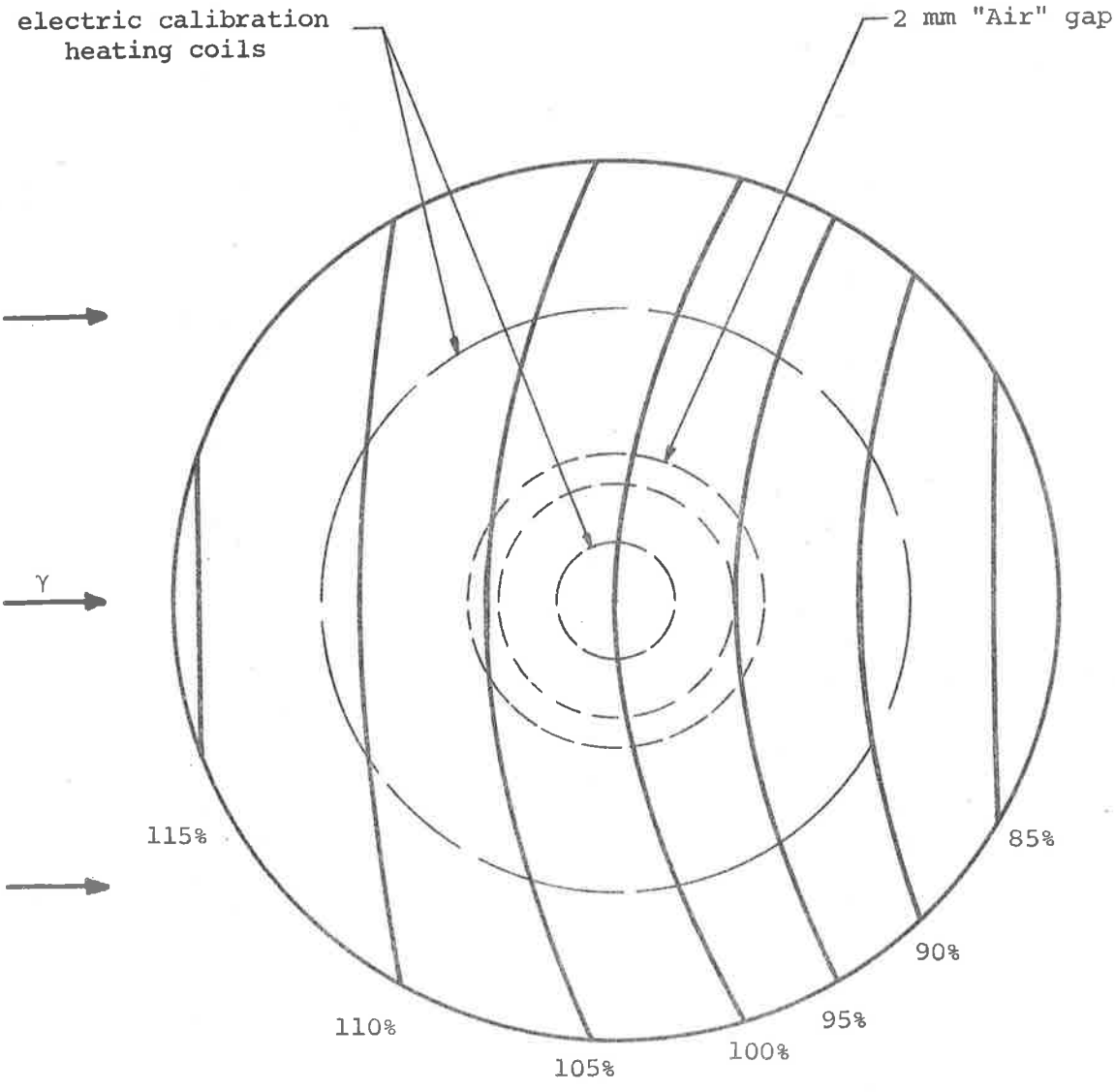

Fig.II.10 Calculated Percentage Dose Distribution in the Graphite Calorimeter, using z = 67 cm.

from data given by JOHNS (1956) and the constants were estimated to be: $a = 0.46\ cm^{-1}$ and $b = 0.10$, for the present geometry.

Combining the above three factors gives the absorbed dose at point P as:

$$\text{Dose} \propto (y^{-2})(e^{-\mu x})\{1 + b(1 - e^{-ax})\} \qquad \ldots(II.21a)$$

In practice, the absorbed dose is experimentally determined at the centre of the calorimeter, so the dose given by equation (II.21a) is normalized to the dose at the point O, that is, D_o. Then equation (II.21a) can be rewritten as:

$$\text{Dose}(r,\phi) = D_o\left(\frac{z}{y}\right)^2\{e^{-\mu(x-d)}\}\left(\frac{1+b(1-e^{-ax})}{1+b(1-e^{-ad})}\right) \qquad \ldots(II.21b)$$

Isodose curves were determined with equation (II.21b), together with the aid of some elementary geometry and the resulting distribution is shown in figure II.10. A value of $z = 67$ cm was used in the calculations, corresponding to the source-to-centre distance used on the "Orbitron" Telecurie Unit. The location of the electric heater coils is shown for comparison. It would appear at this stage that the two distributions are quite different. Furthermore the dose distribution is far from uniform, with a maximum difference of 34% between the doses at the front and back faces. Such a distribution would be difficult to simulate, if required, by using either a discrete heater system or conducting plastic.

II.4.7 Temperature Distribution Due to Radiation Field.

The basic equation to be solved is the "General Heat Conduction Equation".

$$\nabla^2 T(x,y,z,t) + \frac{q(x,y,z)}{k} = \frac{1}{\alpha} \frac{\partial T(x,y,z,t)}{\partial t} \qquad \ldots(II.22)$$

where: $T(x,y,z,t)$ is the temperature distribution to be determined,

$q(x,y,z)$ is the 'source strength' distribution, that is, the distribution of the energy deposited per unit volume per unit time, and

k and α are the thermal conductivity and the diffusivity, respectively, of the graphite.

In the present problem an exact analytical solution of this equation is impossible due to the complex source distribution. To estimate the transient temperature distribution in the present case resort must be made to numerical methods, as shown by SCHNEIDER (1957). The general approach is to consider the cross-section of the calorimeter as being covered by a circular grid network, as shown in Figure II.11, then the transient state heat balance for a general nodal point on this grid, of volume V, is given by the following difference equation:

$$-\sum_i K_i \Delta T_i \Delta t + qV\Delta t = c\rho V \Delta T' \qquad \ldots(II.23)$$

(i) Network for Element and Case Ends

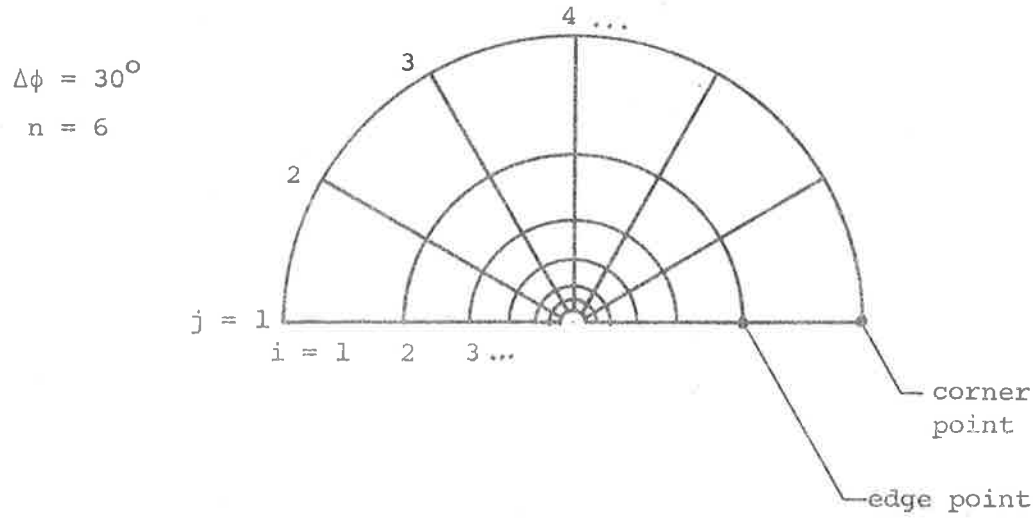

(ii) Network for Case Annulus

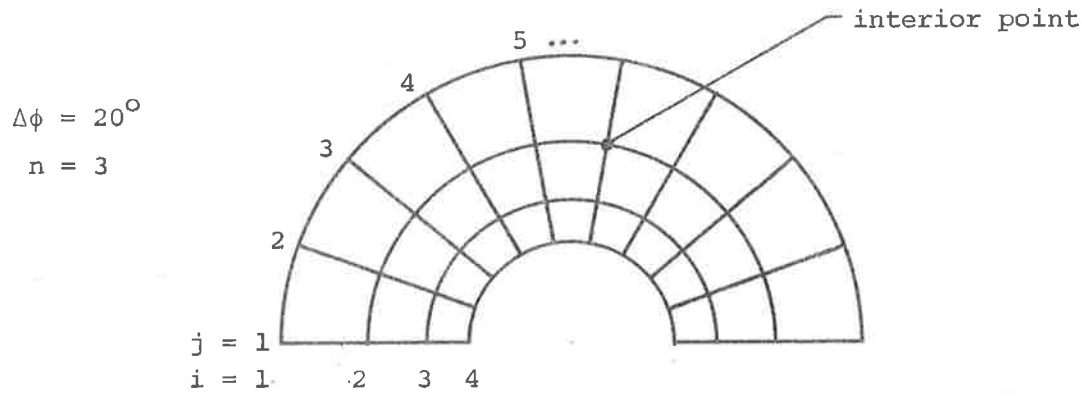

Fig.II.11 Grid Networks used in the Calculation of the Temperature Distribution, due to Radiation Absorption, within the Calorimeter. Nodal Point Positions are represented by the Matrix Notation (i,j), where:

j → 1 to m are the angular positions, and

i → 1 to n are the radial positions.

where: ΔT_i is the temperature difference between the nodal point in question and the ith neighbouring nodal point,

$\Delta T'$ is the increase in temperature of the nodal point in question during the time interval Δt, and

$K_i = k_i(A_i/\ell_i)$ is the thermal conductance between the nodal point in question and the ith neighbouring nodal point, with ℓ_i being the appropriate path length and A_i the appropriate cross-sectional area.

With the aid of equation (II.23) it is possible to generate a difference equation for each nodal point on the grid network, where q is known at each nodal point from the dose distribution determined in section II.4.6, and having due consideration to the boundary conditions.

In the present problem the calorimeter is divided into three regions of interest, namely the element (circular) cross-section, the case (annular) cross-section and the case end (circular) cross-section. Equation (II.23) is greatly simplified by using a logarithmic network which produces curvilinear squares, thus making $(A_i/\ell_i) = 1$ for all nodal points. Also, since k, the thermal conductivity of the graphite, is independent of position, then we can put $K_i = k$ outside of the summation sign in equation (II.23). Unfortunately, however, the logarithmic spacing produces a crowding of the nodal points as the radii are decreased, and when applied

to a circular cross-section produces an infinite number of nodal points. To overcome this effect each circular cross-section was assumed to be annular, with the inner boundary coinciding with a grid circle, which was of negligible size. Also, the grid network applied to the annular case cross-section did not exactly coincide with the inner boundary of the case. The difference was small and assumed negligible. The grid networks used are shown in Figure II.11. Due to the symmetry of the cross-sections, about the direction of the incident radiation, it was possible to simplify the computations by considering only half of each. It was assumed that all boundaries of each of the three cross-sections were perfectly adiabatic. This was a good approximation since, as will be shown in section II.5, the element loses less than 1% of its absorbed energy while the case loses about 7%.

From Figure II.11 it can be seen that there are three basic difference equations involved, depending upon the position of the nodal point under consideration. They are, after some rearrangement:

corner points: $T'(1,1) = 4\Theta_1\left(T(2,1)+T(1,2)+\{\frac{1}{4\Theta_1} - 2\}T(1,1)\right)+Q(1,1)$

edge points: $T'(1,2) = \Theta_1\left(T(1,1)+T(1,3)+4T(2,2)+(\frac{1}{\Theta_1} - 6)T(1,2)\right)+Q(1,2)$

interior points: $T'(2,2) = \Theta_2\left(T(1,2)+T(3,2)+T(2,3)+T(2,1)+(\frac{1}{\Theta_2} - 4)T(2,2)\right) + Q(2,2)$

where we define: $\Theta_i \equiv \left(\frac{\alpha\Delta t}{V_i}\right) = \left(\frac{\alpha\Delta t}{\Delta\phi^2}\right)\frac{1}{r_i^2}$

Case Annulus and Element Cross-Sections

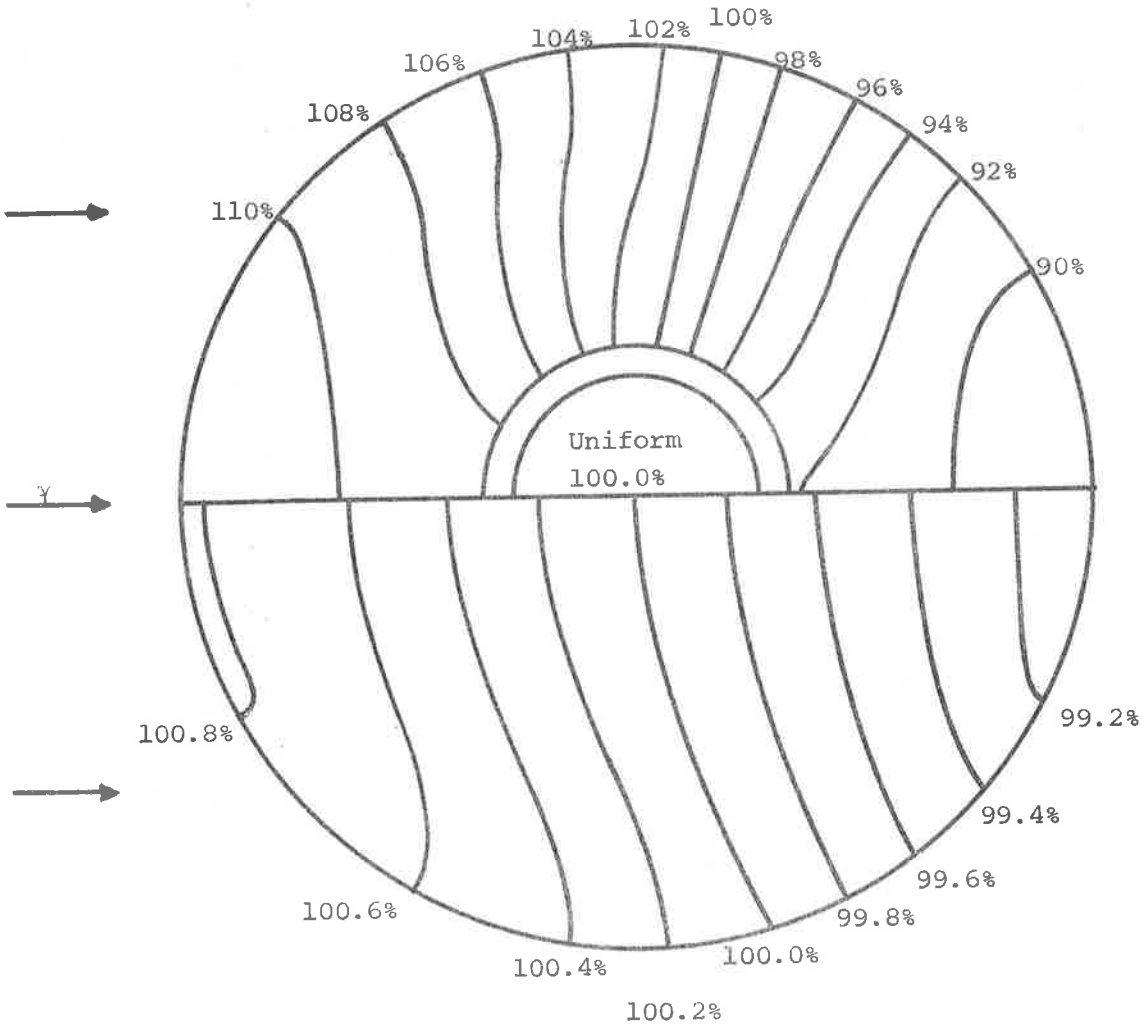

Case End Cross-Sections

Fig.II.12 Calculated Percentage Temperature Distribution in Calorimeter as a Result of the Dose Distribution shown in Fig.II.10, at One Second after Commencing Exposure.

and, $Q(i,j) = \frac{q(i,j)}{c\rho}\,\Delta t = \frac{BD(i,j)\Delta t}{c}$ the 'source temperature' at (i,j) with D(i,j) being the calculated dose rate at (i,j), using D_o = 39.0 rad/min., and B = 3.982 x 10^{-8} (cal/gm sec)/(rad/min).

There is a condition imposed on the allowable values of Θ_i. The first law of thermodynamics requires that $T'(i,j) \geq T(i,j)$, at all nodal points and at all times. For a given network this condition specifies the maximum value of Δt which may be used. For stability and convergence of the results it is best to select a value of Θ_i as small as possible, but this gives very small values of Δt which in turn requires a prohibitively large number of calculations. Values of Δt were selected, for each cross-section, which satisfied the condition for Θ_i a little better than minimally and the values are shown in table II.2. The calculations were programmed in Fortran IV and performed with the aid of a computer. The initial condition was that all T(i,j) = 0, and equilibrium was attained when $\{T'(1,1) - T'(1,m)\} \simeq \{T(1,1) - T(1,m)\}$.

The resulting temperature distributions, when equilibrium is reached, are shown in Figure II.12. Both the periods during which the transients occurred, and the final temperature gradients are very small, as can be seen in Table II.2.

Table II.2

Values of Time Increments used in the Determination of the Temperature Distributions due to Radiation Absorption, and the Resultant Times to reach Equilibrium and the Maximum Temperature Differences, for each Cross-section.

	Element	Case Annulus	Case End
Values of Δt used(secs):	25×10^{-6}	5×10^{-4}	1×10^{-2}
Time to reach equilibrium (secs):	27×10^{-4}	535×10^{-4}	95×10^{-2}
Maximum temperature difference (^{o}C):	2.3×10^{-9}	1.6×10^{-7}	2.0×10^{-6}

After the initial transients have ceased, further addition of energy simply raises the average temperature of the calorimeter at a rate proportional to the rate of absorption of the radiation energy. Figure II.13 shows how the percentage temperature distribution varies with time, in the direction of the incident radiation. From Figure II.13 it can be seen that the percentage temperature distributions are essentially flat (< 1%) within 1 second for the element and case end cross-sections, and by 10 seconds for the case annulus cross-section. In practice, since the temperature measuring equipment has a time constant of the order of 5 seconds, the temperature distribution can be considered as uniform at all significant times, even though the dose distribution is far from uniform. It must now be determined whether the electric calibration heating stimulates this effect.

(i) Element and Case Annulus

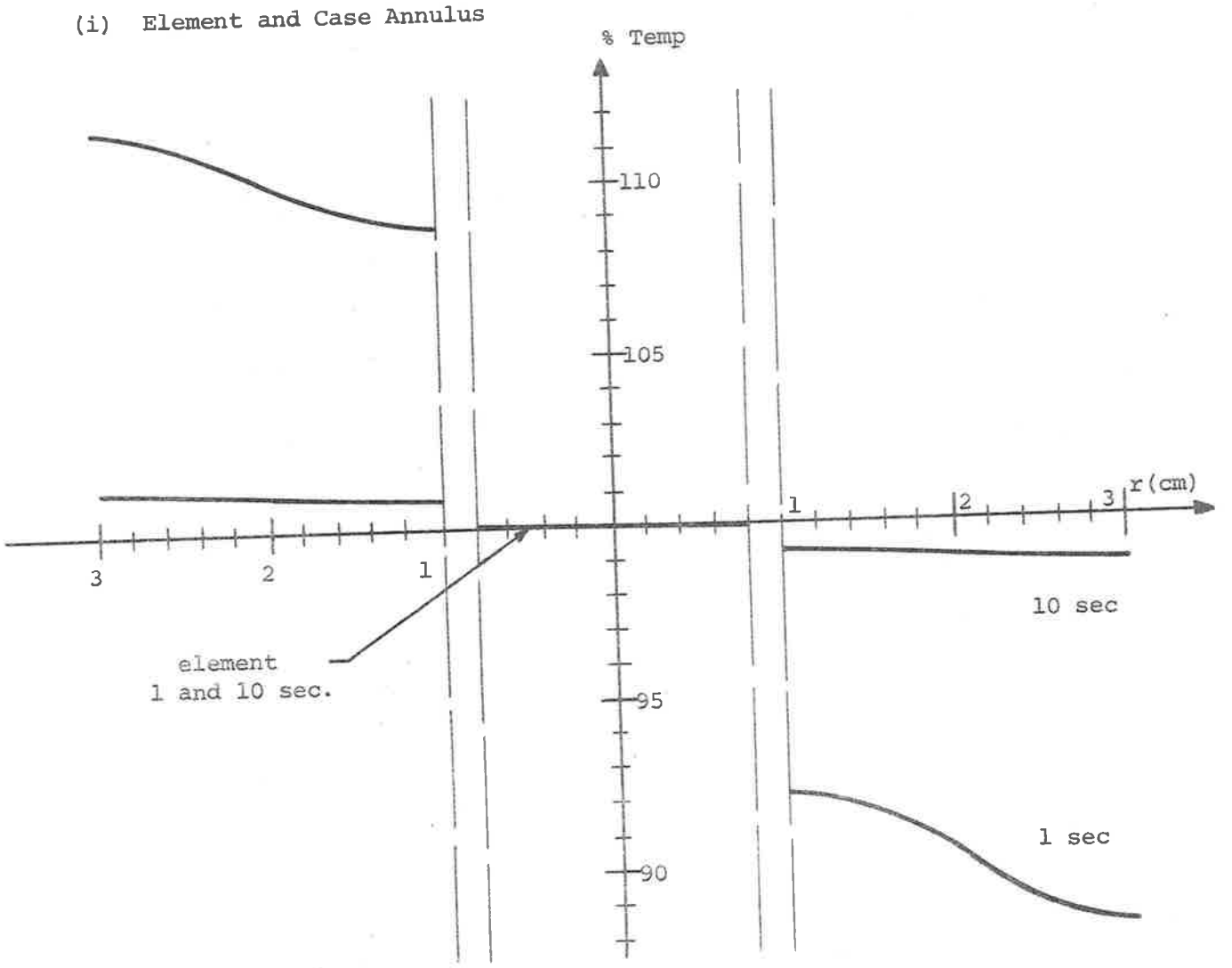

(ii) Case Ends

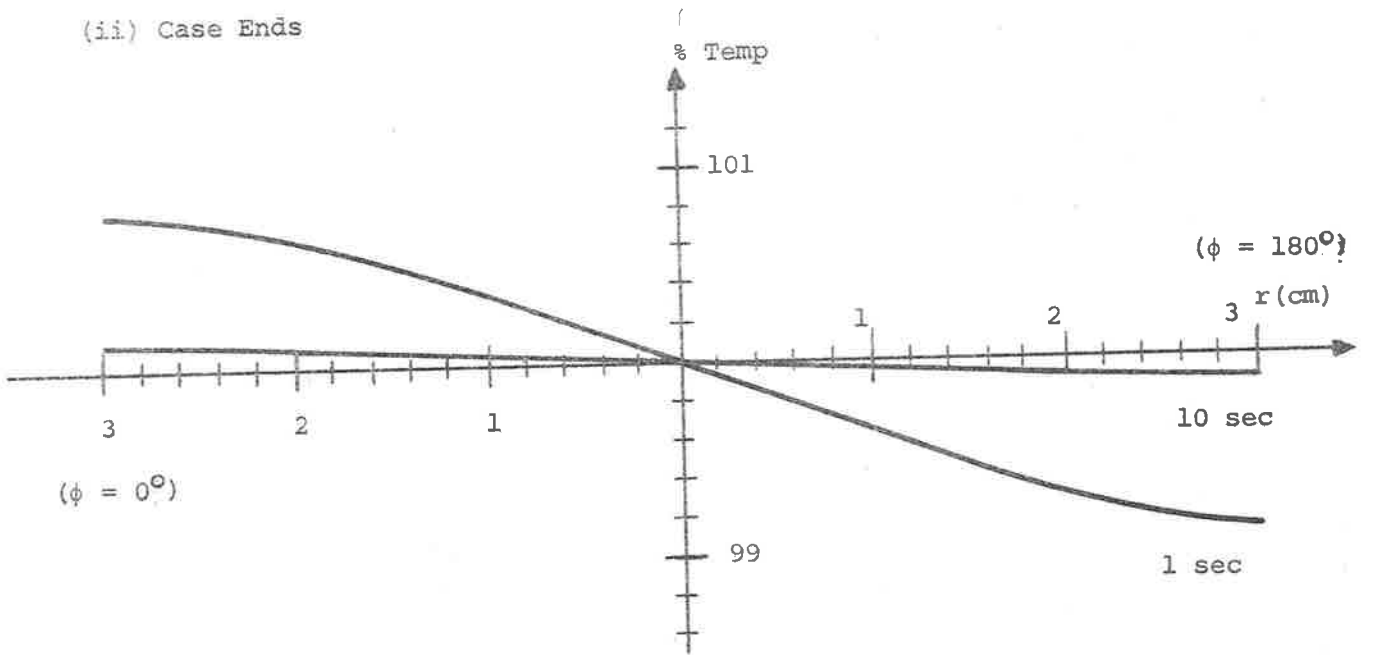

Fig.II.13 Variation of Percentage Temperature Distribution with Exposure Time, in the Direction of Maximum Temperature Gradient, i.e. $\phi = 0$ & 180^{o}.

II.4.8 Temperature Distribution Due to Electric Heating.

As in the previous section the calorimeter is divided into three regions of interest, each with adiabatic boundary conditions. It is also necessary to assume that the thermal resistance between the heater coils and the graphite is negligible. In this analysis, due to the discrete heat source, an analytical solution is possible for each of the three cross-sections considered. The method is due to Kelvin and involves the application of the principle of the 'instantaneous point source of heat in a material of infinite extent'.

It can be shown that the following equation is a solution of the general heat conduction equation (CARSLAW and JAEGER, 1959).

$$T(x,y,z,t) = \frac{Q}{8(\pi\alpha t)^{3/2}} e^{-\{(x-x')^2+(y-y')^2+(z-z')^2\}/4\alpha t} \quad \ldots(II.24)$$

This equation gives the temperature distribution, due to an instantaneous point source of strength Q at point (x', y', z') at time t = 0, as a function of time. Where α is the thermal diffusivity of the conducting material and the total quantity of heat liberated by the source is given by $Q\rho c$.

Integrating equation (II.24) with respect to time, gives the solution for the problem of a continuous point source which releases heat at the rate $q(t)\rho c$ per unit from t = 0 to t = t, at the point (x', y', z'). Integrating equation (II.24)

with respect to the appropriate space variables gives the solution for the problem of the instantaneous distributed source. To obtain solutions for a finite medium use is made of Green's Functions. The solutions which are appropriate for the present case, in cylindrical coordinates, were obtained from CARSLAW and JAEGER (1959), with slight modifications.

1. The solution for a cylinder of infinite axial extent, $0<r<a$, with a continuous distributed source at $r = r'$, with adiabatic boundary conditions is:

$$T = \frac{q}{\pi a^2}\left(t + \sum_{n=1}^{\infty} \frac{J_o(r\beta_n)J_o(r'\beta_n)}{J_o^2(a\beta_n) + J_1^2(a\beta_n)} \frac{(1 - e^{-\alpha\beta_n t})}{\alpha\beta_n^2}\right) \quad \ldots(II.25)$$

where $q(t) = q$ is the source strength per unit axial length (a constant independent of time in the present problem) and β_n are the roots of $J_1(a\beta) = 0$.

Equation (II.25) was applied to the element and case end cross-sections, and the results were normalized to the average temperature and expressed as a percentage. The percentage temperature distributions are shown in Figure II.14, for various times after commencing heat production. The values of r', a and q used in the calculations are shown in table II.3.

Table II.3

Values of the Constants used in the Determination of the Temperature Distributions due to Electric Calibration, for each Cross-section.

cross section	a(cm)	b(cm)	r'(cm)	q(^{o}C cm^2/sec)
(i) element	0.8	-	0.4	27.57×10^{-6}
(ii) case end	3.0	-	2.0	366.1×10^{-6}
(iii) case annulus	1.0	3.0	2.0	366.1×10^{-6}

2. The solution for an annular cylinder of infinite axial extent, $a<r<b$, with a continuous distributed source at $r = r'$, with adiabatic boundary conditions is:

$$T = \frac{q}{\pi(b^2-a^2)}\left(t + \frac{\pi^2(b^2-a^2)}{4\alpha}\sum_{n=1}^{\infty}\frac{\Phi_n J_1^2(b\beta_n)(1-e^{-\alpha\beta_n^2 t})}{J_1^2(a\beta_n)-J_1^2(b\beta_n)}\right) \qquad \ldots(II.26)$$

where

$$\Phi_n = \left(J_o(r'\beta_n)Y_1(a\beta_n)-Y_o(r'\beta_n)J_1(a\beta_n)\right)\left(J_o(r\beta_n)Y_1(a\beta_n)-Y_o(r\beta_n)J_1(a\beta_n)\right)$$

and β_n are the roots of $\left(J_1(a\beta)Y_1(b\beta)-Y_1(a\beta)J_1(b\beta)\right) = 0$

or alternatively $\left(J_1(x)Y_1(\lambda x) - Y_1(x)J_1(\lambda x)\right) = 0$

where $x = a\beta$ and $\lambda = b/a$.

Equation (II.26) was applied to the case annulus and the resulting percentage temperature distribution is shown in Figure II.14. The constants used in the calculation are shown in table II.3.

The percentage temperature distributions for each of the three cross-sections is somewhat as expected. From Figure II.14 it can be seen that after a short initial transient period the actual temperature differences between any two points remains

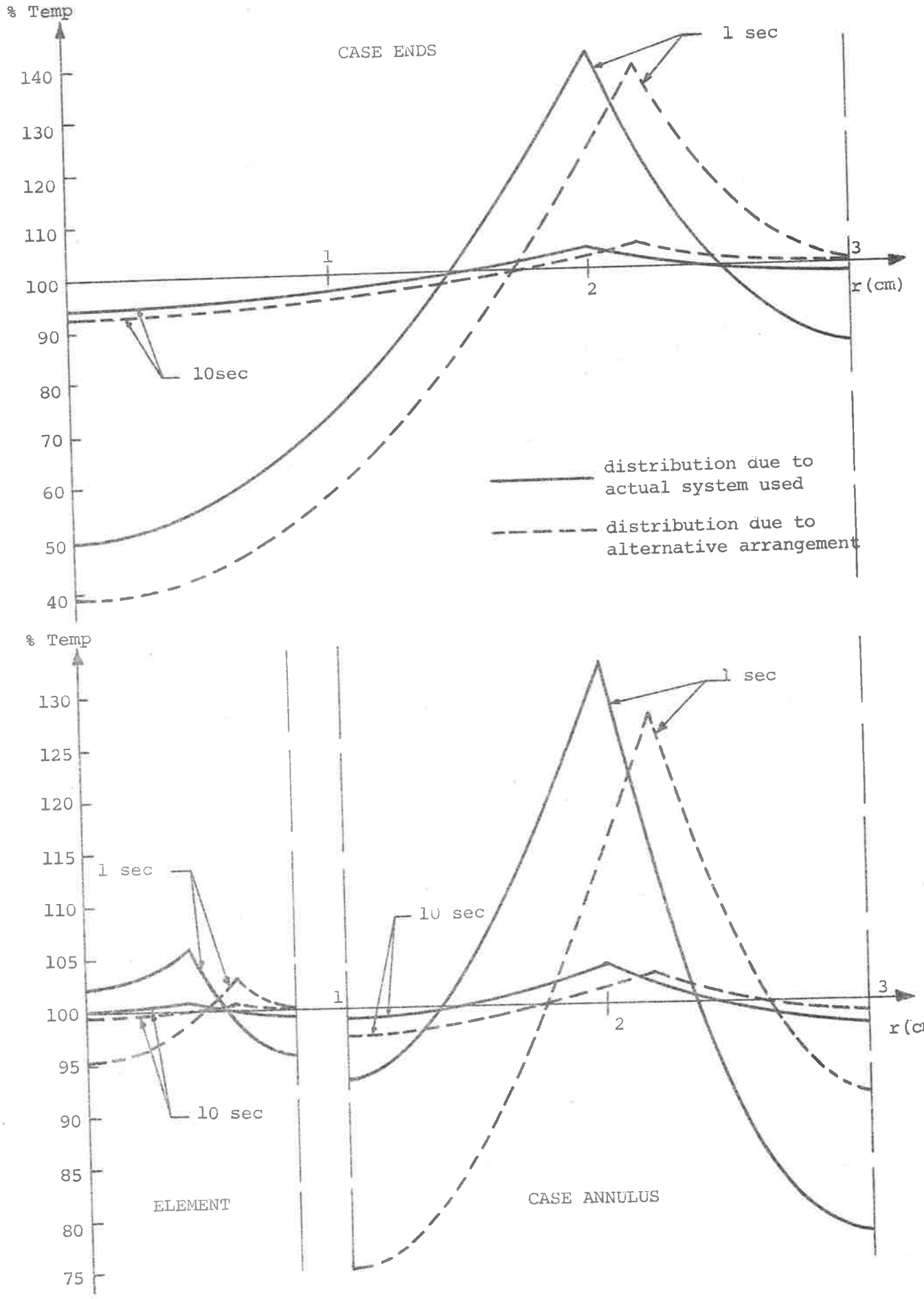

Fig.II.14 Variation of Percentage Temperature Distribution, due to Electric Heating (i_e = 1mA), for each of the Three Cross-Sections.

constant and only the average temperature increases with the further addition of energy. The important result however, is that, while the initial distribution shapes are far from those in the case of radiation heating, the distributions once again become essentially uniform (< 1%) at significant times (>10 secs). From the graphs it can be seen that the temperature on the outside surface of the element is, at all times, very close to that on the inside surface of the case annulus, and that the temperature at the centre of the element is always close to the average temperature, as would be desired in both cases. The numerical solution of equations (II.25) and (II.26) were also performed with the aid of a computer.

The effect of changes in the values of (i) α and (ii) r', upon the percentage temperature distributions, were investigated for design purposes. In the case of (i) the value of α was only an estimate, since the thermal conductivity of the graphite was not accurately measured. An increase in the value of α would be to the advantage of the system, but a decrease would not be so. The result of decreasing α from 1.0 to 0.5 is essentially to double the scale of the percentage temperature axis, while retaining the same distribution shapes. It was concluded that the chosen absorbing material would require a value of $\alpha > 0.5$ to be able to simulate the absorption of radiation energy for the present simple heater coil arrangement. In the case of (ii) it was at

first thought that the best r' values for the heater coils would be such that the coils divided the respective cross-sections into two regions of equal heat capacities. The heater positions necessary to do this, for each of the cross-sections, are: element r' = 0.57 cm, case annulus r' = 2.24 cm and case end r' = 2.12 cm. The present method of placing the case coil requires that the value of r' for the case annulus and the case end be the same, hence the average value of 2.18 cm was used for their positions. The percentage temperature distributions were determined for these heater positions and are shown in Figure II.14 as dotted lines. It is apparent that the distributions in this case are not as good as those actually used. The most obvious defects are that the temperature difference between the element wall and the case inner wall has been increased and the temperature at the centre of the case end is lower, thus increasing heat losses from the element during the transient period; also the temperature at the centre of the element is further from the average temperature. These effects are, however, only significant during the short transient period after which all of the distributions become essentially flat.

Thus it was concluded that the heater positions are not critical, other than that they be within the bulk of the absorbing material and not wound on, or near, the surface. The value of α,

the thermal diffusivity, appears to be the main factor and some care should be taken with regard to this factor when choosing the absorbing material of the calorimeter.

II.5 Thermal Linearity of System.

II.5.1 General Considerations.

In this section the overall response of the system is considered, especially with regard to thermal linearity. There are three main steps, each involving the question of linearity of response, between the absorption of energy in the element and the recording of a response on the chart recorder.

(i) Energy deposited in the element produces an increase in temperature of the element, and thermistor. Because of heat losses the temperature rise may not vary linearly with absorbed dose.

(ii) The temperature increase of the thermistor produces a change in its resistance. This response was seen to be linear over a reasonable temperature range in section II.3.1.

(iii) The resistance change of the thermistor produces an 'out-of-balance' voltage of the bridge, which is recorded. This response was also seen to be linear, although over a more restricted range of temperature than for (ii), in section II.3.4.

Thus, as far as the overall linearity of response of the system is concerned, it is necessary to examine (i) above.

That is, it remains to see how the temperature of the element varies under exposure to either radiation or electric calibration.

II.5.2 Thermal Linearity of Element.

From section II.2.3 it was seen that the specific heat of the graphite has a temperature variation of 1.1%/^{o}C. The specific heat can therefore be considered constant over the temperature range encountered during measurements.

Consider the regions of the calorimeter as shown in Figure II.3. It has been previously shown that the temperatures of the element and of the case are uniform over their cross-sections.

(i) Consider the case and the vacuum chamber walls as a system. The effect of the element within the case may be considered as a small perturbation, if necessary, since both its heat capacity and heat input are only 3.7% of those of the case. The vacuum chamber walls are quite massive and can be considered as a heat reservoir at a constant ambient temperature. The temperature of the case, with respect to ambient temperature, is $T_1(t)$, so that $T_1(0) = 0$. Let the power input to the case be P_1 cal/sec, a constant. At a time t sec after commencing power input into the case, conservation of energy gives the following equation:

$$P_1 t = H_1 T_1(t) + K_1 \int_0^t T_1(t)\,dt \qquad \ldots(II.27)$$

This integral equation is readily solved to give:

$$T_1(t) = \frac{P_1}{K_1}\left(1 - e^{-\xi_1 t}\right) \qquad \ldots(II.28)$$

(ii) Now consider the case and the element as a system. Since the temperature is uniform throughout the case then equation (II.28) also gives the temperature variation of the interior wall of the case. In this system we may consider the case to be a heat reservoir compared with the element, since any small amount of energy given to the case by the element will not significantly alter the temperature of the case. Let the temperature difference between the case and the element be; $T'(t) = \left(T_2(t) - T_1(t)\right)$, where $T_2(t)$ is with respect to the ambient temperature and $T_2(0) = 0$. Further, let the power input to the case be P_2 cal/sec, a constant. Applying the law of the conservation of energy to this system, at a time t secs after commencing exposure, gives:

$$P_2 t = H_2 T_2(t) + K_2 \int_o^t \{T_2(t) - T_1(t)\}dt$$

i.e. $$P_2 t = H_2\{T'(t) + T_1(t)\} + K_2 \int_o^t T'(t)dt \qquad \ldots(II.29)$$

The solution of this integral equation, making use of equation (II.28) is:

$$T'(t) = \chi_2\left(1 - (1 - F)e^{-\xi_2 t} - Fe^{-\xi_1 t}\right) \qquad \ldots(II.30)$$

where $F \equiv (\chi_1/\chi_2)/\left((\xi_2/\xi_1) - 1\right)$

and $\chi \equiv P/K$

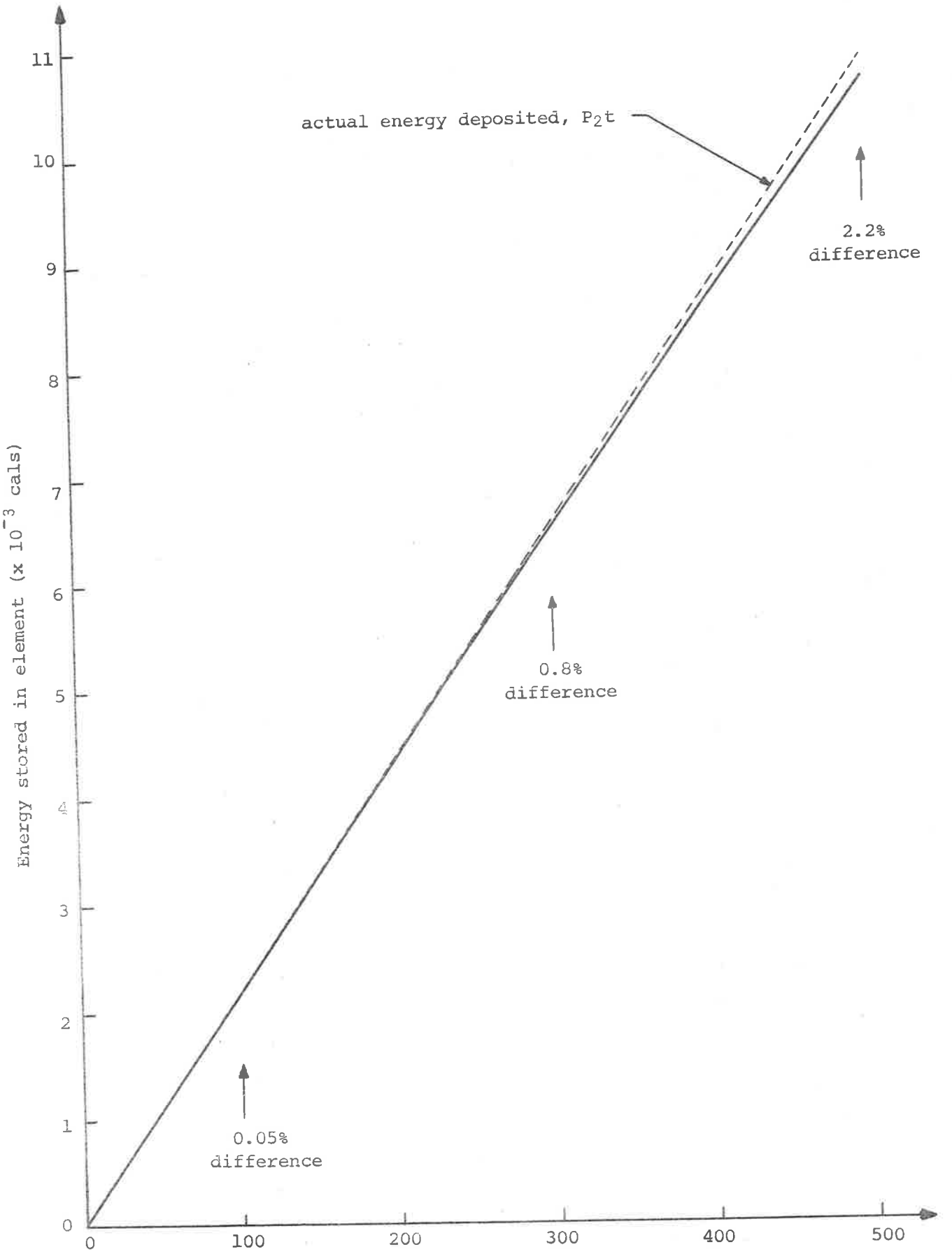

Fig.II.15 Energy Stored in Element, due to an Element Heater Current of 1mA, as a Function of Exposure Time.

Thus tne energy lost from the element to the case in time t is given by:

$$E_{lost}(t) = K_2 \int_o^t T'(t)dt$$

that is,

$$E_{lost}(t) = P_2\left(t - \left(\frac{F}{\xi_1}\right)\{1 - e^{-\xi_1 t}\} + \left\{\frac{F-1}{\xi_2}\right\}\{1 - e^{-\xi_2 t}\}\right) \quad \ldots(II.31)$$

or, alternatively, the energy stored in the element in time t is:

$$E_{stored}(t) = \left(P_2 t - E_{lost}(t)\right)$$

that is, $$E_{stored}(t) = P_2\left(\left(\frac{F}{\xi_1}\right)(1 - e^{-\xi_1 t}) - \left(\frac{F-1}{\xi_2}\right)(1 - e^{-\xi_2 t})\right) \quad \ldots(II.32)$$

Equation (II.32) is shown graphically in figure II.15, for the case of i_e = 1 mA, which gives a value of F = 1.4656. Once again it can be seen that the response is closely linear for practical exposure times. For an exposure of 300 seconds the energy lost from the element is approximately 0.8% and the energy lost from the case to the vacuum chamber walls is approximately 7%. Thus, the element is essentially adiabatic, while the overall system is closely adiabatic and the assumption made in previous temperature distribution determinations is verified.

Consequently, the overall response of the calorimeter is linear under the conditions of its normal use.

II.5.3 Effect of Unbalanced Calibration Heating.

If the same exposure times are used in both calibration and radiation dose measurements, then the energy losses will be the same in both cases. Under this condition the energy losses may be

ignored. This is only strictly true if both the case and the element are heated in proportion to their respective heat capacities during calibration.

It will be remembered that when the values of the weighting resistance were calculated, in section II.4.4, the resistance values were rounded off to the nearest whole ohm. This rounding off in fact produces an excess heating of 0.9% in the case. Thus, during calibration, the heat losses from the element to the case are slightly smaller than the losses experienced during the absorption of radiation. We are now in a position to determine the order of magnitude of this effect and make a correction for it, if necessary. For strictly balanced heating a value of F = 1.4529 is required. Under these conditions the amount of energy loss from the element to the case, for a 5 minute exposure, is 1.0%, compared with 0.8% in the actual case. Thus the electric calibration dose must be increased by 0.2% for a 5 minute exposure. The correction for other exposure times is readily obtained, for example, for exposure times between 100 and 250 seconds a correction of 0.1% is required, between 250 and 500 seconds a correction of 0.2% and between 500 and 800 seconds a correction of 0.3%

With the equations derived in section II.5.2 it is possible to derive corrections for situations where different exposure times are used in calibration and radiation dose measurements. The necessity for such corrections has been avoided in this work.

CHAPTER III AUXILIARY DOSIMETERS

To verify the performance of the calorimetric dosimeter system that was described in Chapter II, two further dosimeters were also designed and constructed. The first of these auxiliary dosimeters was an air-cavity ionization chamber, while the second was a Fricke, or ferrous sulphate, dosimeter. Both of these dosimeters were designed to resemble the calorimeter as closely as possible, with regards to their disturbance on the radiation beam, while retaining their own fundamental calibration.

These two auxiliary dosimeters have the further use in that they may be calibrated in terms of the calorimeter, at any photon energy, and then be used as practical dosimeters independent of the standard calorimetric system.

The theory of the design and operation of both the ionization chamber and Fricke dosimeters is well documented and so the following chapter will be restricted to a discussion of the properties and operation of the actual dosimeters constructed.

III.1 Air-Cavity Ionization Chamber

III.1.1 Materials and Design

The internal structure of the ionization chamber is shown in Figure III.1 and its resemblance to the calorimeter may be seen by refering back to Figure II.1. The ionization chamber and calorimeter

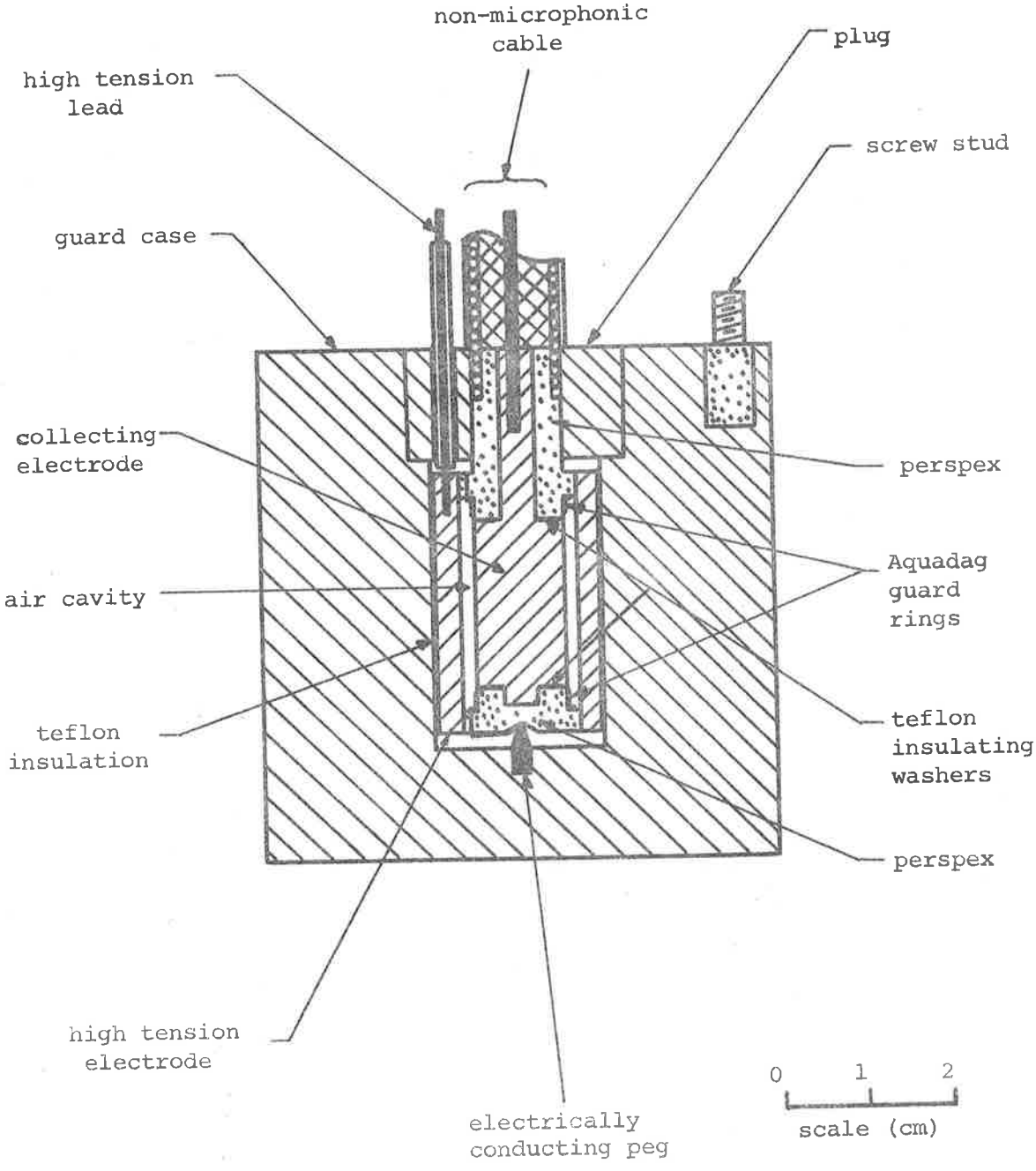

Fig.III.1 Internal Structure of the Air-Cavity Ionization Chamber.

have similar annular air cavities, but a little more perspex is used in the ionization chamber than in the calorimeter. The central collecting electrode is maintained close to earth potential, the charge collected by it being passed along a single-core non-microphonic cable to the charge measuring apparatus. The measuring apparatus is that which is being used currently on the present standard air-cavity ionization chamber and is based on the "Townsend Null Method" as modified by CROMPTON and SUTTON (1952). The annular high tension electrode may have either a high positive, or negative, potential applied to it by means of a simple, single-core lead. The outer guard case is maintained at earth potential because of its electrical continuity with the earthed shielding braid of the non-microphonic cable. The high tension electrode is insulated from the guard case by means of Teflon insulating tape (0.5 inch width and 0.0025 inch thickness) which is wound around the high tension electrode.

Guard rings have been included at each end of the air-cavity to produce a uniform axial and radial field distribution along the length of the collecting electrode, which in turn produces a geometrically well-defined collecting volume for the chamber of about 1.5 cm^3. The guard rings consist of layers of aquadag painted on the roughened surfaces of the perspex insulation as shown in Figure III.1. Both of the guard rings are maintained at earth potential by means of two very fine copper wires which pass through the perspex insulation at each end of the air-cavity, one end of each

wire is in contact with the guard case while the other ends are in contact with the respective guard rings. The guard rings are separated from the collecting electrode by means of Teflon washers of 0.0025 inch thickness.

The electrode assembly, the plug, and the cables form a permanently-assembled system, with only the guard case being removable from the ionization chamber. This proved suitable for the present work but, in future designs, an ionization chamber that could be more fully dismantled would be better, since this would allow periodic checks to be made on the guard rings, which may tend to lift off the perspex surfaces with 'ageing'. This effect can, however, be checked indirectly by making capacitance measurements on the chamber. The present ionization chamber has a capacitance of about 3.4 pF.

The ionization chamber and calorimeter are mounted in the vacuum chambers in different manners. The main requirement in the case of the ionization chamber is that the mounting be somewhat rigid so as to keep the relatively stiff non-microphonic cable under control. This was effected by using a thin-walled perspex tube, of about 2 cm diameter and about 9 cm in length, with flanges at both ends. The bottom flange is attached to the guard case by means of three screws, while the top flange is of similar shape to the perspex lid used in conjunction with the calorimeter but without the electrical leadthrough. The cables were free to pass up the centre of the tube

and out of the vacuum chamber. The positioning of the ionization chamber was checked radiographically.

III.1.2 Electrical Properties

The insulation between the various components was measured by a 'capacitance leak method' using a "Victoreen r-meter". The values of resistances were found to be as follows: $2 \times 10^{15}\Omega$ between the collecting and high tension electrodes, $4 \times 10^{15}\Omega$ between the guard case and the collecting electrode, and $1 \times 10^{11}\Omega$ between the guard case and the high tension electrode. These values were checked periodically during the course of the work and, although they did fluctuate, where found to be acceptable at all times.

The choice of the value of the applied potential to use on the ionization chamber was decided by reference to the following three criteria. (i) The range of permissible field intensities allowable within the ionization chamber is determined, at the lower limit, by the field intensity which will efficiently collect all of the ions produced in the collecting volume, without allowing a significant amount of ion recombination to occur. A field intensity of 250 volt/cm is quoted in the literature as being sufficient to attain reasonable saturation conditions. The upper limit of field intensity is determined by the condition that no extra ions should be produced by secondary collision processes and the value of field intensity where this commences is about 1,000 volt/cm. Thus, the

applied potential must produce field intensities in the ionization chamber within this permissible range. The field intensity, E, within this ionization chamber is readily found to be given by the following equation:

$$E = \frac{V}{r} \frac{1}{\ell n\ (a/b)} \qquad \ldots(III.1)$$

where V is the applied potential, a is the radius of the outer electrode, b is the radius of the inner electrode and r is the radial position at which the field is to be determined, between a and b. In the present ionization chamber we have, a = 0.7 cm and b = 0.5 cm. If we consider V = 100 volts, for example, then the maximum field intensity is 594 volt/cm (at r = b) and the minimum field intensity is 425 volt/cm (at r = a). Since both of these values are within the permissible range then 100 volts is an acceptable applied potential.

(ii) The theoretical efficiency of ion collection, f, for an applied potential of 100 volts, was calculated from the following expression, due to BOAG (1956), according to whom the "generalized saturation equation for parallel plate geometry" is:

$$f \equiv \left(\frac{\text{measured ion current}}{\text{ideal saturated current}}\right) = \frac{2}{1 + \sqrt{(1 + \psi^2)}} \qquad \ldots(III.2a)$$

where $\psi \equiv \frac{md^2\sqrt{q}}{V}$ $\qquad \ldots(III.2b)$

where q is the charge liberated/unit volume/sec (esu/cm^3 sec) and if it is known that conditions are not far from saturation then q may be equated with the measured exposure rate (roentgen/sec); V is the applied potential (volts); d is the plate separation for parallel plate geometry (cm). For other geometries an effective

value of d can be determined. In particular, for cylindrical geometry the value is given by $d = \kappa_{cyl}(a - b)$, where $\kappa_{cyl} = \left(\left(\frac{a/b + 1}{a/b - 1}\right) \frac{\ell n\,(a/b)}{2} \right)^{\frac{1}{2}}$. In the present chamber $\kappa_{cyl} = 1.005$, therefore d = 0.201 cm. The parameter m is a constant defined by $m = \left(\frac{2}{3} \frac{\alpha}{e\, k_+\, k_-}\right)^{\frac{1}{2}}$, where α is the recombination coefficient (cm^3/sec), e is the charge/ion (esu) and k_+ and k_- are the mobilities (cm^2/cm volt) of the positive and negative ions, respectively. GREENING (1964) gives an empirical value of the parameter m (defined above), namely m = 29.7. Although there was a serious error in his algebra, as pointed out by KATOH (1965), this experimental value of m is still acceptable. Thus, with d = 0.201 cm, V = 100 volt and with q = 40 roentgen/min $\simeq$ 0.7 esu/cm^3 sec, we obtain ψ = 0.0101, while the efficiency is calculated to be f = 99.997%. This is an extremely efficient collection of ions. Thus, the correction for non-perfect collection of ions, based on this theory is <0.01% and may be neglected. (iii) It was experimentally tested whether an applied potential of 100 volts did in fact produce saturation. For an applied potential of 50 volts the average measurement of exposure rate with the ionization chamber was found to be 38.77 roentgen/min, while for an applied potential of 155 volts the average result was 38.84 roentgen/min. A difference of only 0.18%, which showed that conditions were not far from saturation. GREENING (1964) indicated that to obtain the saturation value from a set of experimental values, for continuous radiation, one should plot the exposure rate,

ER, as a function of the quotient, ER/V^2, and extrapolate the resulting straight line to the ER axis. By assuming an equation of the form, $ER = A + B(ER/V^2)$, it was possible to gain an estimate of the correction for non-perfect saturation. Using the above two average measurements gave the following values, A = 38.85 roentgen/min (saturation value) and B = -5.0. The original equation may be re-arranged to solve for ER using these values of A and B, and this yields $ER = 38.85/(1 + 5/V^2)$. Therefore, when V = 100 volts, ER = 38.83 roentgen/min. Hence, the correction for non-perfect saturation is <0.1%, and again negligible.

It follows that, from both theoretical and experimental considerations, an applied potential of 100 volts is quite satisfactory.

III.1.3 Determination of Collection Volume.

For the ionization chamber to be calibrated in its own right it was necessary to make an accurate determination of its collection volume. This is, of course, unnecessary if the chamber is simply to be calibrated in terms of the calorimeter. The volume was estimated by three different methods and the weighted mean value used. (i) The volume was firstly estimated from a knowledge of the dimensions of the chamber, which were measured during its assembly and are listed below:

Inner diameter of the high tension electrode: $2R = (1.401 \pm 0.001)$ cm

Outer diameter of the collecting electrode: $2r = (0.999 \pm 0.001)$ cm

Length of the collecting electrode: $L = (2.026 \pm 0.015)$ cm

The volume is given by the following equation:

$$v_g = \pi L(R^2 - r^2) \qquad \ldots(III.3)$$

that is, $v_g = (1.535 \pm 0.009)\,cm^3$

(ii) The second estimation of the collecting volume is based on the measurement of the capacitance of the system. The capacitance of co-axial cylinders, in esu/volt or cm, is given by the following equation, $C = L/2\ell n\,(R/r)$.

Solving for R and substituting into equation (III.3) gives the result:

$$v_g = \pi L r^2 (e^{L/C} - 1) \qquad \ldots(III.4)$$

The capacitance of the ionization chamber was measured on a capacitance bridge against a standard capacitance, which had a nominal value of 10 pF. The measured value was, $C = (3.371 \pm 0.010)$ pF $= (3.030 \pm 0.009)$ cm, from which:

$$v_g = (1.511 \pm 0.013)\ cm^3$$

(iii) The final estimation was made by comparing the graphite chamber against the standard air-cavity ionization chamber. The standard chamber is of the parallel plate design and is constructed from perspex coated with aquadag. The collecting volume is $v_p = (1.563 \pm 0.0005)\ cm^3$, and the correction for attenuation of the radiation in the perspex wall is $\Theta_p = (1.014 \pm 0.0005)$.

NBS HANDBOOK 79 gives the following equation for the comparison of two ionization chambers whose walls are made of material of different atomic number, when exposed to identical fluxes of radiation.

$$\frac{m^{s^g}a}{m^{s^p}a} = \left(\frac{m^{\mu^g}en\ E^p_m}{m^{\mu^p}en\ E^g_m}\right) \qquad \ldots(III.5a)$$

where the superscript p refers to the standard perspex chamber while g refers to the graphite chamber; ${}_{m}s_{a}$ is the ratio of the mass stopping powers for the appropriate material (either perspex or graphite) compared with air; ${}_{m}\mu_{en}$ is the mass energy absorption coefficient for the appropriate material, and E_m is the number of ion pairs formed per unit mass of air in the cavities. If the density of the air is constant for the two measurements then we may replace E_m by E, where E is the number of ion pairs formed per unit volume. In practice, values of E are determined from a measurement of the total charge collected in a given time in a collection volume of v. This charge is measured in terms of the reading, P, on a potentiometer, and so we may write that $E \propto \Theta P/v$, where Θ is a correction factor for attenuation in the chamber wall. Equation (III.5a) may therefore be rewritten in the form that yields an expression for the collection volume of the graphite chamber, namely;

$$v_g = v_p \left(\frac{{}_{m}s_{a}^{g}}{{}_{m}s_{a}^{p}}\right) \left(\frac{{}_{m}\mu_{en}^{p}}{{}_{m}\mu_{en}^{g}}\right) \left(\frac{\Theta_g}{\Theta_p}\right) \left(\frac{P_g}{P_p}\right) \qquad \ldots(III.5b)$$

The values of P_p and P_g, measured under the same conditions, were found to be 0.3668 and 0.3649 volt, respectively (both with an uncertainty of ± 0.0003 volt). The values of ${}_{m}s_{a}$ and ${}_{m}\mu_{en}$ were obtained from NBS HANDBOOK 85, while the constants for the standard perspex chamber were given earlier. Due to the annular geometry involved, the attenuation correction factor for the graphite ionization chamber (Θ_g) was not easily determinable. An effective wall thickness was estimated by a numerical integration method, the principle of

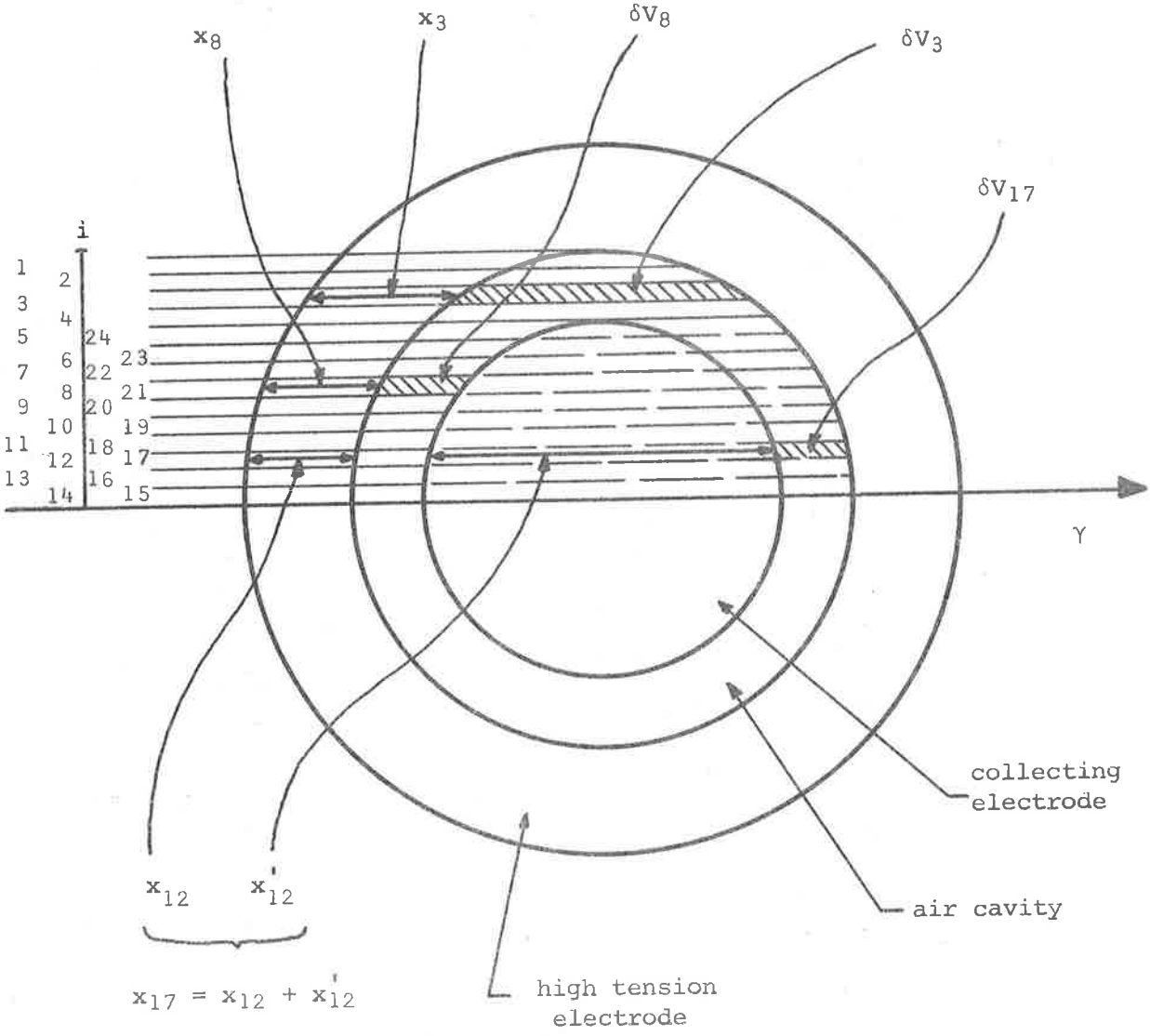

$$\text{Effective wall thickness, } x = \left(\frac{\sum_i x_i \delta V_i}{\sum_i \delta V_i}\right)$$

Fig.III.2 Estimation of Effective Wall Thickness of the Air-Cavity Ionization Chamber.

which may be seen by reference to Figure III.2. The incremental wall thickness was weighted according to the fraction of the collecting volume immediately behind the wall increment being considered. The method assumes that the beam is scattered only in the forward direction and also that the beam suffers insignificant attenuation when passing through air. Both of these assumptions are reasonable for megavoltage radiation. If the cross-section of the ionization chamber is divided into strips of equal width, as shown, then the volume of a particular strip of the air-cavity is proportional to its length. Due to symmetry about the direction of the incident radiation, only half of the cross-section need be considered. From the scaled diagram shown in Figure III.2, the effective wall thickness was found to be $\bar{x}$ = (0.60 ± 0.06) cm. An uncertainty of ±10% was assumed for this estimate of $\bar{x}$, and should be quite generous if one takes into account non-perfect integration, inadequacies in the assumptions made, etc.. However, this large uncertainty in $\bar{x}$ produces an uncertainty of only ±0.3% in the attenuation correction factor. The attenuation correction factor is $\Theta_g = \exp(\mu\bar{x})$, where $\mu = {}_m\mu^g_{en}\,\rho$. Substituting values gives the attenuation correction factor as $\Theta_g = 1.026$.

Thus, the volume of the graphite chamber is, from equation (III.5b):

$$v_g = (1.533 \pm 0.009)\ cm^3$$

Finally, the mean value, weighted according to the uncertainties of the individual estimates, is:

$$\underline{v_g = (1.530 \pm 0.009)\ cm^3}$$

III.1.4 Calibration of the Ionization Chamber

The ionization chamber is able to measure exposure in air on the following principle. The details of the charge measuring system are described by FRY (1954), but basically the system localizes the unknown collected charge in a standard capacitor and then neutralizes it by an equal charge of opposite sign, which is induced in the standard capacitor by varying the potential across its plates. The measurement of exposure rates reduces therefore to the measurement of rates of charge accumulation, and these in practice are further resolved into measurements of rates of change of voltage. Continuously-variable rates of change of voltage are provided by means of two potentiometers, one manually controlled and the other motor-driven. The voltage selected by the wiper of the manual potentiometer is applied to the motor-driven potentiometer and has the value V_{app}. The wiper of the second potentiometer rotates at a uniform rate, and so continuously-variable voltage sweep rates may be obtained by means of which the rate of collection of charge by the ionization chamber may be balanced.

The period of sweep (T) is known from the angular frequency of the motor (ω) and the total effective angle of rotation (ϕ) of the potentiometer wiper. Thus, the rate of change of potential from the motor-driven potentiometer is, $dV/dt = V_{app}/T = V_{app}(\omega/\phi)$ volt/sec. With the system on 'fast sweep' (that is with a

motor speed of about 16 rpm) substituting values for ϕ and ω gives a sweep rate of:

$$\frac{dV}{dt} = 0.3045\ V_{app} \qquad \text{(volt/sec)}$$

Now, the rate of applying charge to the standard capacitor is given by, $i = \dot{Q} = C_{std}\ \dot{V}$,

that is: $$i = 0.3045\ C_{std}\ V_{app} \qquad \text{(coul/sec)}$$

The standard capacitance was designed, constructed and calibrated at the National Standards Laboratory, C.S.I.R.O., Sydney in 1954. It was recalibrated in 1965 and found to have the value 10.003 pF (at 21.8°C). Thus, we have:

$$i = (9.131 \times 10^{-3})\ V_{app} \qquad \text{(esu/sec)}$$

or, $$i = Y_1\ V_{app}$$

The range of the system is coarsely varied by means of a number of secondary capacitors which have been calibrated against the standard 10 pF capacitor, each of which gives a different value of Y in the above equation. A particular capacitance used in the present work had the value 105.03 pF, with the corresponding value $Y_2 = (9.587 \times 10^{-2})$ esu/sec volt.

Now the exposure rate, ER, can be determined from:

$$ER = 60\ C(T, P)\ i/v_g \qquad \text{(roentgen/min)}$$

where C(T, P) is a correction factor, correcting the result to 0°C and 760 torr, and v_g is the collection volume of the chamber (cm^3).

In practice, V_{app} is measured with a "Cambridge" Potentiometer incorporating a potential drop circuit, with a drop ratio of B, on its input. If the measured potentiometer reading is P then, V_{app} = B P. Thus, we can finally write:

$$ER = \{60\ B\ C(T,P)\ Y\ P/v_g\}\ \text{(roentgen/min)} \qquad \ldots(III.6)$$

where, in the present ionization chamber, we have:

$v_g = 1.530\ cm^3$

$Y_1 = 0.009131$ esu/sec volt (for 10 pF)

$Y_2 = 0.09587$ esu/sec volt (for 100 pF)

The resistances in the potential drop circuit were secondary standards known to ±0.01% and B could have the nominal values of either 50 or 100. Overall, the exposure rates could be determined with an uncertainty of ±1.2%.

The ionization chamber measures the exposure rate effectively at the centre of the collecting electrode, while the calorimeter measures the dose rate at a similar position in the element. To all practical extent the environment of both is identical. For a comparison of the two dosimeters it is now necessary to be able to convert exposure rate measurements in the ionization chamber, in roentgen/min, to dose rates, in rad/min. The conversion is made by means of the Bragg-Gray relationship:

$$\text{Dose (in graphite)} = {}_m s_a^g\ W\ E_{air}$$

where E_{air} is the measured exposure in air, in roentgen; W is the

energy necessary to form 1 ion pair in air (33.7 eV/ion pair), and $_{m}s^{g}_{a}$ is the ratio of the mass stopping powers for graphite to air (for Co60 γ-radiation the value is 1.002). Thus, we have:

$$D_{graphite} = 0.871\ E_{air} \quad \text{(rad)} \qquad \ldots(III.7)$$

Thus, doses or dose rates could be determined with the ionization chamber with an overall uncertainty of ±1.4%.

III.1.5 Experimental Procedure

The practical procedure adopted for making measurements with the ionization chamber was as follows. A number of readings were taken with the radiation beam passing from left to right through the ionization chamber which had a positive potential applied to the high tension electrode, and then the same number of readings were taken with the polarity of the high tension reversed. This corrected for any difference in the collection of negative or positive ions. The difference was found to be small in the present graphite chamber. The above procedure was then repeated with the radiation beam passing from right to left through the ionization chamber. The reversal of the beam direction corrected for any slight error in setting the dosimeter at the correct source-to-centre distance. This procedure was adopted when using each of the three dosimeters. A final single result was obtained by averaging all of the above readings, which was usually about 12 in number. A typical calculation of an ionization chamber result is presented in Appendix IV.

This procedure was not very time-consuming, taking only about ½ hour to make the measurements, with about the same time necessary for setting up the equipment and allowing it to 'warm up'. This relatively short time is a distinct advantage of the ionization method over both the calorimetric or chemical methods of dosimetry.

There is the possibility of a small correction due to radiation being scattered from the perspex mount and cable, which does not occur in the case of the calorimeter. But, since the side scatter is of the order of only 1% and the scattered radiation is of lower quality, then the minimum of 1 cm of graphite, through which the scatter must pass to reach the collecting volume, will greatly reduce the contribution of the scatter to less than 0.1% and is thus insignificant.

III.2 The Fricke or Ferrous Sulphate Dosimeter

III.2.1 Materials and Design

The internal structure of the Fricke dosimeter is shown in Figure III.3 and, once again, the similarity to the calorimeter is apparent. The ferrous sulphate container is constructed from polythene (polyethylene) plastic since it is known not to cause appreciable oxidation of the solution that it contains (PETTERSSON and HETTINGER, 1967) (LAW, 1970a). The effects of storing ferrous sulphate solution in some plastics is equivalent to irradiating the solution to a dose rate of about 5 rad/min, due to the oxidizing

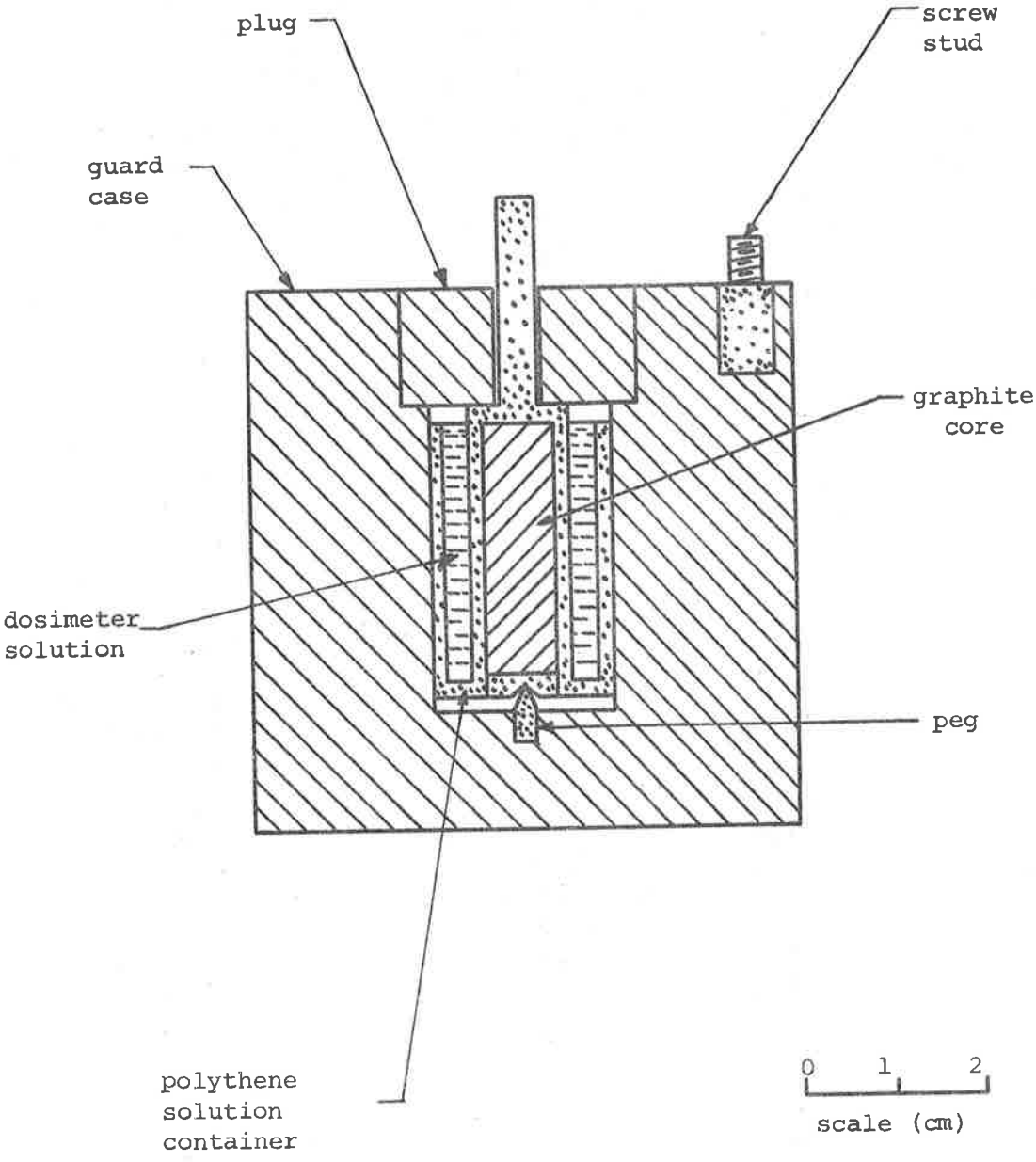

Fig.III.3 Internal Structure of Fricke Dosimeter.

effect of unreacted monomers, etc.. The density of polythene is only about 0.92 gm/cm^3 and so a graphite core was included to increase the average density of the material in the cavity of the guard case. The volume of the solution is limited to a maximum of about 3 cm^3. It is obvious, from Figure III.3, that in this dosimeter there is no 'air' gap as in both the calorimeter and the ionization chamber. The Fricke dosimeter and the calorimeter had the same overall dimensions but were not so alike as to cause identical disturbances on the primary radiation beam and hence, a correction was necessary for the results obtained with the Fricke dosimeter to allow comparisons with the calorimeter. The case is stoppered with the plug as in the other systems, but evaporation of the solution still occured to a small extent. The Fricke dosimeter was held in position in the vacuum chamber in the same manner as the ionization chamber, and the positioning was once again checked radiographically.

The ferrous sulphate solution used in the Fricke dosimeter can be varied somewhat in respect of both the proportions of the basic components and also of the additives which may be used to offset various detrimental effects. Information about the details of these and other such experimental factors may be gained from the work of such persons as, DAVIES and LAW (1963), BATTAERD and TREGEAR (1966), BRYANT and RIDLER (1968), BROSZKIEWICZ and BULHAK (1970) or LAW (1970b).

The particular solution employed in the present work consisted of, (i) 1mM Fe^{++} in the form of Mohr's salt or Ferrous Ammonium Sulphate $\{(NH_4)_2SO_4FeSO_46H_20\}$ which is less readily oxidised by air than is $FeSO_4$, (ii) 0.8N sulphuric acid (H_2SO_4), (iii) 1mM sodium chloride (NaCl) which minimizes the detrimental effects of any impurities present; the exact amount of NaCl present is not critical, and (iv) ultra-distilled water; double distilled and finally distilled over alkaline potassium permanganate.

The proportions of the three chemicals to make 200 ml of the above dosimeter solution were calculated to be; Mohr's salt, 78.43 mgm, assuming fully hydrated; sulphuric acid, 8.529 gm or 4.662 cm^3, assuming 92% concentration; and sodium chloride, 11.69 mgm. The components were measured on a "Sauter" balance and were of Analar grade, since the purity of the chemicals was the most important factor. The degree of hydration of the Mohr's salt and of the concentration of the sulphuric acid were in some doubt, but since these factors are not critical the chemicals on hand were used without extra treatment. Both the distilled water and the sulphuric acid were exposed to radiation, before making the above dosimeter solution, to pre-oxidize any impurities present in them.

The expected density of the dosimeter solution was 1.0239 gm/cm^3 (at 20^oC) but the measured density (using a specific gravity bottle) was found to be 1.0204 gm/cm^3 (at 20^oC); a difference

of 0.36%. Since the density of the solution is determined principally by the density of the sulphuric acid this result would suggest that the concentration of the original acid was, in fact, lower than the 92% assumed.

III.2.2 Calibration of Fricke Dosimeter

A one millimolar solution of Mohr's salt contains 55.85 mgm of Fe^{++}/litre of solution, or $(6.024 \times 10^{23} \times 10^{-3})Fe^{++}$ atoms/litre. If G is the number of molecules oxidized/100eV, then the energy required to produce complete oxidation of ferrous to ferric ions in the solution is, $(6.024 \times 10^{20})(100/G)$ eV/litre. Thus, the dose received in the dosimeter solution is, $(6.187 \times 10^{4}/\rho_{soln})$ rad; where ρ_{soln} is the density of the solution and we have used G = 15.6 mole/100 eV. Thus, the dose for the complete oxidation of 1 mM Fe^{++} solution is (6.063×10^{4}) rad. It is of interest to note that this is the maximum total dose that can be measured by this particular dosimeter solution.

There are a number of ways of measuring the ferric ion yield in the dosimeter solution, probably the most convenient for the physicist is an optical method employing a spectrophotometer. In this method the change in optical density, ΔOD, of the solution per cm of light path is measured at a standard wavelength. If the molar extinction coefficient (the maximum increase in optical density per cm of light path that can be induced in the dosimeter

solution) of ferric ions in 0.8N H_2SO_4, at the specified wavelength, is ε then we have:

$$\text{Dose (in } Fe^{++} \text{ solution)} = (6.063 \times 10^4)\left(\frac{\Delta OD}{\varepsilon}\right) \quad \ldots(III.8)$$

The absorption spectrum of ferric sulphate has two peaks in the ultraviolet region at approximately 224 mμ and 305 mμ, thus providing two suitable wavelengths for the measurement of optical density. The optical density measurements are dependent on the temperature of the solution at the time of measurement, hence a correction is necessary. In the present work the values of ΔOD have been measured at both wavelengths on all occasions, and expressed at 25°C.

NBS HANDBOOK 85 gives the following information for a 1 mM solution at 25°C.

At a wavelength of 304 mμ, ε = 2.196, with a temperature correction of 0.69%/°C;

while at 224 mμ, ε = 4.565, with a temperature correction of 0.13%/°C.

Thus, we have from equation (III.8);

at 304 mμ, Dose(in Fe^{++} solution) = $\Delta OD_{25}(27.60 \times 10^3)$ rad ...(III.8a)

at 224 mμ, Dose(in Fe^{++} solution) = $\Delta OD_{25}(13.28 \times 10^3)$ rad ...(III.8b)

where ΔOD_{25} refers to the measured change in OD due to radiation, corrected to 25°C.

A number of corrections are necessary for the dosimeter to yield a correct measurement of dose. (i) Evaporation losses from the dosimeter solution, between the initial and final measurements of OD, will tend to increase the measured change in OD. The evaporation loss is about 3 mgm of water per hour, which produces a correction of about -0.1%/hour between the initial and final OD measurements. Since exposure times of the order of 6 hours are used in the present work, then this correction is significant. (ii) Other oxidation effects, not due to the radiation or self-oxidation (since OD measurements are made against a control sample of solution) tend to increase the measured dose rate. The order of this effect was determined to be about 0.5 rad/min, which again is significant. The above two corrections were determined each time the Fricke dosimeter was used and will be more fully explained in section III.2.3 and Appendix V. (iii) A further correction involves the conversion of the readings made in the Fricke dosimeter to equivalent readings made in the calorimeter. This conversion involves two considerations. The first is due to the requirement that the disturbance on the primary beam should be the same in both the Fricke dosimeter and the calorimeter. If Compton scattering is the predominant effect at the photon energies under consideration, then we should have that the average electron densities in the cavities of the two guard cases be the same. Since electron density is proportional to the mass density then a correction for the difference in the average cavity densities is,

$(\frac{\text{ave density of calorimeter cavity}}{\text{ave density of Fricke cavity}})$. The second consideration is that the energy absorbed in the dosimeter solution is different from that in graphite, being in the ratio of their mass energy absorption coefficients. Thus, the appropriate correction factor is, $(_{m}\mu^{g}_{en} / _{m}\mu^{Fe}_{en})$, where to a good approximation we have, $_{m}\mu^{Fe}_{en} = \rho_{soln}\ _{m}\mu^{water}_{en}$. Substituting the values for these factors gave this ratio as 0.881. The overall conversion factor is;

$$(\frac{\text{Dose in calorimeter}}{\text{Dose in Fricke dosimeter}}) = (0.881)(\frac{\text{ave density of calorimeter cavity}}{\text{ave density of Fricke cavity}}) \quad \ldots(III.9)$$

Since the mass of the dosimeter solution varies slightly from test to test then the density correction factor must be determined for each test separately, but is usually close to 1.037. A typical calculation is shown in Appendix V. For this density correction factor the final conversion is:

Dose (in calorimeter) = 0.914 Dose (in Fricke dosimeter)

III.2.3 Experimental Procedure

As indicated earlier the effect of impurities can cause inaccuracies thus all glassware and containers storing the dosimeter solution and component chemicals were rigorously cleaned. The dosimeter solution was stored in a stoppered bottle, which was protected from light. The spectrophotometer used in this work was a "UNICAM" SP500 together with "UNICAM" Silica absorption cells of 10 mm light path and approximately 2.6 ml volume.

The following routine was used with this dosimeter. All glassware was previously cleaned and rinsed with the dosimeter solution. Two spectrophotometer cells were filled with the dosimeter solution and the initial density measurements made of one cell and contents, using the other cell and contents as a reference. This initial reading was usually very small and temperature correction was never found necessary.

The solution whose initial optical density was measured was placed in the polythene irradiating container and the mass of the solution determined. A knowledge of the mass of the solution was necessary for both the evaporation correction and for the density correction. The polythene container and solution were then placed in the guard case which, in turn, was mounted in the vacuum chamber. The dosimeter was exposed for half the desired exposure time with the radiation beam passing from left to right through the system, and then irradiated for the remaining time with the beam in the reverse direction.

The mass of the dosimeter solution was again determined, and the amount of water lost by evaporation during the two mass measurements was expressed as a percentage of the original mass of the solution. The irradiated solution was once more placed in the spectrophotometer cell and the OD measured again, noting the temperature of the solution. From the difference between the initial

and this final value of OD one obtained the quantity ΔOD_t, which was then corrected to 25°C to give ΔOD_{25}. This change in OD was then corrected for evaporation losses. The dose calculated by this change in OD had then to be corrected for the effective dose rate due to other oxidizing effects. To obtain an estimate of this effective dose rate the irradiated solution was placed back into the polythene container, and its new mass determined. The container and solution were then allowed to stand in a dark cupboard for at least a day. After a known time the solution was weighed again to determine the mass of the solution lost by evaporation and the final optical density of the solution again determined. The effective dose rate was then determined over the period that the solution was left to stand in the cupboard. This effective dose rate was subtracted from the earlier estimate of dose rate to give a final value. A typical calculation for the Fricke dosimeter is presented in Appendix V.

CHAPTER IV OPERATION OF CALORIMETER AND RESULTS

In this chapter we shall first review the method of analysis of the graphical results and of the operation of the calorimeter. Certain preliminary tests are then described which give a number of experimental properties of the equipment used and, finally, the results of intercomparison tests between the three dosimetric systems are presented.

IV.1 Operation of the Calorimeter

IV.1.1 Analysis of Graphical Results

From the considerations presented in chapter II it is apparent that the output of the millimicrovoltmeter is directly proportional to the dose received by the calorimeter element, or, if we extend the argument further, that the deflection noted on the vertical axis of the chart output, namely X (divs), is proportional to the actual energy deposited, namely E(erg). It is also expected from theoretical considerations that, after the initial transient period, the traces would be essentially linear with time. Figure IV.1 shows how the traces are expected to appear, noting that since the element will rarely, if ever, be at equilibrium temperature then the initial and final portions of the traces will always have some slope. A trace actually obtained in this work, with a typical noise level, is shown in Figure IV.2. It is the aim of the electric calibration procedure to determine the conversion factor

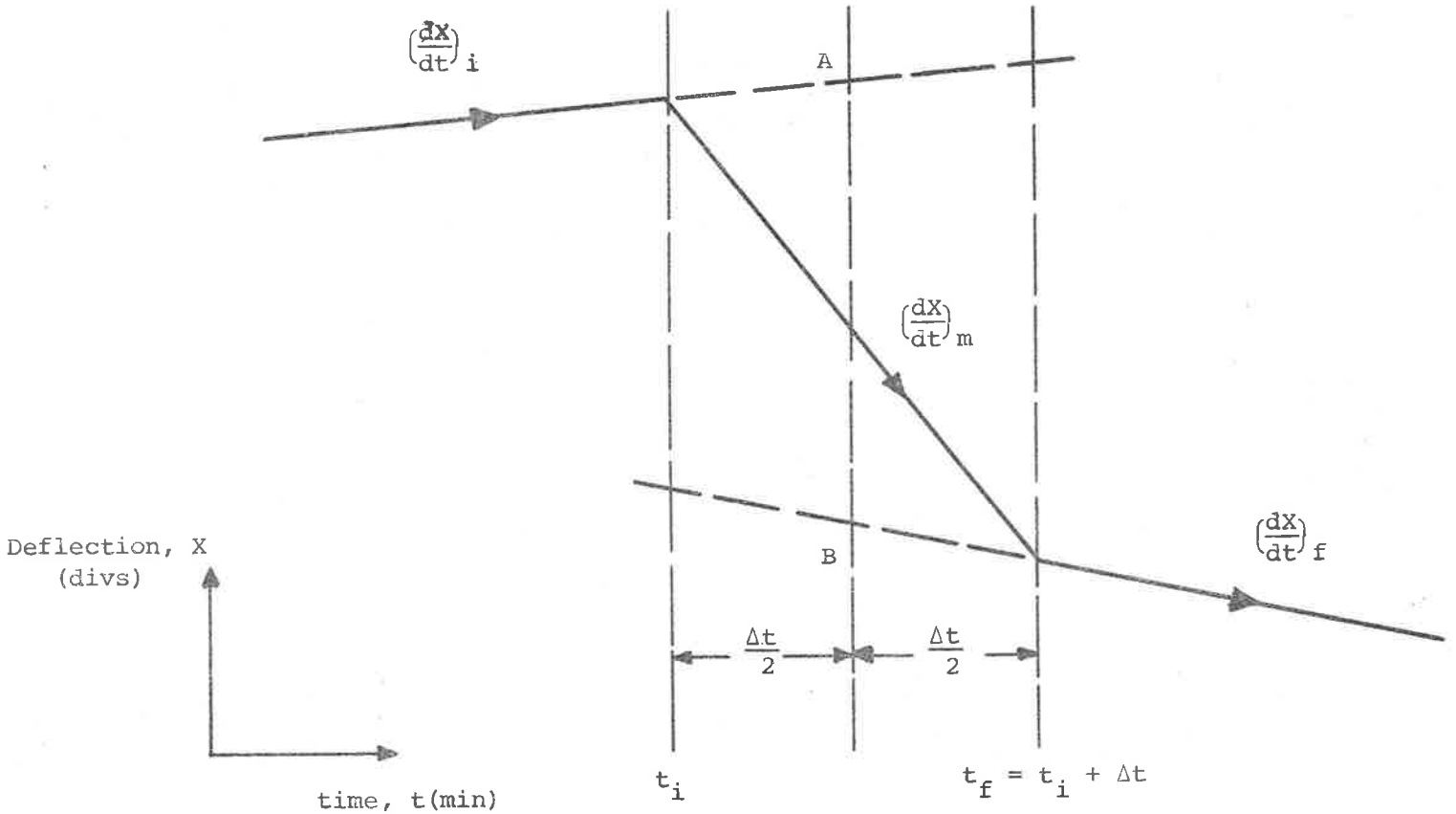

Fig.IV.1 Expected Form of Trace from Calorimeter Output.

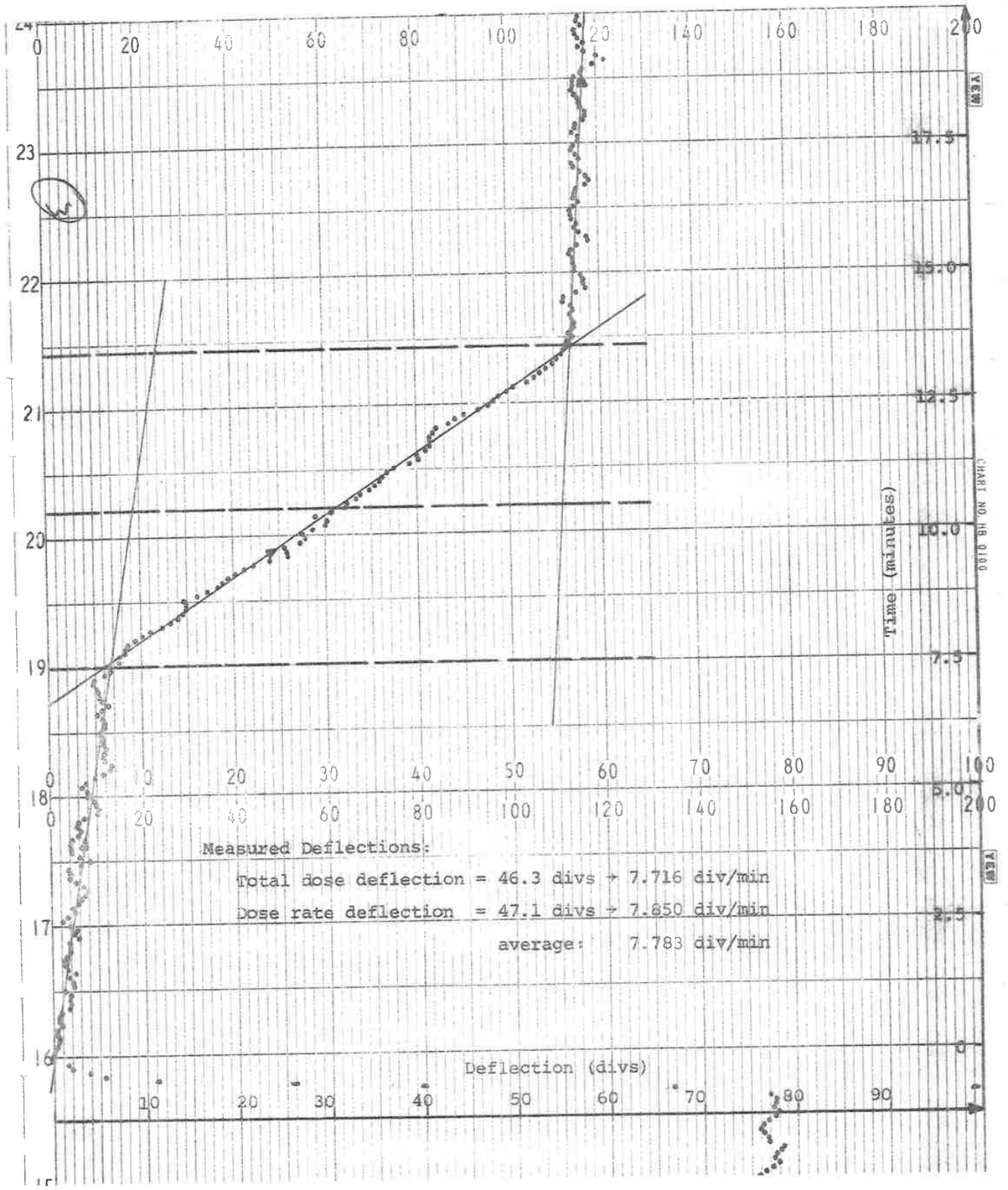

Fiv.IV.2 Actual Trace Obtained during the Course of the Present Work which Shows a Typical Noise Level. The Exposure Time was 6 minutes, and the Temperature Measuring Bridge Employed 2 Hg Cells.

for the deflection axis of the charts. The calibration factor is D_c/X_c (rad/div), where D_c (rad) is the known electric dose input and X_c (div) is the corresponding chart deflection. A problem that remains is that of interpreting the graphical output so as to give the true deflection, X_t, from the measured deflection, X_m, which includes the effect of energy losses or gains. The following analysis leads to two methods of interpreting the charts so as to give the true deflections from the observed or measured deflections.

Applying the conservation of energy to a single calorimetric system, with small heat losses or gains, gives the true rate of change of energy in the element $(dE/dt)_t$ as:

$$\left(\frac{dE}{dt}\right)_t = \left(\frac{dE}{dt}\right)_m + K(T_e - T_o) \qquad \ldots(IV.1)$$

where $(dE/dt)_m$ is the measured rate of change of energy; K is the thermal 'conductance' of the system; while T_e and T_o are the temperatures of the element and its surroundings, respectively. LAUGHLIN and GENNA (1956) have shown that an equation of the form of equation IV.1 can be applied to a twin calorimetric system, where T_o is an effective temperature of the dummy element. This assumes that both the thermistors and the heat transfer coefficients for the test and reference calorimeters are reasonably matched, as is the case in the present work. GENNA *et al* (1963) have shown that the integration of equation (IV.1) with respect to time, between the initial and final times of an exposure t_i and t_f respectively, yields the

result:

$$E_t = \left(E_m - \left(\frac{t_f - t_i}{2}\right)\left\{\left(\frac{dE}{dt}\right)_i + \left(\frac{dE}{dt}\right)_f\right\}\right) \qquad \ldots(IV.2)$$

This integration assumes that T_o remains constant during periods of no external energy input. An analysis taking into account the empirical fact that the reference temperature will be varying slightly, at an essentially constant rate over the periods of interest, yields a result identical with equation (IV.2). Since, X(div) $\propto$ E(erg), then we may write the basic equation as; from equation (IV.2):

$$X_t = \left(X_m - \frac{\Delta t}{2}\left\{\left(\frac{dX}{dt}\right)_i + \left(\frac{dX}{dt}\right)_f\right\}\right) \qquad \ldots(IV.3)$$

where, $\Delta t = (t_f - t_i)$ is the exposure time. This equation leads to one method of chart analysis, referred to as the Total Dose method. This method can be understood by reference to Figure IV.1. The Total Dose method measures the deflection AB on the chart, which is the deflection between the extrapolated initial and final traces at the midpoint of the exposure period. This method requires the time of the exposure to be known accurately and to be defined accurately on the chart, but does not require a knowledge of the slope of the trace during the exposure. The result can be expressed as a rate of change, such as is usually required in practice.

If equation (IV.3) is differentiated with respect to time, we obtain:

$$\left(\frac{dX}{dt}\right)_t = \left(\left(\frac{dX}{dt}\right)_m - \tfrac{1}{2}\left\{\left(\frac{dX}{dt}\right)_i + \left(\frac{dX}{dt}\right)_f\right\}\right) \qquad \ldots(IV.4)$$

This equation leads to a second method of chart analysis, referred to as the Dose Rate method. This method measures the deflection rate during the exposure, which is then corrected by the average deflection rate measured on the initial and final traces. This method does not require the exposure time to be known at all, makes use of the slope of the trace during the exposure, and gives dose rates directly.

The two methods of analysis should, obviously, lead to the same final value but, in practice, due to the effect of noise on the traces, it was not common for the two methods to give the same result. Previous authors have always selected one or the other method of analysis, however, I could see no a priori reason to select one method as being better than the other. Since the two methods are relatively independent of each other, then the use of both methods should permit two estimates of the same quantity from each chart. In practice, both methods of analysis were used at all times and the average taken. This routine also permits a certain degree of checking on the drawing of the construction lines on the charts required by the analysis, since both methods should be self-consistent to a reasonable degree, say a percent or two. The relative merits of the two methods of analysis are examined in more detail in section IV.3.4 from results based on experimental data.

IV.1.2 Experimental Procedure

On the basis of the theoretical considerations discussed so far, the following procedure was adopted and found satisfactory. The same exposure times were used for both electric calibration and for radiation measurement. Similar, although slightly higher, electric dose rates were used in the calibration than those measured from the radiation, so as to gain a slightly more favourable reading-to-noise ratio in the calibration procedure.

The calorimeter box was aligned with the radiation machine about 3 hours before measurements were to be made. The evacuation of the vacuum chambers was commenced and the milli-microvoltmeter turned on to allow time for the unit to stabilize. After about 2 hours the vacuum pressure was sufficiently low (about 10^{-2} torr) to permit the bridge to be turned on (with the potential on either forward or reverse) so as to allow it to reach thermal equilibrium in the following hour.

With all the components in working state, the procedure was to carry out (i) electric calibration, (ii) radiation measurement with beam passing from left to right, (iii) radiation measurement with beam passing from right to left, and (iv) electric calibration. The results of these tests were reduced to give one measurement of dose rate for the given bridge potential polarity. The bridge

polarity was then reversed and the above procedure repeated to give another single measurement of dose rate. As was mentioned earlier, the reversal of the polarity of the potential on the bridge allows compensation for any possible thermoelectric effects present in the bridge. The series of measurements made with the calorimeter, which are given in section IV.3, indicated that, in fact, there was no significant difference between results obtained on either polarity. This indicates that any thermoelectric effects present are certainly no larger than the noise level of the equipment. But, since the average result, of both reverse and forward polarity measurements, should be a better estimate from a purely statistical point of view (being the average of 4 calibrations and 4 radiation measurements, with each of the 8 charts being analysed by two methods), then this procedure was continued.

The recycling time for the calorimetric system is about 15 - 20 minutes, for a 5 or 6 minute exposure, with about the same time for the initial and final traces. The overall procedure described above for taking the measurements took about 4 hours and resulted in one final measurement of radiation dose rate. The internal variations within this final estimate of dose rate were about the same as those obtained when using the air-cavity ionization chamber, which were also averaged out to give one estimate of dose rate. A typical calculation of a calorimeter result is presented in Appendix VI.

IV.2 Preliminary Results

IV.2.1 Initial Tests

A number of small tests were made at the commencement of this work after the dosimeters had been assembled and calibrated. (i) One of the first tests was the determination of a suitable voltage for the air-cavity ionization chamber, as was described in section III.1.2. (ii) The ionization chamber was used to gain an estimate of the attenuation of the radiation due to the wooden box, vacuum chamber wall and guard case, since it could be used freely in air. The attenuation due to the guard case alone was found to be 6.8%, which is considered as quite satisfactory. The attenuation due to the wooden box and vacuum chamber walls together, was found to be 33.4%, thus producing an overall attenuation of the radiation beam reaching the calorimeter element of 37.9%. As mentioned in section II.2.2, this amount of attenuation was considered excessive and sets a limit to the minimum dose rate that can be measured with accuracy by the calorimeter. (iii) The ionization chamber was also used to measure the dose received by the dummy calorimeter, due to scattered radiation reaching it, when the calorimetric system is being used. This was effected by replacing the dummy calorimeter by the ionization chamber and then irradiating the test calorimeter as in a normal test, but without the calorimetric system being on. The dose rate measured by the ionization chamber was expressed as a percentage of the known dose rate

received by the test calorimeter, which was previously determined by the ionization chamber at the test calorimeter position. Since two Teletherapy units were used, under slightly different conditions, this correction for scatter was determined for both units. As a percentage of the dose received by the test calorimeter, the scatter received by the dummy calorimeter with the Picker unit was 0.45% and with the Orbitron unit was 0.40%, each result being the average of a number of measurements. (iv) A time correction was necessary for the Teletherapy units since the exposure timers on the units indicate the time that the radiation is fully on. However, during the time that the exposure shutters of the units are opening and closing, there is a small amount of radiation being emitted from the unit, which makes the actual exposure time slightly larger than indicated on the exposure timer. This small increase in exposure time was determined on a number of occasions, for both the Picker and Orbitron units, by the following method. Exposure readings were made with the aid of a "Victoreen r-meter" for a number of exposure times, as indicated on the timer of the unit. The measured exposure values were then plotted as a function of the presumed exposure times, producing a straight line graph. The extrapolation of this straight line graph back to the exposure time axis gave the desired value of the excess exposure time. The excess time for the Picker unit was found to be 0.03 min and for the Orbitron Unit was found to be 0.01 min. These excess times are small and

insignificant as far as therapeutic use of the unit is concerned, but are significant in the present work.

IV.2.2 Linearity of Response with Exposure Time

Theoretical arguments showing that the response of the calorimeter should be linear with exposure time were presented in section II.5.3. A short test was thought necessary to check these conclusions, with the intention that if the results were found contradictory to expectations, further tests would be performed. These tests were performed using the calibration facility of the calorimeter, with measurements being performed at a number of different exposure times between 4 and 10 minutes, which covered the time intervals of interest.

If (D_c/X_c) is the calibration factor for the calorimeter, then the measured dose, D_m, is determined from the measured deflection, X_m, by the following relation:

$$D_m = \left(\frac{D_c}{X_c}\right) X_m \qquad \ldots(IV.5)$$

Also, from equation (II.32) we have that:

$$E_{stored} = P_2 f(t)$$

where the time function is defined in equation (II.32). For the case of an ideal system with no energy losses we would have that $f(t) = t$. In equation (II.32) E_{stored} corresponds to the measured dose D_m, and if we understand that P_2 is now expressed in rad/min,

while f(t) is in minutes, then we may write:

$$D_m = P_2 f(t) \qquad \ldots(IV.6)$$

Equating equations (IV.5) and (IV.6), and re-arranging gives:

$$\left(\frac{X_m}{P_2}\right) = \frac{f(t)}{(D_c/X_c)} = A\, f(t) \qquad \ldots(IV.7)$$

The function f(t) cannot be expressed in terms of a simple polynomial to a great accuracy, but, for the purposes of the present test, the function $f(t) = t(1 + Bt)$ has been assumed, where B is a small correction factor to take into account energy losses. Thus, equation (IV.7) can be written in the form:

$$y \equiv \left(\frac{X_m}{P_2 t}\right) = A(1 + Bt) \qquad \ldots(IV.8)$$

If the deflection, X_m(div), is measured corresponding to a known electric dose rate, P_2 (rad/min), for various exposure times, t(min), then plotting the function y, defined by equation (IV.8), as a function of exposure time should produce a reasonably straight line graph with slope AB. The results so plotted are shown in Figure IV.3, where each point is the average of a number of measurements made on a given day. Applying the "Method of Least Squares" to these results gave the values of the constants as:
$B = (-0.0024 \pm 0.0029)\text{min}^{-1}$ and, $A = (0.1511 \pm 0.0032)$ div/rad. The limits of uncertainty for these constants were estimated by making least square fits to the two sets of results separately, while the actual values quoted were determined by using all of the results. It is now possible to estimate the percentage of the energy that is lost

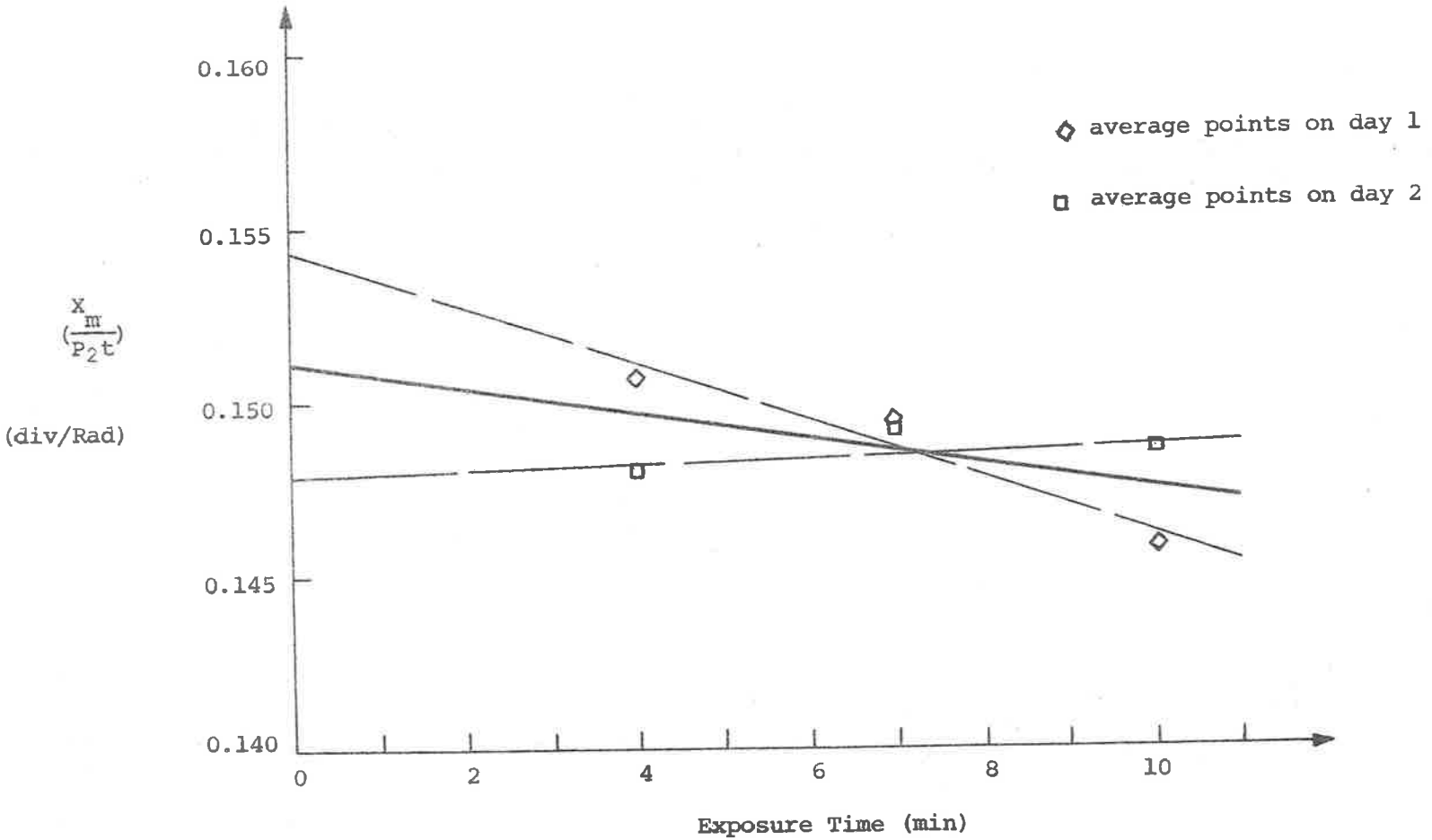

Fig.IV.3 Test of the Linearity of Response of the Calorimeter with Exposure Time.

for a given exposure time and to compare these 'experimental' values with the 'theoretical' values obtained by considering the function f(t). These comparisons are shown in Table IV.1.

TABLE IV.1

Comparison of energy losses from the calorimeter element as predicted by theory and as actually obtained from experiment.

Exposure Times (min)	% Energy Losses	
	Experimental	Theoretical
4	-1.0	-0.7
6	-1.4	-1.1
8	-1.9	-2.0

The agreement between the two sets of values is very good, especially when it is remembered that only a quadratic fit was applied to the experimental results which, in fact, is only a fair approximation to the function f(t). It should also be remembered that the function f(t) is not the only source of non-linearity within the calorimetric system, as was summarized in section II.5.1. Thus, the system is, in practice as well as theory, very closely linear.

IV.3 Results

IV.3.1 Picker Teletherapy Unit

The early tests of intercomparing the calorimeter with

the air-cavity ionization chamber were performed on this unit, entirely for reasons of convenience, since the unit is least used for therapy. However, the unit could not give indefinite exposure times and was, thus, not suitable for use with the Fricke dosimeter. The Picker unit was used with a source-to-centre distance of 55 cm and a field size of 12 x 12 cm. The measurements of dose rate obtained for this unit, each corrected to the 1st January, 1970, are shown in Table IV.2, for both the ionization chamber and the calorimeter. To permit comparison with the results obtained with the Orbitron unit, each measurement of dose rate was normalized by the overall average dose rate for the Picker unit.

TABLE IV.2

Measurement of dose rate on Picker unit, corrected to 1st January, 1970.

Ionization Chamber measurements:

	Date measurement performed.	Measured dose rate (rad/min)		Normalized result.
(i)	19th Dec. 1969	33.67		1.0189
(ii)	7th Jan. 1970	32.81		0.9924
(iii)	9th Jan. 1970	32.90		0.9957
		average (33.13 ± 0.37)		

Calorimeter measurements:

(i)	13th Sep. 1969	39.92)	calori-meter I	0.9963
(ii)	6th Dec. 1969	33.37)		1.0099
(iii)	2nd May 1970	32.60	calori-meter II	0.9864
		average (32.96 ± 0.30)		

....

Overall average dose rate on Picker unit = (33.05 ± 0.32) rad/min

or more correctly, DR = (33.0 ± 0.3) rad/min

The average values obtained by the two dosimeters, separately, agree to 0.5%, which is within the experimental uncertainty of ±1% for both sets of results. These results are quite satisfactory.

IV.3.2 Orbitron Teletherapy Unit

This unit, although in greater demand, allowed indefinite exposure times to be made, thus permitting the Fricke dosimeter to be tested. The unit also had a slightly larger exposure output. The Orbitron unit was used at a source-to-centre distance of 67 cm and a field size of 12 x 12 cm. The measurements of dose rate obtained for this unit, corrected to the 1st July 1970, are shown in Table IV.3, for the three dosimeters under examination. Again each measurement of dose rate was normalized by the overall average dose rate for the Orbitron unit.

The difference between the average values obtained separately for the ionization chamber and the calorimeter is 0.3%, similar to that obtained on the Picker unit; while for the calorimeter and the Fricke dosimeter the difference is 0.2%. The mean deviations of the average results for the calorimeter and for the Fricke dosimeter are both about ±1%, while the mean deviation for the ionization chamber results appears unusually low at ±0.3%. Again these results are quite satisfactory.

TABLE IV.3

Measurement of dose rate on Orbitron unit, corrected to 1st July 1970.

Ionization Chamber measurements:

	Date measurement performed.	Measured dose rate (rad/min)	Normalized result.
(iv)	24th May 1970	38.90	1.0010
(v)	18th Jul. 1970	39.14	1.0072
(vi)	27th Oct. 1970	38.88	1.0005
		average (38.97 ± 0.11)	

Calorimeter measurements:

(iv)	30th May 1970	38.44	0.9891
(v)	31st May 1970	39.14	1.0072
(vi)	14th Jun. 1970	39.28	1.0108
(vii)	9th Aug. 1970	38.36	0.9871
(viii)	14th Nov. 1970	39.01	1.0038
		average (38.85 ± 0.36)	

Fricke Dosimeter measurements:

(i)	19th Jul. 1970	38.51	0.9909
(ii)	25th Jul. 1970	38.61	0.9935
(iii)	8th Aug. 1970	39.12	1.0066
(iv)	22nd Aug. 1970	38.93	1.0018
		average (38.79 ± 0.24)	

Overall average dose rate on Orbitron unit = (38.86 ± 0.25) rad/min

or more correctly, DR = (38.9 ± 0.3) rad/min

IV.3.3 Observations from Results

The average of the normalized results, together with their mean deviations, were determined for the three dosimeters to be:

Calorimeter:	(0.9988 ± 0.009)	(average of 8 results)
Ionization chamber:	(1.0026 ± 0.007)	(average of 6 results)
Fricke dosimeter:	(0.9982 ± 0.006)	(average of 4 results)

It is readily seen from these figures that each of the dosimeters gave results which were within their mean deviations, which was of the order of ±1% in each case.

To give some physical significance to these results it is possible to determine effective values of both W for the ionization chamber and G for the Fricke dosimeter. In section III.1.4 it was stated that the value W = 33.7 eV/ion pair was used in the calibration of the ionization chamber. By considering the following ratio it is possible to calculate an effective value of W from the above results.

$$\left(\frac{\text{average normalized ion chamber result}}{\text{average normalized calorimeter result}}\right) = (1.004 \pm 0.016)$$

therefore, the effective W = (33.6 ± 0.5) eV/ion pair

This value suggests a slightly lower value of W but the difference from the accepted value of (33.73 ± 0.15) eV/ion pair (NBS HANDBOOK 85) is not significant.

Similarly, the value of G = 15.6 mole/100 eV was used in the calibration of the Fricke dosimeter and by considering the

following ratio an effective value of G can be determined from the above results.

$$\left(\frac{\text{average normalized Fricke dosimeter result}}{\text{average normalized calorimeter result}}\right) = (0.999 \pm 0.015)$$

therefore, the effective G = (15.6 ± 0.2) moles/100 eV

Again there is no significant difference from the accepted value of (15.69 ± 0.19) mole/100 eV (NBS HANDBOOK 85).

The calculation of these effective values of W and G indicate that the results obtained with the calorimeter are comparable with those obtained with both the ionization chamber and the Fricke dosimeter. The work, however, was not designed to estimate the values of W and G with any precision.

It is now possible to determine if there is any significant difference between the results obtained with calorimeter I compared with those obtained with calorimeter II. The average normalized result for calorimeter I is (1.0031 ± 0.0068) and the average normalized result for calorimeter II is (0.9974 ± 0.0099). The ratio of these results is (1.006 ± 0.017). This value suggests that the calorimeter I results are slightly higher than those for calorimeter II, by 0.6%, but the result is not significant, especially due to the limited number of results obtained with calorimeter I.

IV.3.4 Tests on the Methods of Chart Analysis

The calorimeter results were used to examine the two methods of chart analysis described in section IV.1.1. It will be remembered that, on each day of making measurements with the calorimeter, 8 charts were recorded and the results of each were averaged to give a single result of dose rate for the day. Tests were performed with the calorimeter on 8 days, over 12 months, giving a total of 64 charts, each being analysed by both the Total Dose and the Dose Rate methods. These 64 pairs of results are shown in Figure IV.4. The first, and probably most obvious, test was to calculate the correlation coefficient for the results obtained by the two methods. Since it is expected that the distribution of the points from the line of 'perfect correlation' should obey a normal distribution, then the correlation coefficient, r, is given by equation (IV.9).

$$r = \frac{\sum (x_i - \bar{x})(y_i - \bar{y})}{\left(\sum (x_i - \bar{x})^2 \sum (y_i - \bar{y})^2\right)^{\frac{1}{2}}} \qquad \ldots(IV.9)$$

where x_i are the deflections (divs) obtained by the Total Dose method, with $\bar{x}$ being the mean of these results, and y_i are the deflections (divs) obtained by the Dose Rate method, with $\bar{y}$ being the mean of these results. The value of the correlation coefficient was calculated to be, $r = 0.98$, which indicates a very strong correlation between the two sets of results. This is, as would be expected, with the non-perfect correlation being due to the effect of noise on the traces.

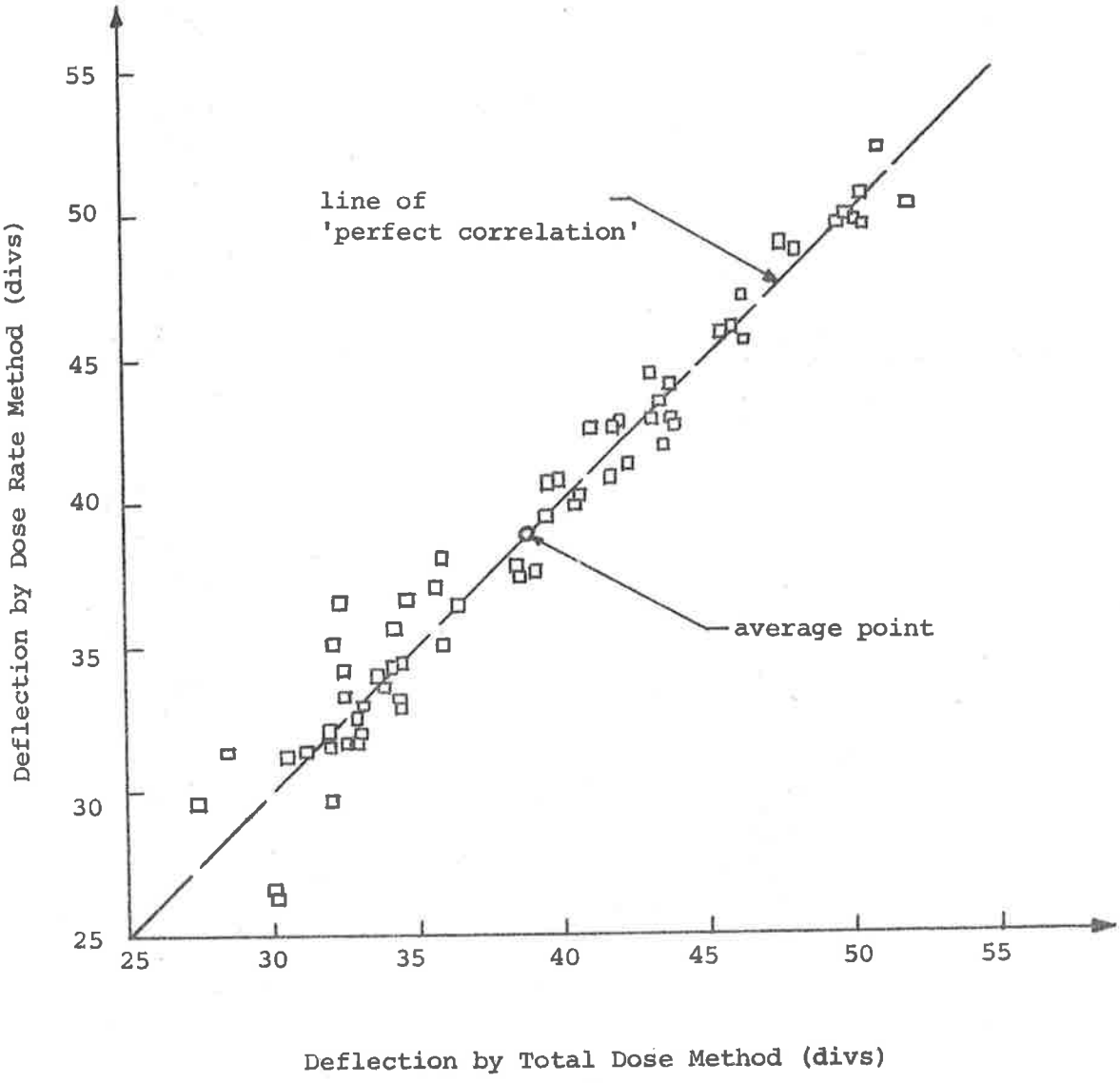

Fig.IV.4 Scatter Diagram showing the Correlation between Results Obtained by the Two Methods of Chart Analysis.

As a means of further comparing the results obtained by the two methods, the deflections obtained by each method were averaged over each set, that is over the 8 charts obtained on each day of measurement. This is because this average is the more relevant quantity in the final analysis. The internal mean deviations within each set were also calculated for each method of analysis. The following ratios were then considered for each set separately, and then the average of the ratios determined for the 8 sets.

(i) $\left(\frac{\text{average deflection from the Dose Rate method}}{\text{average deflection from the Total Dose method}}\right) = (1.000 \pm 0.011)$

This indicates that the average results obtained, by both methods of analysis, for a set, are the same, at least when averaged over 8 sets. This is also as would be expected since there is no a priori reason to expect the results of one method to be different from, or better than, the other. The average deviation of ±1.1% between the two methods is also quite reasonable.

(ii) $\left(\frac{\text{ave internal mean deviation from Dose Rate method}}{\text{ave internal mean deviation from Total Dose method}}\right) = (1.014 \pm 0.056)$

This suggests that the Total Dose method gives slightly more consistent results for a set than does the Dose Rate method, at least when averaged over 8 sets, but the conclusion is not significant.

These tests support the earlier conclusion that neither method of analysis has any advantages over the other, at least in the present work. Thus, for this reason, and for those given in section IV.1.1, both methods of analysis should be used at all times and the average taken.

CHAPTER V CONCLUSIONS

Both the preliminary tests and the intercomparison tests with the ionization chamber and the Fricke dosimeter indicate that the calorimeter, which was designed and constructed in this work, behaves essentially as expected from the theoretical considerations discussed in chapter II.

Each of the three dosimeters tested gave essentially the same readings within their respective mean deviations, which were each of the order of ±1%. The calorimetric system is more tedious to use than the ionization chamber, both in time of making the measurements and in reducing the results. The Fricke dosimeter, however, is equally as tedious as the calorimeter, but the equipment used is both simple and cheap. A problem with the Fricke dosimeter is that the G-value, which varies with photon energy, must be known at the particular energy at which measurements are to be made. It is a disadvantage to use the calorimetric system at photon energies less than about 3 MeV, where the ionization methods are still applicable. Notwithstanding the extra trouble involved, the calorimetric system must be used for photon energies greater than about 3 MeV, for the reasons given in section I.3. In practice, the calorimetric system would be the fundamental standard of dose measurement by means of which either the ionization chamber, or the Fricke dosimeter, would be calibrated at any photon energy, with specified

quality. The calibrated, or secondary, dosimeters would then be used independently of the calorimeter.

Due to the diversity of designs of the calorimetric systems described in the various publications, many of which have specialized applications, it is difficult to make accurate comparisons with the system developed in the present work. If generalizations are permitted, then the following points appear relevant. The design of the present calorimeter is basically simple, both in theory and construction. It does not require an ultrahigh vacuum, temperature-controlled water bath, or auxiliary circuits to control the temperature of the calorimeter case, etc., as are not uncommon in other calorimeters. The temperature-measuring circuit, based on the D.C. Wheatstone bridge, is simpler than many of the other systems which use relatively complex A.C. bridges, in an endeavour to remove noise. The extra noise in the present bridge is, even if only partly, compensated for by the method of chart analysis. The system is quite portable, permitting it to be used readily within the Radiotherapy department. Many authors, although indicating that their final quoted measurements of dose rate are averages over a number of measurements, do not indicate over how many such measurements the average has been obtained. Those who do indicate the number of measurements usually quote between 4 and 20, for both calibrations and for radiation measurements. The present system, which averages

over only 4 such measurements, would appear to be somewhat conservative. The quoted uncertainties in the final estimates of dose rates in the literature appear to average about ±1%, with a range from about ±0.5% to about ±2%. The present system achieves a similar experimental uncertainty by averaging over a smaller number of results, and could thus be said to be more efficient with the actual measurements made. The recycling times have varied from about 5 to 30 minutes, where the calorimeters having the smaller recycling times have used either, special techniques to restore thermal equilibrium in a short time, or have employed radiation machines with very high exposure outputs thus permitting short exposure times. The recycling time of the present system is from 15 to 20 minutes, which, combined with the small number of measurements necessary, makes this system less time-consuming than many of the other systems to attain a similar uncertainty of the final averaged result.

Preliminary tests for adaptability have been carried out on the 4 MeV "Metropolitan-Vickers", series I, Linear Accelerator, which is at the present the highest energy radiation machine at the Royal Adelaide Hospital. A number of minor modifications were necessary in the operating procedure due to the properties of this particular accelerator. The exposure rate, in air at 1 metre from the source, is nominally 150 roentgen/min, but, in fact, the rate fluctuates in time, especially just after commencing the exposure. However, the fluctuations were not apparent on the chart output of

the calorimeter and both methods of chart analysis could still be performed. The exposure output of the accelerator is monitored by an inbuilt ionization chamber and the maximum possible total exposure is limited to about 600 roentgen, or a dose of about 350 rad in the calorimeter element. Because of the particular type of mounting of this accelerator, it was not possible to irradiate the dosimeters from both sides, thus making the initial setting up a little more critical. The basic operation of the calorimeter, however, remained unchanged, and further tests on this machine were not warranted, since the effective photon energy of the x-radiation from the accelerator was very close to that of Co 60 γ-radiation, with which extensive tests had already been performed.

The work described in this thesis was prompted by the coming installation of a 13 MeV "Toshiba", LMR-13, Linear Accelerator. Both the exposure rate and the maximum possible exposure output of this accelerator will be about twice that of the present accelerator, thus improving the signal-to-noise ratio for the calorimeter. The new accelerator will also permit the irradiation of the calorimeter from both sides. The calorimetric dosimeter system will be an important accessory to this, and to any further high-energy machines that may be installed in the future.

APPENDICES

APPENDIX I MASSES AND HEAT CAPACITIES OF CALORIMETER COMPONENTS

(i) Test Calorimeter, mark I.

Element

Part	Material	Mass (gm)	Specific Heat (cal/gm°C)	Heat Capacity (cal/°C)	% Mass
element	graphite	8.910	0.165	1.470	96.02
aquadag	graphite	0.009	0.165	0.001	
ring	perspex	0.274	0.35	0.096	3.89
heater insul.	rayon	0.001	0.40	0.000	
silicone grease		0.036	0.45	0.028	
thermistor	glass& araldite bead & leads	0.050	0.50	0.025	0.09
		0.005	0.09	0.000	
heater wire	eureka	0.004	0.10	0.000	

Total Mass=9.289 gm Total H.C.=1.620 cal/°C

Case

case	graphite	235.537	0.165	38.864	97.54
aquadag	graphite	0.879	0.165	0.145	
plug	graphite	9.547	0.165	1.575	

.....

studs	perspex	1.707	0.35	0.597	)	
screws	perspex	2.723	0.35	0.953	)	
nuts	perspex	1.242	0.35	0.435	)	2.26
peg	perspex	0.011	0.35	0.004	)	
heater insul.	rayon	0.023	0.40	0.009	)	
heater wire	eureka	0.260	0.10	0.026	)	
heater leads	copper	0.248	0.09	0.022	)	0.20

Total Mass=252.177gm Total H.C.=42.630 cal/^{o}C

Total mass of calorimeter = 261.466 gm

and the element is 3.55% of this total mass.

Ratio of masses = 27.15

Ratio of H.C. = 26.31

(ii) Reference Calorimeter, mark I.

Element

Part	Material	Mass (gm)	Specific Heat (cal/gm°C)	Heat Capacity (cal/°C)	% Mass
element	graphite	8.999	0.165	1.485	96.02
ring	perspex	0.291	0.35	0.102	
silicone grease		0.030	0.45	0.013	3.93
thermistor (glass & araldite		0.047	0.50	0.023	
((bead & leads		0.005	0.09	0.000	0.05

Total Mass=9.372gm Total H.C.=1.623 cal/°C

Case

case	graphite	237.185	0.165	39.136	97.80
plug	graphite	9.594	0.165	1.583	
studs	perspex	1.707	0.35	0.597	
screws	perspex	2.677	0.35	0.937	2.20
nuts	perspex	1.166	0.35	0.408	
peg	perspex	0.011	0.35	0.004	

Total Mass=252.340gm Total H.C.=42.665 cal/°C

Total mass of calorimeter = 261.712 gm

and the element is 3.58% of this total mass.

(iii) Test Calorimeter, mark II.

Element

element	graphite	8.910	0.165	1.470	)	96.65
aquadag	graphite	0.009	0.165	0.001	)	
ring	perspex	0.189	0.35	0.066	)	3.25
heater insul.	rayon	0.001	0.40	0.000	)	
silicone grease		0.062	0.45	0.028	)	
thermistor	(glass & (araldite	0.048	0.50	0.024	)	0.10
	(bead & (leads	0.005	0.09	0.000	)	
heater wire	eureka	0.004	0.10	0.000	)	

Total Mass=9.228gm. Total H.C.=1.589 cal/^{o}C

Case same as for Test Calorimeter, mark I.

Total Mass of calorimeter = 261.405 gm

and the element is 3.53% of this total mass.

Ratio of Masses = 27.33

Ratio of H.C. = 26.83

(iv) Reference Calorimeter, mark II.

Element

part	Material	Mass (gm)	Specific Heat (cal/gm^{o}C)	Heat Capacity (cal/^{o}C)	% Mass
element	graphite	8.999	0.165	1.485	96.95
ring	perspex	0.169	0.35	0.059	
silicone grease		0.062	0.45	0.028	2.00
thermistor (glass&araldite		0.047	0.50	0.023	
(bead & leads		0.005	0.09	0.000	0.05

Total Mass=9.282gm Total H.C. =1.595 cal/^{o}C

Case

case	graphite	237.185	0.165	39.136	97.79
plug	graphite	9.565	0.165	1.578	
studs	perspex	1.707	0.35	0.597	
screws	perspex	2.677	0.35	0.937	2.21
nuts	perspex	1.166	0.35	0.408	
peg	perspex	0.011	0.35	0.004	

Total Mass=252.311gm Total H.C.=42.660 cal/^{o}C

Total mass of calorimeter = 261.593 gm

and the element is 3.51% of this total mass.

APPENDIX II CALCULATION OF THERMAL TRANSFER COEFFICIENTS

The following calculations are considered to provide only estimates since the thermal properties involved have been obtained from various handbook values. They should, however, be at least of the correct order of magnitude.

Convection Losses

LAUGHLIN and GENNA (1956) have shown that no natural convection will occur when the following condition is satisfied:

$$(p/760)^2 < 16.2/d^3\Delta T$$

where p is the pressure in torr, d is the separation between components in cm. and ΔT is the temperature difference in ^{o}C.

In the present calorimeter the maximum distances involved are about 10 cm and the temperature differences are always less than $1^{o}C$, thus no convection transfer will occur if the pressure is less than, p = 100 torr. Since the pressure is always much less than 100 torr in practice, no convection losses will occur in this calorimeter.

Element/Case System.

(i) Radiation Losses.

The general equation for radiation heat transfer is:

$$\frac{dE}{dt} = -A\sigma F(T^4 - T_o^4) \text{ cal/sec} \qquad \ldots.(1)$$

where A is the surface area of the emitting surface, σ is the Stefan-Boltzman constant, T and T_o are the absolute temperatures of the emitting and absorbing surfaces, respectively, and F is the configuration factor for grey bodies. F is a complex function solvable for only a few simple cases. An approximation for F, for an object suspended in an enclosure, is given by McADAMS (1942) as:

$$F = 1/\left(1/\varepsilon + \frac{A}{A_o}(1/\varepsilon_o - 1)\right)$$

where ε and ε_o are the emissitivities of the emitting and absorbing surfaces respectively.

It is readily shown that if the difference between T and T_o is less than 1^oC, then equation (1) can be simplified to:

$$\frac{dE}{dt} = - A\sigma F(4T_o^3)(T - T_o) = - K_r(T - T_o)$$

where K_r is the thermal conductance for radiation. In the present case the various values are:

$A = 19.10\ cm^2$, $A_o = 27.64\ cm^2$, $\varepsilon = \varepsilon_o = 0.85$, with $T_o = 22^oC$.

thus, $K_r = 2.08 \times 10^{-3}\ cal/^oC\ sec$

(ii) Losses by Conduction through low pressure air.

Pressure in cavity $\simeq 5 \times 10^{-3}$ torr

The mean free path (M.F.P.) at this pressure $\simeq$ 1 cm.

Separation between element and case $\simeq$ 0.2 cm.

Thus, in this system the M.F.P. > dimensions of the system, and LAUGHLIN and GENNA (1956) state that the thermal transfer coefficient for this condition is given by:

$$h_a = 0.0022\ p\ \text{cal/cm}^2\ ^\circ\text{C sec}$$

thus, in the present case $h_a = 11.0 \times 10^{-6}$ cal/cm^2 $^\circ$C sec

and $K_a = 0.21 \times 10^{-3}$ cal/$^\circ$C sec

(iii) Losses by Conduction through the perspex ring.

An estimation of this loss is complicated since the ring is in poor thermal contact with the case, thus both conduction and radiation are involved. Conduction occurs from the inner edge of the ring, at temperature T, to its outer edge, at temperature T_1. The rate of heat loss flowing radially across a cylinder is given by:

$$\frac{dE}{dt} = \frac{2\pi kL(T - T_1)}{\ln(r_1/r_2)}$$

Due to the porous nature of the ring it is necessary to determine an effective value of its axial length, L, while retaining the same r_1 and r_2 values, and knowing both its mass and density. The calculated value is L = 0.14 cm which, together with the value $k = 5 \times 10^{-4}$ cal cm/cm^2 $^\circ$C sec, gives:

$$\frac{dE}{dt} = 2.0 \times 10^{-3}(T - T_1)\ \text{cal/sec} \qquad \ldots(2)$$

The thermal barrier at the outer edge of the ring to the case, at temperature T_o, is bridged by radiation. In this case we have: $A = A_o = 1$ cm^2, $\varepsilon = \varepsilon_o = 0.85$, which gives:

$$\frac{dE}{dt} = 0.10 \times 10^{-3}(T_1 - T_o)\ \text{cal/sec} \qquad \ldots(3)$$

Eliminating T_1 from equations (2) and (3) gives:

$$K_p = 0.09 \times 10^{-3} \text{ cal/}^{o}\text{C}$$

(iv) Losses through perspex peg.

The pressure acting on the peg is approximately 2 kgm/cm^2 which gives reasonable, although not perfect, thermal contact. For simplicity perfect contact is assumed. Conduction losses are given by the elementary relation:

$$\frac{dE}{dt} = \frac{kA}{d}(T - T_o) \qquad \ldots(4)$$

In the present case we have: A = 0.008 cm^2, d = 0.3 cm and the value of k is given in the previous section, thus we have:

$$K_e = 0.01 \times 10^{-3} \text{ cal/}^{o}\text{C sec}$$

(v) Losses along copper leads

There are four leads involved, two for the thermistor (a and b) and two for the heater (c and d). The gauge is the same for each, namely 45 SWG (7.8 cir mil area). k_{cu} = 0.92 cal cm/cm^2 ^{o}C sec. Leads a, b and c. Each of same length, 1.5 cm, with total area 118.5 x 10^{-6}cm^2, hence, using equation (4), gives:

$$K_b = 0.07 \times 10^{-3} \text{ cal/}^{o}\text{C sec.}$$

Lead d. Length 5.0 cm. and area 39.5 x 10^{-6}cm^2, hence:

$$K_d = 0.01 \times 10^{-3} \text{ cal/}^{o}\text{C sec.}$$

Thus, finally $K_c = 0.08 \times 10^{-3}$ cal/^{o}C sec

Total thermal conductance for Element/Case System: $K_2 = 0.244 \times 10^{-2}$ cal/^{o}C sec

Case/Vacuum Chamber System

(i) Radiation Losses.

In this situation, $A = 169.6\ cm^2$ $A_o = 1445\ cm^2$

$\varepsilon = 0.85$ $\varepsilon_o = 0.6$

thus, from equation (1), $K_r = 19.2 \times 10^{-3}$ cal/^oC sec

(ii) Losses by Conduction through low pressure air.

M.F.P. at 5×10^{-3} torr $\simeq$1 cm.

Separation between case and Vacuum chamber wall $\simeq$ 10 cm.

Thus, in this system the M.F.P.(L) < dimensions of the system, and LAUGHLIN and GENNA (1956) state that the thermal transfer coefficient for this condition is given by:

$$h_a = k/(d + g_1 + g_2)$$

where k is the thermal conductivity of the air (11×10^{-5} cal cm/cm^2 ^oC sec), and g_1 and g_2 are the temperature jump distances, usually $g_1 = g_2 \simeq 2.7L$.

Hence, $K_a = 1.20 \times 10^{-3}$ cal/^oC sec

(iii) Losses along copper leads.

In this case there are two leads, each with two sections of different diameter wire.

(a) 4.4 cm of 40 SWG + 1.9 cm of 44 SWG

(b) 2.4 cm of 40 SWG + 7.8 cm of 44 SWG

The relevant equation for conduction along paths of two different cross-section areas in series is:

$$\frac{dE}{dt} = \frac{k(T - T_o)}{\left(\frac{d_1}{A_1} + \frac{d_2}{A_2}\right)}$$

thus, we have for (a) $K_f = 1.2 \times 10^{-5}$ cal/^oC sec

and (b) $K_g = 0.51 \times 10^{-5}$ cal/^oC sec

hence, $K_c = 1.7 \times 10^{-5}$ cal/^oC sec

(iv) Losses along nylon supports

There are three cords, each 6 cm long and 0.3 mm diameter.

$k_{nylon} = 0.2 \times 10^{-6}$ cal/^oC sec

Thus, $K_n = 0.2 \times 10^{-6}$ cal/^oC sec

Total thermal conductance for Case/Vacuum chamber System:

$K_1 = 2.04 \times 10^{-2}$ cal/^oC sec.

APPENDIX III CALIBRATION HEATER RESISTANCE VALUES

Calorimeter I. (average of 3 sets of measurements)

Element heater:	at VC*	96.42 ± 0.02 Ω
	at box	97.42 ± 0.02 Ω
Case heater:	at VC	3.339 ± 0.01 Ω
	at box	4.323 ± 0.01 Ω

Calorimeter II. (average of 6 sets of measurements)

Element heater:	at VC	91.03 + 0.05 Ω
	at box	91.94 ± 0.04 Ω
Case heater:	at VC	3.193 ± 0.05 Ω
	at box	4.210 ± 0.05 Ω

(*Vacuum chamber electrical leadthroughs)

APPENDIX IV CALCULATION OF A TYPICAL IONIZATION CHAMBER RESULT

Example (iii) from Table IV.2

Conditions: Fry electrometer on 16 rpm and 10 pF

Voltage drop ratio, B = 100.82

Anode potential on chamber 100 volts

T = 24.3°C and P = 745.1 torr

The correction factor for temperature and pressure is thus,

$$C(T,P) = \left(\frac{760.0}{745.1}\right)\left(\frac{273.2 + 24.3}{273.2}\right) = 1.1106$$

The average measured potentiometer reading, P = 0.9396 volt

Substituting the above data into equation (III.6) gives:

$$ER = \left(\frac{0.009131 \times 60 \times 100.82 \times 1.1106}{1.530}\right)(0.9396) = 37.67 \text{ roentgen/min}$$

Making use of equation (III.7) gives the dose rate on the 9th Jan. 1970 as:

$$\underline{DR = 32.81 \text{ rad/min}}$$

Taking the half-life of Co 60 as 5.26 years, the correction factor for radioactive decay can be expressed to a very good approximation, if t < 300 days, in the form:

$$(I/I_o) = \exp(\pm\lambda t) = \left(1 \pm (3.609 \times 10^{-4}t) + (3.609 \times 10^{-4}t)^2/2\right)$$

where the time interval, t, is in days.

For the present example, t = 8 days, and the correction factor is 1.0029, giving the dose rate on the 1st Jan.1970 as:

$$\underline{\underline{DR = 32.90 \text{ rad/min}}} \quad \text{(as shown in Table IV.2)}$$

APPENDIX V CALCULATION OF A TYPICAL FRICKE DOSIMETER RESULT

Example (iv) from Table IV.3

Preliminary measurements:	304 mμ	224 mμ
OD measured at 22.1°C	+0.003	+0.004

Mass of solution before irradiating = 2.937 gm.

.....

Calculation of density correction factor:

Volume of central cavity of guard case = 10.68 cm^3

mass of components in calorimeter cavity = 9.232 gm

hence, average density in calorimeter cavity = 0.8644 gm/cm^3

mass of components in Fricke cavity (less solution) = 5.969 gm

total mass, including mass of solution from above = 8.906 gm

hence, average density in Fricke cavity = 0.8335 gm/cm^3

thus, $\left(\frac{\text{average density of Calor. cavity}}{\text{average density of Fricke cavity}}\right)$ = 1.037

from equation (III.9) we now have that the overall conversion factor is 0.914

.....

Solution was irradiated for a total of 5.5 hours.

Mass of solution after irradiating = 2.919 gm

thus, mass of water lost by evaporation (in 6.25 hours) = 0.018 gm

or 0.61% of the original mass of the solution

.....

Intermediate measurements:	304 mμ	224 mμ
OD at 24.0°C, OD_t	0.509	1.058
temperature correction	1.0069	1.0013
OD at 25.0°C, OD_{25}	0.512	1.059
change in OD_{25}, ΔOD_{25}	0.509	1.055
corrected for evaporation	0.506	1.049

Using equation (III.8a) gives the total dose = 13.97×10^3 rad

Using equation (III.8b) gives the total dose = 13.93×10^3 rad

thus, average dose in 5.5 hours = 13.95×10^3 rad

which gives the dose rate, in Fe^{++} solution = 42.27 rad/min (i)

The irradiated solution was stored for a further 44.0 hours

Mass of solution (in polythene container) before storing = 2.859 gm

mass of solution after storing = 2.769 gm

thus, mass of water lost (in 44.0 hours) by evaporation = 0.090 gm

or 3.15% of the mass of the solution before storing

Final measurements:	304 mμ	224 mμ
OD at 23.0°C, OD_t	0.552	1.157
temperature correction	1.0138	1.0026
OD at 25.0°C, OD_{25}	0.560	1.160
change in OD_{25}, ΔOD_{25}	0.048	0.101
corrected for evaporation	0.046	0.098

.....

Using equation (III.8a) gives the total dose = 1.27×10^3 rad

Using equation (III.8b) gives the total dose = 1.30×10^3 rad

thus, average dose in 44.0 hours = 1.285×10^3 rad

which gives the effective dose rate, in

Fe^{++} solution = 0.48 rad/min (ii)

The final measurement of dose rate, measured in the Fricke dosimeter, obtained from results (i) and (ii) = 41.79 rad/min.

Using equation (III.9), and the conversion factor determined above, gives the equivalent dose rate in the calorimeter on the 22nd Aug. 1970;

DR = 38.20 rad/min

The correction factor for radioactive decay over a period of 52 days is 1.0190, thus giving the dose rate on the 1st July 1970 as;

DR = 38.93 rad/min (as shown in Table IV.3)

APPENDIX VI CALCULATION OF A TYPICAL CALORIMETER RESULT

Example (vii) from Table IV.3

Operating conditions:

Bridge potential, 2 Hg Cells

Millimicrovoltmeter range, 0.3 mV

Chart recorder paper speed, 600 mm/hour

Exposure time, 6 minutes (plus 0.01 min for radiation measurements)

Bridge on forward polarity.

Chart No. (i) Electric calibration: v = 24.115 mV

Substituting this value of v into equation (II.20b), and applying a +0.2% correction (refer section II.5.3), gives the electric dose rate as DR = 55.18 rad/min.

The average measured deflection of the trace is 49.6 divs, which corresponds to a deflection rate of 8.267 div/min.

Therefore, the calibration factor is 6.675 rad/div.

Chart No. (iv) Electric calibration: v = 24.103 mV

The electric dose rate in this case is, DR = 55.12 rad/min.

The average measured deflection of the trace is 49.9 divs, which corresponds to a deflection rate of 8.312 div/min.

Therefore, the calibration factor is 6.631 rad/div.

Thus, the average calibration factor, for forward polarity, is:

$$(D_C/X_C)_f = 6.653 \text{ rad/div.}$$

Chart No. (ii) Radiation measurement: radiation beam from right to left. The average measured deflection of the trace is 35.45 divs, which corresponds to a deflection rate of 5.899 div/min.

Chart No. (iii) Radiation measurement: radiation beam from left to right. The average measured deflection of the trace is 34.4 divs, which corresponds to a deflection rate of 5.724 div/min.

Thus, the average measured deflection rate, including a +0.4% correction for scatter (refer section IV.2.1), is:

$$(dX/dt)_{mf} = 5.835 \text{ div/min.}$$

The average measured radiation dose rate, using forward polarity, is therefore:

$$DR_f = 38.82 \text{ rad/min.}$$

Bridge on reverse polarity.

Chart No. (v) Electric calibration: v = 24.110 mV

The electric dose rate is, DR = 55.16 rad/min.

The average measured deflection of the trace is 49.9 divs, which corresponds to a deflection rate of 8.317 div/min.

Therefore, the calibration factor is 6.632 rad/div.

Chart No.(viii) Electric calibration: v = 24.100 mV

The electric dose rate is, DR = 55.11 rad/min.

The average measured deflection of the trace is 49.9 divs, which corresponds to a deflection rate of 8.317 div/min.

Therefore, the calibration factor is 6.626 rad/div.

Thus, the average calibration factor, for reverse polarity, is:

$$(D_c/X_c)_r = 6.629 \text{ rad/div.}$$

Chart No. (vi) Radiation measurement: radiation beam from left to right.

The average measured deflection of the trace is 33.7 divs, which corresponds to a deflection rate of 5.607 div/min.

Chart No. (vii) Radiation measurement: radiation beam from right to left.

The average measured deflection of the trace is 32.85 divs, which corresponds to a deflection rate of 5.466 div/min.

Thus, the average measured deflection rate, including a +0.4% correction for scatter, is:

$$(dX/dt)_{mr} = 5.558 \text{ div/min.}$$

The average measured radiation dose rate, using reverse polarity, is therefore:

$$DR_r = 36.84 \text{ rad/min.}$$

Finally, the average measured radiation dose rate, for both forward and reverse bridge polarity, for the 9th August, 1970 is:

DR = 37.83 rad/min.

The correction factor for radioactive decay over a period of 39 days is 1.0141, thus giving the dose rate on the 1st July 1970 as:

DR = 38.36 rad/min. (as shown in Table IV.3)

BIBLIOGRAPHY

ALMOND, P.R. (1967) *Phys.Med.Biol.*, 12, 13.

BARNARD, G.P., MARSH, A.R.S. and HITCHMAN, D.G.I. (1964) *Phys.Med.Biol.*, 9, 295.

BATTAERD, H.A.J.B. and TREGEAR, G.W. (1966) *Rev.Pure and Appl.Chem.*, 16, 83.

BECQUEREL, H. and CURIE, P. (1901) *Compt.Rend.*, 132, 1289.

BEHNKEN, H., KAY, G.W.C., SOLOMON, I. and TAYLOR, L.S. (1934) *Am.J.Roentgenol.*, 31, 815.

BERNIER, J.P., SKARSGARD, L.D., CORMACK, D.V. and JOHNS, H.E. (1956) *Rad.Res.*, 5, 613.

BEWLEY, D.K. (1963) *Brit.J.Radiol.*, 36, 865.

BOAG, J.W. (1956) Ionization Chambers, *In* "Radiation Dosimetry" (G.J. Hine and G.L. Brownell, editors), Academic Press, New York, chapter 4.

BROSZKIEWICZ, R.K. and BULHAK, Z. (1970) *Phys.Med.Biol.*, 15, 549.

BRYANT, T.H.E. and RIDLER, T.P. (1968) *Health Phys.*, 15, 263.

CARSLAW, H.S. and JAEGER, J.C. (1959) "Conduction of Heat in Solids", Clarendon Press, Oxford, chapters 10 and 14, 2nd edition.

CROMPTON, R.W. and SUTTON, D.J. (1952) *Proc.Roy.Soc.*, A215, 467.

DAVIES, J.V., GREENE, D., KEENE, J.P., LAW, J. and MASSEY, J.B. (1963) *Phys.Med.Biol.*, 8, 97.

DAVIES, J.V. and LAW, J. (1963) *Phys.Med.Biol.*, 8, 91.

DEWING, S.B. (1962) "Modern Radiology in Historical Perspective", Charles C. Thomas, Springfield.

DOLPHIN, G.W. and INNES, G.S. (1956) *Phys.Med.Biol.*, 1, 161.

EDWARDS, P.D. and KERST, D.W. (1953) *Rev.Sci.Instr.*, 24, 490.

EWING, J. (1934) *Am.J.Roentgenol.*, 31, 153.

FAILLA, G. (1937) *Radiology*, 29, 202.

FAILLA, G. (1955) *Radiology*, 65, 406.

FANO, U. and TAYLOR, L.S. (1950) *Radiology*, 55, 743.

FLEMING, D.M. (1970) *Health Phys.*, 18, 135.

FLEMING, D.M. and GLASS, W.A. (1969) *Rad.Res.*, 37, 316.

FRICKE, H. and GLASSER, O. (1925) *Am.J.Roentgenol.*, 13, 453.

FRICKE, H. and MORSE, S. (1929) *Phil.Mag.*, 7, 129.

FRY, R.M. (1954) *J.Sci.Instrum.*, 31, 269.

GEISSELSODER, J., KOEPKE, K. and LAUGHLIN, J.S. (1963) *Rad.Res.*, 20, 423.

GENNA, S. and LAUGHLIN, J.S. (1955) *Radiology*, 65, 394.

GENNA, S. and LAUGHLIN, J.S. (1956) AEC Contract Report, AT (30-1) 1451.

GENNA, S., JAEGER, R.G., NAGL, J. and SANIELEVICI, A. (1963) *At.Energy Rev.*, 1, 239.

GLASSER, O. (1941) *Radiology*, 37, 221.

GOODWIN, P.N. (1959) *Rad.Res.*, 10, 6.

GRAY, L.H. (1929) *Proc.Roy.Soc.*, A122, 647.

GRAY, L.H. (1936) *Proc.Roy.Soc.*, A156, 578.

GREENING, J.R. (1964) *Phys.Med.Biol.*, 9, 143.

GREENING, J.R., RANDLE, K.J. and REDPATH, A.T. (1968) *Phys.Med.Biol.*, 13, 359.

GRUBBE, E.H. (1933) *Radiology*, 21, 156.

ICRU Rept. 10a, "Radiation Quantities and Units" published as *National Bureau of Standards (U.S.) Handbook 84*, 1962.

JOHNS, H.E. (1956) X-Rays and Teleisotope γ-Rays. *In* "Radiation Dosimetry" (G.J. Hine and G.L. Brownell, editors), Academic Press, New York, chapter 12.

KATOH, K. (1965) *Phys.Med.Biol.*, 10, 565.

KEENE, J.P. and LAW, J. (1963) *Phys.Med.Biol.*, 8, 83.

KERST, D.W. and PRICE, G.A. (1950) *Phys.Rev.*, 79, 725.

LAUGHLIN, J.S. and BEATTIE, J.W. (1951) *Rev.Sci.Instr.*, 22, 572.

LAUGHLIN, J.S., BEATTIE, J.W., HENDERSON, W.J. and HARVEY, R.A. (1953) *Am.J.Roentgenol.*, 70, 294.

LAUGHLIN, J.S. and GENNA, S. (1956) Calorimetric Methods. *In* "Radiation Dosimetry" (G.J. Hine and G.L. Brownell, editors), Academic Press, New York, chapter 9.

LAW, J. (1970a) *Phys.Med.Biol.*, 15, 117.

LAW, J. (1970b) *Phys.Med.Biol.*, 15, 301.

LAZO, R.M., DEWHURST, H.A. and BURTON, M.J. (1954) *J.Chem.Phys.*, 22, 1370.

McADAMS, W.H., (1942), "Heat Transmission", McGraw-Hill, New York, chapter 3, 2nd Edition.

MILVY, P., GENNA, S., BARR, N. and LAUGHLIN, J.S. (1958) *Proc. 2nd Intern. Conf. on Peaceful Uses of Atomic Energy*, 21, 142.

NBS Handbook 79, "Stopping Powers for Use with Cavity Chambers" (NCRP Report), published as *National Bureau of Standards (U.S.) Handbook* 79, 1961.

NBS Handbook 84, "Radiation Quantities and Units" (ICRU Report 10a), published as *National Bureau of Standards (U.S.) Handbook* 84, 1962.

NBS Handbook 85, "Physical Aspects of Irradiation" (ICRU Report 10b), published as *National Bureau of Standards (U.S.) Handbook* 85, 1964.

PETREE, B. (1958) *Rad.Res.*, 9, 166.

PETREE, B. and WARD, G. (1962) *NBS (U.S.) Technical Notes*, No.163.

PETTERSSON, C. and HETTINGER, G. (1967) *Acta.Radiol.(Therapy)*, 6, 160.

Recomm. Of I.C.R.U., LONDON 1950, (6th Intern.Cong. of Radiology) published in *Radiology*, 56, 117.

REED, G.W. (1964) editor "Radiation Dosimetry", Academic Press, New York and London.

REID, W.B. and JOHNS, H.E. (1961) *Rad.Res.*, 14, 1.

ROLLO, F.D., KATCHIS, L.J. and DAUER, M. (1968) *Phys.Med.Biol.*, 13, 79.

RUTHERFORD, E. and ROBINSON, H. (1913) *Phil.Mag.*, 25, 312.

SCHLEIGER, E.R. and GOLDSTEIN, N. (1964) *Rev.Sci.Instr.*, 35, 890.

SCHNEIDER, P.J. (1957) "Conduction Heat Transfer", Addison-Wesley, Massachusetts, chapter 12.

SCOTT, P.B. and GREENING, J.R. (1963) *Phys.Med.Biol.*, 8, 51.

SPIERS, F. (1956) Radiation Units, *In* "Radiation Dosimetry" (G.J. Hine and G.L. Brownell, editors), Academic Press, New York, chapter 1.

WOOD, F.C. (1929) *Radiology*, 12, 461.